

Finite- and infinite-volume study of $DD\pi$ scattering

Sebastian M. Dawid^a , Fernando Romero-López^{b,c} , and Stephen R. Sharpe^a

^a*Physics Department, University of Washington, Seattle, WA 98195-1560, USA*

^b*Albert Einstein Center, Institute for Theoretical Physics, University of Bern, 3012 Bern, Switzerland*

^c*Center for Theoretical Physics, Massachusetts Institute of Technology, Cambridge, MA 02139, USA*

E-mail: dawids@uw.edu, fernando.romero-lopez@unibe.ch, srsharpe@uw.edu

ABSTRACT: We develop a comprehensive framework for extracting the pole position and properties of the doubly-charmed tetraquark $T_{cc}^+(3875)$ from lattice QCD data using the relativistic three-particle formalism. This approach incorporates the effect of the one-pion exchange diagram in $DD\pi$ and DD^* scattering, making it applicable at energies coinciding with the left-hand cut in the partial-wave projected DD^* amplitude. We present an example application of this framework to existing lattice QCD data at $m_\pi = 280$ MeV. We solve the integral equations describing the $DD\pi$ reaction, use LSZ reduction to determine the corresponding DD^* amplitude, and find the values of the infinite-volume two- and three-body K matrices that lead to agreement with lattice DD^* phase shifts within their uncertainties. Using these K matrices in the three-particle quantization condition, we describe the finite-volume DD^* spectrum and find good agreement with the lattice QCD energies. Our results suggest that, at this pion mass, the tetraquark appears as a pair of subthreshold complex poles whose precise location strongly depends on the value of the $DD\pi$ three-particle K matrix.

Contents

1	Introduction	2
2	Infinite-volume formalism for the T_{cc}^+	4
2.1	$DD\pi$ scattering amplitude and kinematics	4
2.2	Three-body integral equations	7
2.2.1	The ladder equation	7
2.2.2	Three-body forces	11
2.2.3	Numerical solution	14
2.3	Connecting $DD\pi$ and DD^* scattering amplitudes	15
3	Finite-volume formalism	17
3.1	QC2 for DD^* scattering	17
3.2	QC3 for $DD\pi$ scattering	19
4	Numerical results	21
4.1	Physical setup and two-body interactions	22
4.2	The $J^P = 1^+$ ladder amplitude	25
4.3	The $J^P = 1^+$ amplitude with non-zero \mathcal{K}_3	27
4.4	The $J^P = 0^-$ amplitude	32
4.5	Comparison with the finite-volume energies	34
5	Summary and outlook	39
A	Partial-wave projection of OPE and \mathcal{K}_3	41
A.1	Basic results	41
A.2	Projection formula for OPE kernel G	43
A.3	Projection of \mathcal{K}_3	46
A.4	Projection of \mathcal{M}_2	47
B	Expressions for the partial-wave projection of OPE	47
B.1	$J^P = 1^+$	48
B.2	$J^P = 0^-$	49
C	Expressions for the partial-wave projection of \mathcal{K}_3	49
C.1	$J^P = 1^+$	49
C.2	$J^P = 0^-$	51
D	Residue of D^* pole	52

1 Introduction

The doubly-charmed tetraquark, $T_{cc}^+(3875)$, has been observed by the LHCb collaboration as a resonance between the rest energies of DD^* and $DD\pi$ [1, 2]. Various phenomenological models have been able to predict a $(I)J^P = (0)1^+$ state in this mass window [3–7]. As for many other heavy-flavor multi-quark exotics, its proximity to the relevant threshold makes it a promising meson-meson molecule candidate; however, parallel descriptions as a compact diquark-antidiquark state or a mixture of different configurations were also successful. A recent review can be found in ref. [8]. A fully controlled determination of this state from QCD has not been yet achieved; however, lattice computations are already exploring the T_{cc}^+ at heavier-than-physical (and equal) light quark masses [9–14].

The physical tetraquark decays exclusively into the $DD\pi$ state, requiring the inclusion of three-body thresholds and physical one-pion exchanges (OPEs) in phenomenological analyses [15–20]. However, when the pion is sufficiently heavy, the D^* meson becomes a $D\pi$ bound state, and the DD^* and $DD\pi$ thresholds are inverted. Rather than a three-body unstable resonance, the tetraquark may appear as a shallow two-body bound or a virtual state pole in the DD^* scattering amplitude for a considerable range of quark masses [13, 20]. Although threshold inversion could, in principle, allow one to effectively describe T_{cc}^+ as a two-body system, it has become clear that a rigorous determination of the DD^* amplitude must incorporate three-body effects [20–22].

The main reason is that, at heavy pion masses, one-pion exchanges become virtual and induce a non-analyticity (left-hand cut) in the partial-wave projected DD^* scattering amplitude near the expected T_{cc}^+ energy. A near-threshold branch point invalidates the application of commonly used finite- and infinite-volume two-body techniques, such as the Lüscher formalism [23] or naïve effective-range expansions (ERE) [24, 25]. It complicates the extraction of the tetraquark pole position using lattice QCD and has motivated several authors to resolve this issue using different methods [21, 22, 26, 27].

Among these proposals, ref. [22] advocates using the three-body finite-volume formalism [28–46], specifically that in the generic relativistic field theory (RFT) approach of refs. [30, 31], to describe the DD^* and $DD\pi$ spectrum, since it naturally includes the effects from the OPE diagrams. The first step in this approach is to apply the three-body quantization condition to the finite-volume DD^* and $DD\pi$ energy levels to determine the properties of $DD\pi$ scattering at generic isospin in isosymmetric QCD (including $I = 0$ for the T_{cc}^+). The resulting infinite-volume information takes the form of two- and three-meson K matrices. The former describe interactions of particles in the two-particle subchannels, DD and $D\pi$, and incorporate the D^* meson as a resonance or bound-state pole in the $I = 1/2$, p -wave $D\pi$ scattering amplitude. The three-body K matrix parametrizes short-range three-particle interactions.

In this approach, there is then a second step, in which two- and three-meson K matrices are translated into the elastic $DD\pi$ scattering amplitude by using relativistic integral equations [22, 31, 47–50]. The solutions of the integral equations provide a three-body amplitude consistent with S matrix unitarity, which can be analytically continued to energies near the OPE branch points and D^* pole. By applying the Lehmann-Symanzik-Zimmermann

(LSZ) reduction formula to the $DD\pi$ solution of these equations, one can extract the DD^* amplitude at energies below the left-hand branch point and reliably determine the pole position of T_{cc}^+ [22, 51]. One of the advantages of this approach is that it is applicable at any pion mass, allowing one to analyze and connect results obtained from lattice ensembles characterized by both stable and unstable D^* .

In this work, we present a complete implementation of the strategy sketched above, in which we carry out all the steps needed to connect lattice QCD energies to the T_{cc}^+ . We numerically implement the proposal of ref. [22] in both finite and infinite volume and show how to extract the pole position of the tetraquark. To make contact with existing lattice QCD results, we focus on the case of a bound D^* meson, such that the tetraquark appears in the DD^* scattering amplitude. For concreteness, we tune the scattering parameters to resemble the lattice QCD setting of Refs. [9, 13].

Our work consists of three main parts. In the first, we solve the relativistic three-body integral equations in the $J^P = 0^-$ and $J^P = 1^+$ channel corresponding to the T_{cc}^+ . This requires generalization of existing tools [49, 51–54] to a system with non-zero partial waves, non-degenerate masses, and general three-body couplings.¹ We constrain the two-body subchannel interactions using the available $D\pi$ lattice data [56–60] and heavy-light meson Chiral Perturbation Theory (ChPT) [61–63], and tune the three-body K matrix such that the results are in reasonable agreement with the s -wave DD^* scattering phase shift of ref. [9]. The resulting amplitude is continued to the unphysical Riemann sheet and evaluated below the DD^* threshold where we identify the T_{cc}^+ as a sub-threshold complex pole, in agreement with other analyses [13, 20, 21, 24, 64].

In the next part, we solve the three-particle quantization condition using the same K matrices that appear in the infinite-volume equations. This allows us to calculate the $DD\pi$ and DD^* energy levels and compare them to lattice DD^* levels obtained from ref. [9]. Our approach reproduces the lattice spectrum closely, aside from states that can be interpreted as having primarily a $DD\pi$ composition, which were not determined in the lattice calculation. This agreement provides a test of the full formalism.

In refs. [9, 13] the lattice energies are analyzed using the two-particle quantization for the DD^* system, leading to results for the $J^P = 1^+$ (s -wave) and $J^P = 0^-$ (p -wave) phase shifts. As noted above, it is known that this approach fails near the left-hand cut, and we investigate this issue in the final part of this work. We do so by solving the two-particle quantization condition using the $J^P = 1^+$ and 0^- phase shifts obtained from the solution to the integral equations. We observe that, as expected, the two- and three-particle quantization conditions give similar energy levels above the DD^* threshold, while there are significant discrepancies between the levels lying near the left-hand cut. Consequently, several low-lying energy levels observed in the lattice simulations cannot be used as input into the two-body quantization condition but can be analyzed using the three-body one.

We organize this paper as follows. In section 2, we describe the scattering kinematics and the details of the infinite-volume formalism: relativistic integral equations, partial-

¹While this work was in preparation, ref. [55] appeared, which also addresses non-zero partial waves.

wave projection, and the models of two- and three-body K matrices. We also discuss the singularities of the $DD\pi$ amplitude and its LSZ reduction to that for DD^* . In section 3, we review the finite-volume formalism derived in ref. [22], as well as the two-body quantization condition for the DD^* system, including partial-wave mixing. In section 4, we present the results of the numerical implementation of the formalism. We show the DD^* amplitude extracted from the solutions of the integral equations for $DD\pi$ in the $J^P = 1^+$ and 0^- channels. We also present the finite-volume energies obtained from the quantization conditions and compare them to the original data set of ref. [9]. Based on these numerical results, we discuss the applicability of the three- and two-particle formalisms near the left-hand cut. We summarize this work in section 5.

We include four appendices. In appendix A, we discuss formal aspects of the partial-wave projection of the OPE amplitude, the three-body K matrix, and the two-particle amplitude \mathcal{M}_2 . In appendices B and C, we summarize, respectively, the projected matrix elements of the OPE and the three-body K matrix in the channels used in this work. In appendix D, we compare our $D\pi$ amplitude model to the tree-level result in the heavy-light meson ChPT.

2 Infinite-volume formalism for the T_{cc}^+

To describe the T_{cc}^+ , we consider an elastic three-body scattering process, $DD\pi \rightarrow DD\pi$, in the isospin $I = 0$ channel. In line with existing lattice QCD results, the isospin limit is assumed throughout. We consider heavier-than-physical pions, such that the D^* is a $D\pi$ bound state rather than a resonance.

The formalism that we use has been developed in the Relativistic Field Theory (RFT) approach of refs. [30, 31]. The integral equations relevant to the $DD\pi$ system were derived in ref. [22]; here, we give a more detailed presentation, focusing on the aspects relevant to practical implementation. Methods of solution of the RFT integral equations have been developed in refs. [49, 51, 52, 65–67]. In the following, we present the extensions necessary for nondegenerate systems with multiple subchannels, as well as allow for the inclusion of three-particle K matrices.

2.1 $DD\pi$ scattering amplitude and kinematics

The connected $3 \rightarrow 3$ scattering amplitude, \mathcal{M}_3 , depends on eight independent variables. To organize them conveniently, we divide the three particles into a *pair* and a *spectator*, analyzing the process as a quasi-two-body coupled-channel reaction. It is described by the so-called unsymmetrized amplitude², $\mathcal{M}_3^{(ij)}$. Indices i, j label, respectively, the final and initial pair-spectator channels. Both indices are drawn from $\{1, 2\}$: the choice “1” indicates that the D is a spectator and $D\pi$ forms the isospin $I = 1/2$ pair, while “2” means that the π spectates and the pair is DD , which has isospin $I = 1$. Similarly, we denote the mass of the D and π mesons as $m_1 = m_D$ and $m_2 = m_\pi$, respectively. Once $\mathcal{M}_3^{(ij)}$ is known, it can

²For simplicity, we drop the superscript (u, u) used in ref. [22], as we work exclusively with the pair-spectator amplitudes.

be symmetrized with respect to all possible pair-spectator choices to recover the genuine amplitude \mathcal{M}_3 . This procedure is described in Sec. 3.3 of ref. [22].

We consider the reaction in the three-body center-of-mass (c.m.) frame, where the total four-momentum of three particles is $P = (P^0, \mathbf{P}) = (E, \mathbf{0})$. We label the momentum of the incoming and outgoing spectator as \mathbf{k}_j and \mathbf{p}_i , respectively. In the following, to lighten the notation, we will drop the i, j subscripts from the momentum variables as long as it does not lead to ambiguity. It should be kept in mind, however, that the masses of the spectator and pair particles depend upon the choice of indices. All momenta are on-shell, and their magnitudes are denoted $p = |\mathbf{p}|$ and $k = |\mathbf{k}|$. A spectator momentum \mathbf{q} fixes the invariant mass of the corresponding pair to be

$$\sigma_q^{(i)} \equiv \sigma_{q_i} = (E - \omega_{q_i})^2 - q_i^2. \quad (2.1)$$

Here, $\omega_q^{(i)} = \omega_{q_i} = \sqrt{m_i^2 + q_i^2}$, denotes the particle's energy. Again, when no ambiguity is present, we drop indices i, j .

In addition to the total energy and two-body invariant masses, the amplitude depends on five angular variables describing the orientation of the external momenta. Following ref. [67], we choose one of them to be the angle Θ between the incoming and outgoing spectator momenta in the three-body c.m. frame, i.e. $\hat{\mathbf{p}} \cdot \hat{\mathbf{k}} = \cos \Theta$. We specify the next two variables in the c.m. frame of the initial pair, a frame defined by the condition $\mathbf{P}_k^* = \mathbf{P}^* - \mathbf{k}^* = 0$, where we use \star to denote momenta boosted to that frame. The variables are the polar and azimuthal angle of the momentum of one of the particles in the pair,³ $\Omega_k^* = (\vartheta_k^*, \varphi_k^*)$. These are defined in a coordinate system such that the z axis in the pair c.m. frame is aligned along the pair's momentum in the overall c.m. frame, $\hat{\mathbf{z}}_k = -\hat{\mathbf{k}}$. In all these variables, the subscript, here k , indicates the momentum of the corresponding spectator. The dependence on Ω_k^* is decomposed into spherical harmonics, with the angular momentum of the pair denoted s , and its z component denoted λ . The latter is the helicity of the pair, given the choice of z axis described above.⁴ The last two variables are analogous angles for the final-state pair, defined in the $\mathbf{P}_p^* = \mathbf{P}^* - \mathbf{p}^* = 0$ frame. For simplicity, we use the same \star symbol to denote variables in the final and initial pair reference frames, even though they are different. It will always be clear from the context to which frame we refer. The angular variables are $\Omega_p^* = (\vartheta_p^*, \varphi_p^*)$, and the corresponding angular momentum and helicity are denoted s' and λ' . The reader can find further details on the angular variables in Refs. [67, 68] and in App. A.

To summarize, given the pair-spectator division, the amplitude depends on a triplet of energy-like variables, either (p, k, E) , or, equivalently, (σ_p, σ_k, E) , and on five scattering angles, for which we choose Θ , $(\vartheta_p^*, \varphi_p^*)$, and $(\vartheta_k^*, \varphi_k^*)$. Since, in the overall c.m. frame, angular momentum and parity are good quantum numbers, we wish to project the amplitude onto definite J^P . The projected amplitude is obtained in three steps [67–69]. The details

³The chosen particle is denoted the “primary” member of the pair and is taken to be the D in the $D\pi$ pair, following Refs. [22, 40, 42]. For the DD pair, the choice is arbitrary.

⁴Note that all previous papers using the RFT approach, e.g., refs. [22, 30], use the notation ℓ instead of s . Also, the azimuthal component m in these works is defined relative to an unspecified choice of z axis, whereas here we use the helicity λ .

are reviewed in appendix A; here, we provide a summary. First, we project onto the basis of definite spin and helicity of external pairs,

$$\mathcal{M}_{3,s'\lambda';s\lambda}^{(ij)}(p,k;E,\Theta) = \frac{1}{4\pi} \int d\Omega_p^* \int d\Omega_k^* Y_{s'\lambda'}^*(\Omega_p^*) \mathcal{M}_3^{(ij)}(p,\Omega_p^*,k,\Omega_k^*;E,\Theta) Y_{s\lambda}(\Omega_k^*). \quad (2.2)$$

Here $Y_{s'\lambda'}$ are the standard spherical harmonics, and the normalization follows that of ref. [30].⁵ The overall phase of the amplitude on the left-hand side depends on the choice of x and y axes used for the helicity projections. While the choice is arbitrary, a consistent convention must be used throughout, and one such is described in appendix A. The second step projects the amplitude onto definite J and is achieved by,

$$\mathcal{M}_{3,s'\lambda';s\lambda}^{(ij)J}(p,k;E) = \frac{1}{2} \int d\cos\Theta \mathcal{M}_{3,s'\lambda';s\lambda}^{(ij)}(p,k;E,\Theta) d_{\lambda\lambda'}^J(\Theta). \quad (2.3)$$

The final step is to transform from the spin-helicity basis to the LS basis, in which ℓ' and ℓ refer, respectively, to the relative orbital angular momenta between the final and initial spectator and the corresponding pair. This is done using the recoupling coefficients,

$$C_{\ell s\lambda}^J = \sqrt{\frac{2\ell+1}{2J+1}} \langle J, -\lambda | \ell, 0; s, -\lambda \rangle, \quad (2.4)$$

leading to the result,

$$\mathcal{M}_{3,\ell'\ell';\ell s}^{(ij)J}(p,k;E) = \sum_{\lambda'=-s'}^{s'} \sum_{\lambda=-s}^s C_{\ell'\ell's'\lambda'}^J \mathcal{M}_{3,s'\lambda';s\lambda}^{(ij)J}(p,k;E) C_{\ell s\lambda}^J. \quad (2.5)$$

The negative signs appearing in eq. (2.4) are explained in appendix A. In fact, for the channels we consider here, the properties of Clebsch-Gordon coefficients are such that the result holds with these negative signs removed.

Given that the amplitude depends on many variables, we implement a compact notation in which it is treated as a generalized matrix in a multi-dimensional space,

$$\mathcal{M}_{3,\ell'\ell';\ell s}^{(ij)J}(p,k;E) \equiv \mathcal{M}_{3,\ell'\ell';\ell s}^{(ij)}(p,k) = [\mathcal{M}_3]_{ip\ell's';jk\ell s}, \quad (2.6)$$

Moreover, since E and J are both conserved, we keep the dependence on these quantities implicit. We define matrix multiplication via the summation over discrete indices and integration over continuous momenta,

$$[\mathcal{A}\mathcal{B}]_{ip\ell's';jk\ell s} = \sum_{n=1}^2 \sum_{\ell_n''=0}^{\ell_{\max}^{(n)}} \sum_{s_n''=0}^{s_{\max}^{(n)}} \int_0^{q_{\max}^{(n)}} \frac{dq_n q_n^2}{(2\pi)^2 \omega_{q_n}} \mathcal{A}_{\ell'\ell';\ell_n''s_n''}^{(in)}(p,q_n) \mathcal{B}_{\ell_n''s_n'';\ell s}^{(nj)}(q_n,k). \quad (2.7)$$

Here, we keep the intermediate on-shell pair-spectator channel index n explicit in all related variables: the magnitude of the spectator's momentum, q_n , intermediate pair's spin s_n'' , and

⁵The choice of which spherical harmonic is complex-conjugated is opposite from that introduced in ref. [30] and used in all subsequent works in the RFT approach. While this choice is ultimately a convention, we prefer that given here as it is consistent with the standard choice in Quantum Mechanics, namely $\langle \hat{n} | \ell m \rangle = Y_{\ell m}(\hat{n})$.

pair-spectator's orbital angular momentum, ℓ_n'' . The momentum cutoff $q_{\max}^{(n)}$ depends on the intermediate channel n and is determined by the positions of the left-hand singularities in the two-body scattering amplitudes. We specify it below.

In principle, infinitely many (ℓ, s) combinations contribute to the sums in eq. (2.7). In practice, they must be truncated to reduce the equations for \mathcal{M}_3 to a numerically solvable problem. Such a truncation is justified by the fact that amplitudes with higher values of angular momentum are suppressed near the threshold. For the $J^P = 1^+$ tetraquark channel considered here, we neglect spins higher than $s_{\max}^{(1)} = 1$ in the $D\pi$ subchannels. Due to the presence of D^* , we assume dominance of the $D\pi$ p -wave interactions and include the lower s -wave scattering for consistency. The DD channel is considered weakly interacting, and we restrict the spin space even further by including only the s -wave interaction in our description, $s_{\max}^{(2)} = 0$. Finally, we set $\ell_{\max}^{(n)} = 2$. These restrictions lead to the following (ℓ, s) combinations in the $J^P = 1^+$ channel,

$$(\ell_1, s_1) = (1, 0), (0, 1), (2, 1), \quad (\ell_2, s_2) = (1, 0). \quad (2.8)$$

Note that this choice allows for the partial-wave mixing between the LS quantum numbers $(\ell_1, s_1) = (0, 1)$ and $(\ell_1, s_1) = (2, 1)$. To compare our results to those of ref. [9], we also study scattering in the $J^P = 0^-$ partial wave, for which the combinations considered are

$$(\ell_1, s_1) = (0, 0), (1, 1), \quad (\ell_2, s_2) = (0, 0). \quad (2.9)$$

2.2 Three-body integral equations

The pair-spectator amplitude \mathcal{M}_3 is given by a sum of two terms [22, 31, 40],

$$\mathcal{M}_3 = \mathcal{D} + \mathcal{M}_{\text{df},3}. \quad (2.10)$$

The first is called the *ladder* amplitude and is determined solely by the pair two-body amplitude, \mathcal{M}_2 , and by the kernel describing one-particle exchange between the initial and final pair, \mathbf{G} . The second term, the “divergence-free” amplitude, requires the presence of at least one short-range three-body interaction, given by the three-particle K matrix, \mathcal{K}_3 , and involves final and initial two-body rescatterings.⁶ In the following, we recall the expressions for \mathcal{D} and $\mathcal{M}_{\text{df},3}$ using our compact notation.

2.2.1 The ladder equation

The ladder amplitude is given by the on-shell partial-wave-projected integral equation, written here in generalized matrix form,

$$\mathcal{D} = -\mathcal{M}_2 \mathbf{G} \mathcal{M}_2 - \mathcal{M}_2 \mathbf{G} \mathcal{D}. \quad (2.11)$$

To simplify its solution, one typically removes the external two-body amplitudes,

$$\mathcal{D} = \mathcal{M}_2 d \mathcal{M}_2, \quad (2.12)$$

⁶In previous RFT works, the three-particle K matrix has been referred to as $\mathcal{K}_{\text{df},3}$ [22]. Here, for the sake of brevity, we drop the subscript “df”.

defining the “amputated” partial-wave projected ladder amplitude, \mathbf{d} , free of the two-body singularities in the σ_p and σ_k variables. It satisfies

$$\mathbf{d} = -\mathbf{G} - \mathbf{G} \mathcal{M}_2 \mathbf{d}, \quad (2.13)$$

whose formal solution is,

$$\mathbf{d} = -[\mathbf{1} + \mathbf{G} \mathcal{M}_2]^{-1} \mathbf{G}. \quad (2.14)$$

Two-body amplitudes: The ladder equation depends on the partial-wave-projected two-body amplitude \mathcal{M}_2 , fully describing interactions in the $D\pi$ and DD subchannels. In our generalized notation, due to the energy and angular momentum conservation, it is a diagonal matrix,

$$[\mathcal{M}_2]_{ip\ell's';j\ell s} = \eta_i \delta_{ip\ell's';j\ell s} \mathcal{M}_{2,s}^{(i)}(p), \quad (2.15)$$

where the generalized Dirac delta function is,

$$\delta_{ip\ell's';j\ell s} = \tilde{\delta}(p - k) \delta_{ij} \delta_{\ell'\ell} \delta_{s's}, \quad (2.16)$$

with the momentum part,

$$\tilde{\delta}(p - k) = (2\pi)^2 (\omega_p/p^2) \delta(p - k). \quad (2.17)$$

The symmetry factors are $\eta_1 = 1$ and $\eta_2 = 1/2$, corresponding to the fact that the pair is composed of identical particles if the spectator is a pion. The derivation of this projected form of \mathcal{M}_2 is described in appendix A.4. We represent the diagonal elements of \mathcal{M}_2 in K -matrix form,

$$[\mathcal{M}_{2,s}^{(n)}(p)]^{-1} = [\mathcal{K}_{2,s}^{(n)}(\sigma_p)]^{-1} - i\rho^{(n)}(\sigma_p). \quad (2.18)$$

Here the two-body phase space is,

$$\rho^{(n)}(\sigma_p) = \frac{\eta_n q_p^*}{8\pi \sqrt{\sigma_p}}. \quad (2.19)$$

where,

$$q_{p_n}^* = \frac{\lambda^{1/2}(\sigma_p^{(n)}, m_{n_1}^2, m_{n_2}^2)}{2\sqrt{\sigma_p^{(n)}}}, \quad (2.20)$$

and $\lambda(x, y, z)$ is the Källen triangle function. Equation (2.20) gives the magnitude of the relative momentum (in the pair’s rest frame) between particles in the pair corresponding to the spectator of momentum p_n (here, we explicitly indicate the spectator’s channel for clarity.) Note that it is different from the intermediate spectator integration momentum of eq. (2.7). The indices n_1, n_2 label the two particles in the pair corresponding to spectator n , which, in the conventions of ref. [22], are $\{n_1, n_2\} = \{D, \pi\}$ for $n = 1$, and $\{n_1, n_2\} = \{D, D\}$ for $n = 2$. We orient the cuts of \mathcal{M}_2 to run to complex infinity, i.e., we write,

$$\lambda^{1/2}(\sigma_p^{(n)}, m_{n_1}^2, m_{n_2}^2) = i\sqrt{\sigma_p^{(n)} - (m_{n_1} - m_{n_2})^2} \sqrt{(m_{n_1} + m_{n_2})^2 - \sigma_p^{(n)}}, \quad (2.21)$$

assuming the canonical definition of the complex square root. The branch point at $\sigma_{\text{thr}}^{(n)} = (m_{n_1} + m_{n_2})^2$ is required by elastic two-body unitarity and corresponds to the two-body thresholds, $\sigma_{\text{thr}}^{(1)} = (m_D + m_\pi)^2$ for $D\pi$ and $\sigma_{\text{thr}}^{(2)} = 4m_D^2$ for DD .

Dynamical information about two-body scattering is contained in the two-body K matrix, \mathcal{K}_2 . We model these interactions using the effective-range expansion (ERE) [70, 71], truncating to two terms,

$$[\mathcal{K}_{2,s}^{(n)}(\sigma_p)]^{-1} = \frac{\eta_n}{8\pi\sqrt{\sigma_p}(q_p^*)^{2s}} \left(-\frac{1}{a_s^{(n)}} + \frac{1}{2} r_s^{(n)} (q_p^*)^2 \right). \quad (2.22)$$

In the following, we choose values of the parameters $a_s^{(n)}$ (two-body scattering lengths), and $r_s^{(n)}$ (two-body effective ranges), such that there are no poles on the physical sheet in s -wave $D\pi$ or DD scattering. For p -wave $D\pi$ scattering, however, we choose values such that a D^* bound-state pole develops in $\mathcal{M}_{2,1}^{(1)}$. In general, a pole occurs when the relative momentum takes the purely imaginary value $q_p^* = q_0 = i|q_0|$ satisfying,

$$-\frac{1}{a_s^{(n)}} + \frac{1}{2} r_s^{(n)} q_0^2 - i q_0^{2s+1} = 0. \quad (2.23)$$

Furthermore, the left-hand side must be a decreasing function of q_p^{*2} at $q_p = q_0$ for the pole to correspond to a physical state; see chapter 12 in ref. [72]. Explicitly, we tune the ERE parameters such that,

$$q_0 = \frac{\lambda^{1/2}(m_{D^*}^2, m_D^2, m_\pi^2)}{2m_{D^*}}, \quad (2.24)$$

or,

$$m_{D^*} = \sqrt{m_\pi^2 + q_0^2} + \sqrt{m_D^2 + q_0^2}. \quad (2.25)$$

We discuss this tuning in more detail in section 4.

To complete the discussion of the two-body amplitudes, we briefly comment on their other singularities. As can be seen from eq. (2.21), our parametrization of $\mathcal{M}_{2,s}^{(n)}$ has an (unphysical) pseudo-threshold left-hand branch point at $\sigma_{\text{psth}}^{(n)}$, where $\sigma_{\text{psth}}^{(1)} = (m_D - m_\pi)^2$ and $\sigma_{\text{psth}}^{(2)} = 0$. Moreover, the partial-wave projected amplitudes should include two-pion exchange left-hand cuts at $\sigma_{2\pi,\text{lhc}}^{(1)} = (m_D^2 - m_\pi^2)$ and $\sigma_{2\pi,\text{lhc}}^{(2)} = 4(m_D^2 - m_\pi^2)$ that are absent from our model. All these singularities, however, lie outside of the allowed region for our choice of cutoff momentum $q_{\text{max}}^{(n)}$, as will be discussed below. Another issue concerns the fact that, as is well known, the ERE parametrization can produce unphysical poles for a wide range of scattering parameters, some of which can occur at complex energies on the first Riemann sheet of the two-body amplitude [73, 74]. When choosing values of the ERE parameters, we ensure that such poles are distant from the $D\pi$ and DD thresholds, so that they do not significantly affect the physics of the two-body subchannels.

The OPE amplitude: The second important quantity in the ladder equation is the kinematic one-particle exchange amplitude. In our generalized notation, it is, [22, 40]

$$[\mathbf{G}]_{ip\ell's';jk\ell s} = c_{ij} (-1)^{s'd_{ij}} G_{\ell's';\ell s}^{(ij)J}(p, k) (-1)^{sd_{ji}}, \quad (2.26)$$

where the double-index symmetry factor, c_{ij} , takes the values $c_{11} = 1, c_{12} = c_{21} = -\sqrt{2}$, and $c_{22} = 0$, while the additional phases are controlled by d_{ij} , which vanishes except for $d_{12} = 1$. Note that the d on the right-hand side of $G^{(ij)}$ has indices reversed compared to that on the left-hand side. The amplitude vanishes for the $(ij) = (22)$ channel since it is impossible to exchange a particle between two DD pairs. In the spin-helicity basis, the one-particle exchange amplitude has the form,⁷

$$G_{s'\lambda';s\lambda}^{(ij)}(p, \Omega_p^*; k, \Omega_k^*; E, \Theta) = Y_{s'\lambda'}^*(\hat{\mathbf{k}}_p^*) \left(\frac{k_p^*}{q_p^*} \right)^{s'} \frac{4\pi H_{ij}(p, k)}{b_{pk}^2 - m_{ij}^2 + i\epsilon} \left(\frac{p_k^*}{q_k^*} \right)^s Y_{s\lambda}(\hat{\mathbf{p}}_k^*), \quad (2.27)$$

where $b_{pk}^2 = (E - \omega_p - \omega_k)^2 - (\mathbf{p} + \mathbf{k})^2$ and m_{ij} is a mass of exchanged particle, $m_{11} = m_\pi$, $m_{12} = m_{21} = m_D$. The vector \mathbf{k}_p^* (\mathbf{p}_k^*) denotes the momentum of the initial (final) spectator in the final (initial) pair's rest frame.

The function $H_{ij}(p, k)$ is a smooth cutoff function that enters in the derivation of the three-body formalism in the RFT approach [30, 31, 40], and takes the separated form $H_{ij}(p, k) = H_i(p)H_j(k)$. It always equals unity at the position of the pole in eq. (2.27), and smoothly drops to zero as p, k increase. There is a family of allowed choices of $H(p)$ and the specific choice we use is⁸,

$$H_i(p) = J(f_i(\sigma_p)) \quad \text{and} \quad f_i(\sigma_p) = (1 + \epsilon_H) \frac{\sigma_p - \sigma_{\min}^{(i)}}{\sigma_{\text{thr}}^{(i)} - \sigma_{\min}^{(i)}}, \quad (2.28)$$

with $\sigma_{\min}^{(1)} = \sigma_{2\pi, \text{lhc}}^{(1)}$ and $\sigma_{\min}^{(2)} = \sigma_{2\pi, \text{lhc}}^{(2)}$. The J function is,

$$J(x) = \begin{cases} 0, & x \leq 0, \\ \exp\left(-\frac{1}{x} \exp\left[-\frac{1}{1-x}\right]\right), & 0 < x \leq 1, \\ 1, & 1 < x. \end{cases} \quad (2.29)$$

This form implies that the integration in eq. (2.7) is performed up to the energy-dependent momentum cutoff,

$$q_{\max}^{(n)} = \frac{\lambda^{1/2}(E^2, \sigma_{\min}^{(n)}, m_D^2)}{2E}. \quad (2.30)$$

⁷We remind the reader that we are using a convention for the complex conjugation of spherical harmonics that is opposite from that in the previous RFT literature. We also note that G is usually presented using spherical harmonics corresponding to a space-fixed z axis. The transformation to the helicity basis used here (defined relative to the pair's momentum) is unitary and can be consistently applied throughout the integral equations.

⁸The cutoff function in eq. (2.27), while equaling unity at the pole, serves as an effective form factor for the $D^*D\pi$ vertices that drops below unity when the pair invariant mass equals $m_{D^*}^2$.

As noted earlier, our choices of $\sigma_{\min}^{(i)}$ ensure that the πD and DD amplitudes are evaluated only above the left-hand cuts arising from a two-pion exchange.

The parameter ϵ_H entering in $f_i(\sigma_p)$ is a positive constant introduced to ensure that the cutoff function reaches unity below the pair threshold, thus avoiding a potential source of power-law finite-volume effects [38]. In practice, for our choice of J , such effects are highly suppressed even if $\epsilon_H = 0$, and we choose this value.

To convert $G^{(ij)}$ in eq. (2.27) to the JLS basis appearing in eq. (2.26), we must perform the integrations and basis transformations applied to \mathcal{M}_3 in eqs. (2.2) and (2.5) above. This non-trivial task was accomplished in ref. [67] at a high level of generality. In appendix A, we describe the relevant manipulations in the specific case of interest, and in appendix B we list all the relevant matrix elements for $J^P = 1^+$ and 0^- .

2.2.2 Three-body forces

In the previous sections, we considered the ladder amplitude alone. Here, we describe the second term of eq. (2.10), the matrix $\mathcal{M}_{\text{df},3}$, which parametrizes the effect of short-range interactions. It is given by [22, 31],

$$\mathcal{M}_{\text{df},3} = \mathcal{L} \mathcal{T} \mathcal{R}, \quad (2.31)$$

where the “endcap” matrices \mathcal{L} , \mathcal{R} describe all rescattering processes within and between external pairs that do not involve short-range three-particle interactions. After projection to the JLS basis, they are given by

$$[\mathcal{L}]_{ip\ell's';jkl s} = \left(\frac{1}{3} - \tilde{\rho}_s^{(i)}(k) \mathcal{M}_{2,s}^{(i)}(k) \right) \delta_{ip\ell's';jkl s} - \mathcal{D}_{\ell's';\ell s}^{(ij)}(p, k) \tilde{\rho}_s^{(j)}(k), \quad (2.32)$$

$$[\mathcal{R}]_{ip\ell's';jkl s} = \left(\frac{1}{3} - \tilde{\rho}_s^{(i)}(k) \mathcal{M}_{2,s}^{(i)}(k) \right) \delta_{ip\ell's';jkl s} - \tilde{\rho}_{s'}^{(i)}(p) \mathcal{D}_{\ell's';\ell s}^{(ij)}(p, k), \quad (2.33)$$

and contain the modified two-body phase space,

$$\tilde{\rho}_s^{(i)}(\sigma_p) = H_i(p) \left(-i\rho^{(i)}(\sigma_p) + \frac{\eta_i}{8\pi\sqrt{\sigma_p}} \frac{c_{\text{PV},s}^{(i)}}{(q_p^*)^{2s}} \right). \quad (2.34)$$

Comparing this to the phase space factor in eqs. (2.18) and (2.19), we note the presence of the cutoff function as well as the addition of the so-called I_{PV} term (proportional to the coefficients $c_{\text{PV},s}^{(i)}$) introduced in ref. [75]. The latter is needed in the derivation of the finite-volume quantization condition (to be discussed in section 3) in the presence of bound-state poles and resonances in two-particle subchannels. Since we must use the same definition of \mathcal{K}_3 in the finite-volume formalism and the integral equations, we need to include the I_{PV} term here. In our case, non-zero $c_{\text{PV},s}^{(i)}$ are needed due to the presence of D^* and D_0^* poles in the $D\pi$ p - and s -wave amplitudes, respectively.

The \mathcal{T} matrix is given by the integral equation,

$$\mathcal{T} = \mathcal{K}_3 - \mathcal{K}_3 \tilde{\rho} \mathcal{L} \mathcal{T}, \quad (2.35)$$

where we promote the modified phase space into a matrix,

$$[\tilde{\rho}]_{ip\ell's';jkl s} = \delta_{ip\ell's';jkl s} \tilde{\rho}_s^{(i)}(k). \quad (2.36)$$

The quantity \mathcal{K}_3 is the partial-wave projection of the symmetrized three-body K matrix,

$$[\mathcal{K}_3]_{ip\ell's';jkl s} = \mathcal{K}_{3,\ell's';\ell s}^{(ij)J}(p, k; E) \equiv \mathcal{K}_{3,\ell's';\ell s}^{(ij)}(p, k), \quad (2.37)$$

which is a regularization-scheme-dependent object parameterizing short-range three-body interactions. It is closely related to the three-body element of the genuine on-shell multi-particle K matrix [50] and allows for a convenient description of three-body forces in the RFT formalism. For the physical three-body kinematics, it is a real function of momenta that satisfies the same symmetries as the full $3 \rightarrow 3$ amplitude, including Lorentz invariance. In particular, unlike the pair-spectator amplitudes $\mathcal{M}_3^{(ij)}$ are different objects for different choices of i, j , the $\mathcal{K}_3^{(ij)}$ all correspond to the same underlying amplitude, although expressed in a different coordinate system. This is the meaning of a “symmetrized” K matrix.

In the following, we assume a form of \mathcal{K}_3 in which dependence on the initial and final channel variables separates between “left” and “right” functions,

$$\mathcal{K}_{3,\ell's';\ell s}^{(ij)}(p, k) = \sum_{a=1}^{a_{\max}} \mathcal{K}_{L,\ell's'}^{a,(i)}(p) \mathcal{K}_{R,\ell s}^{a,(j)}(k). \quad (2.38)$$

Although not the most general parametrization of \mathcal{K}_3 , for large enough a_{\max} , and appropriately chosen functions $\mathcal{K}_L^a, \mathcal{K}_R^a$, it is capable of describing many practical models of interest, including those with energy- and momentum-dependent contact interactions and explicit resonance poles. Models satisfying this property have been suggested and successfully used for the three-body couplings in recent studies, see for instance [19, 46, 54, 76–78]. In our generalized matrix notation, the separable ansatz becomes a sum of the outer products of vectors,

$$\mathcal{K}_3 = \sum_a \vec{\mathcal{K}}_L^a \otimes \vec{\mathcal{K}}_R^a. \quad (2.39)$$

Using this form, the solution of the integral equation for \mathcal{T} is reduced to the problem of computing a set of double integrals. This can be seen by employing the form (2.39) in eq. (2.35),

$$\mathcal{T} = \mathcal{K}_3 - \sum_a \vec{\mathcal{K}}_L^a \otimes \vec{\alpha}^a. \quad (2.40)$$

where,

$$\vec{\alpha}^a = \vec{\mathcal{K}}_R^a \tilde{\rho} \mathcal{L} \mathcal{T}. \quad (2.41)$$

By multiplying eq. (2.40) by $\vec{\mathcal{K}}_R^b \tilde{\rho} \mathcal{L}$ from the left, one arrives at an algebraic equation,

$$\vec{\alpha}^b = \vec{\beta}^b - \sum_a \mathcal{I}_{ba} \vec{\alpha}^a, \quad (2.42)$$

where we introduced,

$$\mathcal{I}_{ba} = \vec{\mathcal{K}}_R^b \tilde{\rho} \mathcal{L} \vec{\mathcal{K}}_L^a, \quad (2.43)$$

$$\vec{\beta}^a = \vec{\mathcal{K}}_R^b \tilde{\rho} \mathcal{L} \mathcal{K}_3 = \sum_b \mathcal{I}_{ab} \vec{\mathcal{K}}_R^b, \quad (2.44)$$

and $b \in \{1, \dots, a_{\max}\}$. Note that in the definition of \mathcal{I} the “left” function $\vec{\mathcal{K}}_L$ is on the right side of the expression while the “right” vector $\vec{\mathcal{K}}_L$ is on the left side. In the generalized matrix notation, \mathcal{I} is a scalar, i.e., it carries no dependence on external channel variables, which allowed us to drop the \otimes sign in eq. (2.42). In consequence, the solution to eq. (2.42) is obtained simply by inverting the $a_{\max} \times a_{\max}$ matrix,

$$\vec{\alpha}^a = \sum_b (\mathbf{1} + \mathcal{I})_{ab}^{-1} \vec{\beta}^b. \quad (2.45)$$

Finally, using the above formula in eq. (2.40) yields the solution for the \mathcal{T} amplitude,

$$\mathcal{T} = \sum_{a,b} \vec{\mathcal{K}}_L^a \otimes (\mathbf{1} + \mathcal{I})_{ab}^{-1} \vec{\mathcal{K}}_R^b. \quad (2.46)$$

For completeness, the $\mathcal{M}_{3,\text{df}}$ amplitude is given by the expression with the endcap matrices restored,

$$\mathcal{M}_{3,\text{df}} = \sum_{a,b} \vec{L}^a \otimes (\mathbf{1} + \mathcal{I})_{ab}^{-1} \vec{R}^b, \quad (2.47)$$

where we introduced the “left” and “right” generalized endcap vectors,

$$\vec{L}^a = \mathcal{L} \vec{\mathcal{K}}_L^a, \quad \vec{R}^a = \vec{\mathcal{K}}_R^a \mathcal{R}. \quad (2.48)$$

To conclude, the task of solving eq. (2.35) is reduced to an algebraic problem of inverting a small matrix entering eq. (2.47). In cases when the two- and three-body parameters can be fixed independently, the solution of the ladder integral equation, \mathcal{D} , is obtained just once, tabulated, and reused in eq. (2.47) for any model of \mathcal{K}_3 satisfying the property (2.39).

Threshold expansion: More concretely, in this work, we implement a model of the three-body K matrix based on the threshold expansion of ref. [42]. Working to given order in powers of an expansion about the three-particle threshold, it is the most general low-energy form of any smooth \mathcal{K}_3 constrained by Lorentz invariance, PT invariance, and the symmetry under the interchange of the D mesons separately in the initial and final three-body state. Through linear order, the result is

$$\mathcal{K}_3(\{\mathbf{p}\}, \{\mathbf{k}\}) = \mathcal{K}_3^{\text{iso},0} + \mathcal{K}_3^{\text{iso},1} \Delta + \mathcal{K}_3^B \Delta_2^S + \mathcal{K}_3^E \tilde{t}_{22}. \quad (2.49)$$

where $\{\mathbf{p}\}$ ($\{\mathbf{k}\}$) indicates the set of final (initial) state momenta, $\mathcal{K}_3^{\text{iso},0}$, $\mathcal{K}_3^{\text{iso},1}$, \mathcal{K}_3^B , \mathcal{K}_3^E are real coefficients, and

$$\begin{aligned} \Delta &= \frac{E^2 - M^2}{M^2}, \quad \Delta_2^S = \Delta_2 + \Delta'_2, \quad \tilde{t}_{22} = \frac{(k_\pi - p_\pi)^2}{M^2}, \\ \Delta_2 &= \frac{\sigma_{k,DD} - 4m_D^2}{M^2}, \quad \Delta'_2 = \frac{\sigma_{p,DD} - 4m_D^2}{M^2}, \end{aligned} \quad (2.50)$$

Here, k_π, p_π are energy-momentum four-vectors of initial and final pion, respectively, while $\sigma_{k,DD}$, and $\sigma_{p,DD}$ are the two-body invariant masses squared of the initial and final DD subsystems. The $DD\pi$ threshold energy, $M = 2m_D + m_\pi$, is introduced to make all the above kinematic variables dimensionless.

We note that, although, in the RFT approach, \mathcal{K}_3 is guaranteed to be a smooth function within the kinematic regime of the validity of the formalism, the low-order polynomial form of Eq. (2.49) will become increasingly inaccurate as one approaches the boundaries of this regime. In particular, a breakdown is expected as one approaches the left-hand singularity associated with the two-particle exchange in D^*D system. In the following, we stay away from these boundary regions.

To implement this form for \mathcal{K}_3 in the integral equations described above, we have to partial-wave project it onto a definite J in the LS basis and decompose it into the separable form. We describe these steps in appendix A and provide an explicit expression for $J^P = 1^+$ and 0^- in appendix C. We find that all terms of eq. (2.49) contribute to $J^P = 0^-$, while only the \mathcal{K}_3^E term contributes to the $J^P = 1^+$ amplitude. Additional contributions from higher-order terms will be present but are not considered here. The only additional subtlety is the need to include symmetry factors in $\mathcal{K}_3^{(ij)}$. These are given by multiplying the elements obtained in appendix C by e_{ij} , where $e_{11} = 1$, $e_{12} = e_{21} = -1/\sqrt{2}$ and $e_{22} = 1/2$. Equivalently, the results for the factorized quantities $\mathcal{K}_L^{a,(i)}$ and $\mathcal{K}_R^{a,(i)}$ should both be multiplied by e_i , where $e_1 = 1$ and $e_2 = -1/\sqrt{2}$.

2.2.3 Numerical solution

The solutions to integral equations for \mathcal{M}_3 , eqs. (2.14) and (2.47), can be obtained numerically by discretizing the momentum variables and rewriting the equations in a purely algebraic form. The discrete solutions approach the continuum one for increasingly dense meshes, and the asymptotic value is extracted using the techniques described in Refs. [49, 51].

To improve the stability and convergence of the solution, it is useful to implement complex deformed contours for numerical integration. Note that, in principle, one is free to independently deform integration intervals in pair-spectator channels $n = 1$ and $n = 2$ in eq. (2.7). The shape of a contour is chosen such that it avoids all singularities of the integration kernel, $\mathbf{G}\mathcal{M}_2$. These occur in \mathbf{G} in the form of OPE cuts and in \mathcal{M}_2 as unitarity and unphysical cuts and the D^* pole. Moreover, deformed contours must avoid so-called domains of non-analyticity generated by the motion of these momentum- and energy-dependent singularities in the kernel [51].

In the context of T_{cc}^+ , the energies of interest are real and near the DD^* threshold, $E_{DD^*} = m_D + m_{D^*}$ since this is where the virtual-state pole is expected to appear. However, for energies that satisfy the following condition [51],

$$E > \frac{1}{2m_D} \left(m_D^2 - m_\pi^2 + m_{D^*}^2 + \sqrt{4m_D^2 + \lambda(m_D^2, m_\pi^2, m_{D^*}^2)} \right), \quad (2.51)$$

only the D^* pole causes a relevant obstruction in the numerical solution. The above constraint is caused by the development of the circular cut in the integration kernel, which

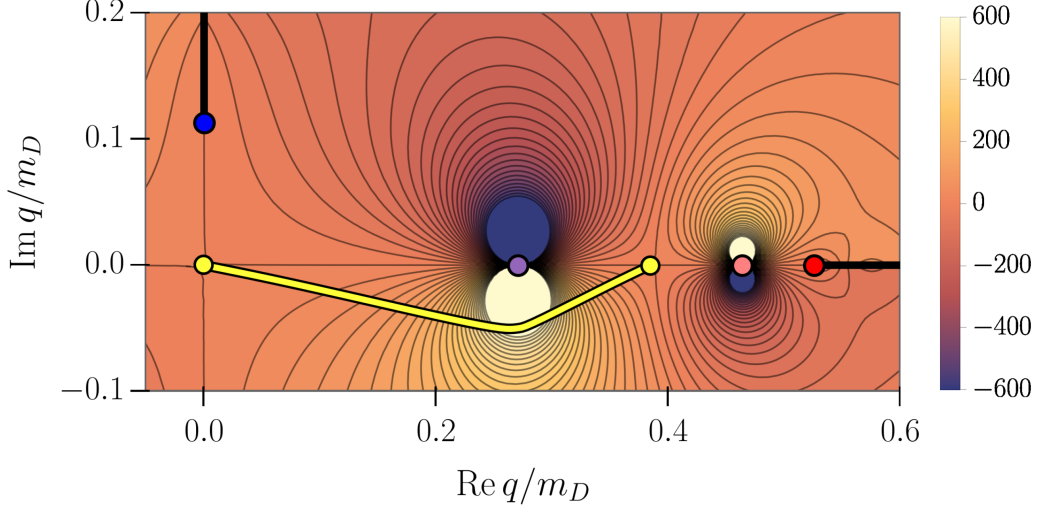


Figure 1: Imaginary part of $\mathcal{M}_{2,1}^{(1)}(q)$ in the complex q momentum plane for $E/m_D = 2.133$, $\kappa = 0.1453$, $a_1^{(1)}m_D^3 = -7.9^3$, and $r_1^{(1)} = 0$. The amplitude contributes singularities to the integration kernel $\mathbf{G}\mathcal{M}_2$ of the ladder equation in the intermediate channel $n = 1$. Branch cuts are shown as black lines and singularities as colored points. The threshold branch point is shown in blue, the pseudo-threshold in red, the D^* bound-state pole in purple, and the unphysical pole in pink. The deformed integration contour is shown in yellow. Note that the upper endpoint of the integration contour is placed below the unphysical singularities, as discussed in the text.

requires more sophisticated methods as discussed in ref. [51]. We thus constrain our solutions to higher energies and deform the integration contour in the intermediate $D\pi$ p -wave channel, $n = 1$, $s_n = 1$, such that the D^* pole is safely avoided, as shown in figure 1. For the s -wave channels, both with $n = 1$ and $n = 2$, we use the straight, purely real contour.

Contour deformation allows one to probe the integration kernel away from the D^* pole position, making the integrated functions smooth and slowly varying. In consequence, a good numerical convergence can be achieved by using Gauss-Legendre quadratures with meshes of size $N = 50$ to 100.

2.3 Connecting $DD\pi$ and DD^* scattering amplitudes

In the vicinity of the D^* pole, the $D\pi$ p -wave scattering amplitude, $\mathcal{M}_{2,1}^{(1)}$ is,

$$\mathcal{M}_{2,1}^{(1)}(q) \simeq \frac{\zeta^2}{\sigma_q - m_{D^*}^2}, \quad (2.52)$$

where m_{D^*} is the D^* mass and ζ^2 is the residue. As discussed above, for a p -wave bound state, the residue is positive, and thus ζ is real and can be chosen positive. This pole appears as a singularity of the $DD\pi$ amplitude through its dependence on the two-body scattering in external states. The LSZ reduction formula for bound states [79–81] implies that continuation of the $D(D\pi) \rightarrow D(D\pi)$ pair-spectator scattering amplitude to external invariant masses $\sigma_p = \sigma_k = m_{D^*}^2$ allows one to extract the particle-bound-state amplitude

from the solution of the three-body integral equations. We apply this reasoning to the $i = j = 1$, $s' = s = 1$ matrix elements [49, 53],

$$\lim_{\sigma_p, \sigma_k \rightarrow m_{D^*}^2} \left(\frac{\sigma_p - m_{D^*}^2}{\zeta} \right) \mathcal{M}_{3, \ell'1, \ell1}^{(11)}(p, k; E) \left(\frac{\sigma_k - m_{D^*}^2}{\zeta} \right) = -[\mathcal{M}_{DD^*}(E)]_{\ell'1, \ell1}^J, \quad (2.53)$$

to obtain the partial-wave projected DD^* amplitude, $\mathcal{M}_{DD^*}(E)$.

Since D^* has a non-zero spin, we employ a generalized K matrix parametrization of the DD^* amplitude,

$$[\mathcal{M}_2^{-1}]_{\ell's', \ell s}^J = [\mathcal{K}_2^{-1}]_{\ell's', \ell s}^J - i\rho \delta_{\ell's', \ell s}, \quad (2.54)$$

where $\rho = q_b/(8\pi E)$ is the two-body phase space and $q_b = \lambda^{1/2}(E^2, m_D^2, m_{D^*}^2)/2E$. Here, the two-body K matrix, \mathcal{K}_2 , is diagonal in J , but the orbital angular momenta and spins are not conserved individually. However, since parity is conserved, even and odd values of ℓ do not mix in \mathcal{K}_2 .

If the value of J^P allows for only a single LS combination, one may use one phase shift to describe the low-energy scattering,

$$(8\pi E) q_b^\ell [\mathcal{K}_2^{-1}]_{\ell s, \ell s}^J q_b^\ell = q_b^{2\ell+1} \cot(\delta_J). \quad (2.55)$$

Here we have added the threshold factors q_b^ℓ such that the quantities are finite as $q_b \rightarrow 0$. By contrast, if several LS channels mix, more complicated forms are required, such as the Blatt-Biedenharn parametrization [82]. This is the case of $J^P = 1^+ DD^*$ scattering, where transitions between $(\ell, s) = (0, 1)$ and $(\ell, s) = (2, 1)$ are possible. In this parametrization, the $[\mathcal{K}_2]_{\ell's'=1, \ell s=1}^{J^P=1^+} \equiv [\mathcal{K}_{DD^*}]_{\ell', \ell}$ matrix is described by three real energy-dependent angles: two phase shifts, $\delta_\alpha, \delta_\beta$, and a mixing angle ϵ ,

$$(8\pi E) [\mathcal{K}_{DD^*}^{-1}] = \begin{pmatrix} \cos(\epsilon) & -\sin(\epsilon) \\ \sin(\epsilon) & \cos(\epsilon) \end{pmatrix} \begin{pmatrix} q_b \cot(\delta_\alpha) & 0 \\ 0 & q_b \cot(\delta_\beta) \end{pmatrix} \begin{pmatrix} \cos(\epsilon) & \sin(\epsilon) \\ -\sin(\epsilon) & \cos(\epsilon) \end{pmatrix}. \quad (2.56)$$

In practice, it is useful to rewrite this in terms of quantities that remain finite as $q_b \rightarrow 0$. Introducing a threshold-factor matrix Q such that $[Q]_{\ell'\ell} = \delta_{\ell'\ell} q_b^\ell$, the expression eq. (2.56) can be written in terms of finite quantities as

$$(8\pi E)[Q] [\mathcal{K}_{DD^*}^{-1}] [Q] = \begin{pmatrix} \cos(\epsilon) & -\frac{1}{q_b^2} \sin(\epsilon) \\ q_b^2 \sin(\epsilon) & \cos(\epsilon) \end{pmatrix} \begin{pmatrix} q_b \cot(\delta_\alpha) & 0 \\ 0 & q_b^5 \cot(\delta_\beta) \end{pmatrix} \begin{pmatrix} \cos(\epsilon) & q_b^2 \sin(\epsilon) \\ -\frac{1}{q_b^2} \sin(\epsilon) & \cos(\epsilon) \end{pmatrix}. \quad (2.57)$$

Note that, below the left-hand branch point at energy E_2^{lhc} (defined below), the scattering phase shifts and the mixing angle in general acquire non-zero imaginary parts.

The DD^* amplitude has several important singularities on the real energy axis. The threshold right-hand branch cut occurs at the energy E_{DD^*} . If the T_{cc}^+ is a bound state, then there will be a pole below the threshold on the physical Riemann sheet. It can be computed through the formula,

$$[(\mathcal{M}_{DD^*})^{-1}]_{\ell', \ell} = [\mathcal{K}_{DD^*}^{-1}]_{\ell \ell} - i\rho \delta_{\ell' \ell}. \quad (2.58)$$

We note that the orthogonal transformation that diagonalizes $\mathcal{K}_{DD^*}^{-1}$ (see eq. (2.56)) also diagonalizes the phase-space term, and thus \mathcal{M}_{DD^*} . It follows that the bound-state pole condition takes a form analogous to eq. (2.23) separately for both $\cot \delta_\alpha$ and $\cot \delta_\beta$. If the T_{cc}^+ is a virtual state, the pole appears on the real axis of the second Riemann sheet, and can be computed via,

$$\left[(\mathcal{M}_{DD^*}^{\text{II}})^{-1}\right]_{\ell',\ell} = \left[\mathcal{K}_{DD^*}^{-1}\right]_{\ell\ell} + i\rho \delta_{\ell'\ell}. \quad (2.59)$$

It is also possible that the pole moves into the complex plane on the second sheet, as discussed below.

Finally, the two-body K matrix has a left-hand branch point below the threshold due to the virtual π exchange between the interacting mesons. In our LSZ-reduction-based approach this singularity is inherited from the $J^P = 1^+$ OPE amplitude $G_{\ell'1,\ell1}^{(11)}(p,k)$ continued to the momentum $p = k = q_b$. The cut is placed between branch points at

$$E_1^{\text{lh}} = \frac{m_D^2 - m_{D^*}^2}{m_\pi}, \quad E_2^{\text{lh}} = \sqrt{2(m_D^2 + m_{D^*}^2) - m_\pi^2}. \quad (2.60)$$

In general, scattering phase shifts and the mixing angle are complex for energies between these two values.

3 Finite-volume formalism

We aim to demonstrate how the formalism from ref. [22] maps lattice QCD results for DD^* and $DD\pi$ energy levels to conclusions about the T_{cc}^+ . Here, we focus on the first step: using quantization conditions to constrain the K matrices from the lattice spectrum, which in a typical application would be then used as input for the integral equations discussed earlier.

Specifically, we summarize the two quantization conditions that we use in this work: first the standard Lüscher QC2 for D^*D systems, and then the QC3 for $DD\pi$. We emphasize that our main focus in this paper is to demonstrate the applicability of the QC3 approach, while we use the QC2 to show where and how badly it breaks down near the left-hand cut. We also note, as mentioned already in the introduction, that there are versions or extensions of the QC2 that are able to solve the left-hand cut problem [26, 27, 95]. While it would be interesting to compare the results of the QC3 to those from these alternate QC2s, this is beyond the scope of the present work.

We also note that the QC2 and QC3 are valid up to terms that are exponentially suppressed in the size of the spatial box (here taken to be cubic of length L). Dropped terms are generically suppressed by $O(e^{-m_\pi L})$. In the DD^* case, the suppression factor is determined by the binding momentum of the D^* .

3.1 QC2 for DD^* scattering

We consider heavier than physical pion masses such that the D^* meson is stable, i.e. a $D\pi$ bound state with binding momentum q_0 , defined via $m_{D^*} = \sqrt{m_D^2 - |q_0|^2} + \sqrt{m_\pi^2 - |q_0|^2}$. Thus, the mass of the D^* in finite volume receives corrections that are proportional to $\exp(-|q_0|L)$ [83]. For near-physical pion masses, $|q_0| \lesssim m_\pi$, and so these corrections are

the dominant terms that are dropped in the DD^* finite-volume formalism. Thus, up to these exponentially-suppressed effects, the DD^* spectrum can be described by the two-body finite-volume formalism of ref. [84] extended to include particles with spin [85]. The range of applicability of this method is given by,

$$E_2^{\text{lh}} < E^* < \min[2m_D + m_\pi, 2m_{D^*}], \quad (3.1)$$

where $E^* = \sqrt{E^2 - \mathbf{P}^2}$ is the c.m. frame energy, with \mathbf{P} the total momentum in the finite-volume frame. The upper bound is set by the first inelastic threshold, either $DD\pi$ or D^*D^* , depending on the pion mass.⁹ The lower bound is determined by the location of the one-pion exchange left-hand cut. For energies $E \lesssim E_2^{\text{lh}}$, the non-analytic behavior of the two-meson Bethe-Salpeter kernel invalidates the derivation of the formalism, as explained in detail in ref. [26].

In the presence of spin, the QC2 can be written as,

$$\det_{Jm_J\ell} [\hat{\mathcal{K}}_2^{-1}(E, \mathbf{P}) + \hat{U} \cdot \hat{F}_2(E, \mathbf{P}, L) \cdot \hat{U}^\dagger] = 0. \quad (3.2)$$

The hats indicate that the quantities are matrices in the space corresponding to the combination of orbital angular momentum ℓ with the spin, $s = 1$, of the D^* , to give total angular momentum J , and azimuthal component m_J . This space can be spanned either by the $\{Jm_J\ell\}$ basis (in which \mathcal{K}_2 is most naturally expressed) or the $\{\ell m m_s\}$ basis (most natural for F_2). The unitary matrix \hat{U} transforms between these bases, and is given by

$$[\hat{U}]_{Jm_J\ell; \ell m m_s} = \langle J, m_J | \ell, m; s = 1, m_s \rangle. \quad (3.3)$$

In practice, one must truncate the QC2 by keeping partial waves $J < J_{\text{max}}$, such that all matrices have finite dimensionality. For the T_{cc}^+ case, we set $J_{\text{max}} = 2$, which means keeping $J^P = 0^-, 1^+$ and 1^- .

We now define the objects in the QC2. $\hat{\mathcal{K}}_2$ is the DD^* K matrix, whose form has been discussed above; see in particular eq. (2.54) and subsequent discussion. The matrix \hat{F}_2 is a known kinematic function, most naturally expressed in the $\{\ell m m_s\}$ basis, and takes the form,¹⁰

$$[\hat{F}_2]_{\ell' m' m'_s; \ell m m_s} = \delta_{m'_s m_s} \left[\frac{1}{L^3} \sum_{\mathbf{a}}^{\text{UV}} -\text{p.v.} \int \frac{d^3 a}{(2\pi)^3} \right] \frac{\mathcal{Y}_{\ell' m'}(\mathbf{a}^*) \mathcal{Y}_{\ell m}^*(\mathbf{a}^*)}{2\omega_a^D (b^2 - m_{D^*}^2)} \frac{1}{(q^*)^{\ell' + \ell}}. \quad (3.4)$$

Here (ω_a^D, \mathbf{a}) is the four-momentum of the D meson, four-vector $b = P - a$ where $P^\mu = (E, \mathbf{P})$. The vector \mathbf{a}^* is the spatial part of a four-vector resulting from boosting a to the overall c.m. frame. Harmonic polynomials are defined as $\mathcal{Y}_{\ell m}(\mathbf{a}) = \sqrt{4\pi} a^\ell Y_{\ell m}(\hat{a})$. The sum over \mathbf{a} runs over the finite-volume set, $\mathbf{a} = (2\pi/L)\mathbf{n}$, with \mathbf{n} a vector of integers. The integral over the pole is regulated using the principal value prescription, and a consistent ultraviolet regulator (denoted by “UV”) is implicit for both sum and integral. Finally, $q^* = \lambda^{1/2}(E^{*2}, m_D^2, m_{D^*}^2)/(2E^*)$, where $E^* = \sqrt{E^2 - \mathbf{P}^2}$ is the c.m. frame energy. \hat{F}_2 can be evaluated following the method described in appendix B of ref. [86].

⁹If the first inelastic threshold is D^*D^* , a two-body multi-channel approach is possible [85].

¹⁰In this section, we revert to the standard RFT convention of which of the spherical harmonics to complex conjugate. We stress that the resulting energy levels do not depend on this choice.

3.2 QC3 for $DD\pi$ scattering

In this section, we describe the finite-volume three-particle formalism of ref. [22], which connects the finite-volume energy levels of the $DD\pi$ system to the elastic scattering amplitude. We focus on the T_{cc}^+ channel, with overall isospin $I = 0$. The formalism is agnostic as to whether the D^* meson is stable or not—this is determined by the $I = 1/2$ $D\pi$ scattering amplitude, which is one of the inputs. Assuming a stable D^* meson, the range of validity of the formalism is,

$$E_{2\pi}^{\text{lh}} = \sqrt{2m_{D^*}^2 + 2m_D^2 - 4m_\pi^2} < E^* < \min[2m_D + 2m_\pi, 2m_{D^*}] . \quad (3.5)$$

The lower limit is the position of the left-hand branch point associated with a virtual two-pion exchange between D and D^* . It is typically relatively far from the physical region of interest. The upper limit is given by the lowest inelastic threshold, either $DD\pi\pi$ or D^*D^* , depending on the pion mass.

The QC3 takes the form,

$$\det_{i,\mathbf{k},sm} [\mathbb{1} + \hat{\mathcal{K}}_3 \hat{F}_3] = 0 . \quad (3.6)$$

As for the integral equations discussed in the previous section, the three mesons are divided into a pair and a spectator. The flavor of the spectator is labeled by i (either D or π), with three-momentum denoted by \mathbf{k} , drawn from the finite-volume set. Discrete indices s, m label the orbital angular momentum of the pair in its c.m. frame, defined as in section 2.1 except that here we revert to using a space-fixed coordinate system to define the azimuthal component. This is just a convention, but it has become the standard choice in implementations of the finite-volume quantization condition [86]. The determinant in eq. (3.6) is evaluated on matrices living in the multidimensional space with all these indices. The cutoff function $H_i(k)$ (which appears in \hat{F}_3 , as seen below) ensures that the sum over \mathbf{k} is truncated, while we truncate in s in the same manner as for the integral equations—see the end of section 2.1. In the following, we describe the building blocks of the above equation in detail.

First, the matrix \hat{F}_3 is given in terms of three components, \hat{F} , \hat{G} and $\hat{\mathcal{K}}_2$, as,

$$\hat{F}_3 \equiv \frac{\hat{F}}{3} - \hat{F} \frac{1}{1 + \hat{\mathcal{M}}_{2,L} \hat{G}} \hat{\mathcal{M}}_{2,L} \hat{F}, \quad \hat{\mathcal{M}}_{2,L} \equiv \frac{1}{\hat{\mathcal{K}}_{2,L}^{-1} + \hat{F}} . \quad (3.7)$$

The first component is,

$$\hat{F} = \text{diag}(\tilde{F}^D, \tilde{F}^\pi) , \quad (3.8)$$

where flavor indices are displayed explicitly, and

$$\begin{aligned} [\tilde{F}^{(i)}]_{p's'm';psm} &= \delta_{\mathbf{p}'\mathbf{p}} \frac{H^{(i)}(p)}{2\omega_p^{(i)} L^3} \left\{ \left[\frac{1}{L^3} \sum_a^{\text{UV}} -\text{p.v.} \int \frac{d^3a}{(2\pi)^3} \right] \right. \\ &\times \left[\frac{\mathcal{Y}_{s'm'}^*(\mathbf{a}_{p'})}{(q_{p'}^*)^{s'}} \frac{1}{4\omega_a^{(j)} \omega_b^{(k)} (E - \omega_p^{(i)} - \omega_a^{(j)} - \omega_b^{(k)})} \frac{\mathcal{Y}_{sm}^*(\mathbf{a}_p^*)}{(q_p^*)^s} \right] \\ &\left. + \frac{1}{8\pi \sqrt{\sigma_p^{(i)}}} \frac{c_{\text{PV},s}^{(i)}}{(q_p^*)^{2s}} \right\} . \quad (3.9) \end{aligned}$$

Much of the notation is as for F_2 above—see eq. (3.4)—while the c_{PV} coefficients have been introduced in eq. (2.34). Here, however, there are three particles: the initial spectator with momentum \mathbf{p} and flavor i , and the corresponding pair, consisting of a primary with momentum \mathbf{a} and flavor j , and a secondary with momentum $\mathbf{b} = \mathbf{P} - \mathbf{p} - \mathbf{a}$ and flavor k . The momentum \mathbf{a}_p^* is the result of boosting $a = (\omega_a^{(j)}, \mathbf{a})$ to the c.m. frame of the pair, while q_p^* is defined in eq. (2.20). We have kept flavor indices explicit, as there is an ambiguity as to which member of the pair is primary if $i = D$. Our choice in this case is $j = D$, $k = \pi$. If $i = \pi$, then we have $j = k = D$.

The flavor structure of \hat{G} is given as,

$$\hat{G} = \begin{pmatrix} \tilde{G}^{DD} & -\sqrt{2}P^{(s)}\tilde{G}^{D\pi} \\ -\sqrt{2}\tilde{G}^{\pi D}P^{(s)} & 0 \end{pmatrix}, \quad (3.10)$$

where the entries are defined by,

$$[\tilde{G}^{(ij)}]_{ps'm';rsm} = \frac{1}{2\omega_p^{(i)}L^3} \frac{\mathcal{Y}_{s'm'}(\mathbf{r}_p^*)}{(q_p^*)^{s'}} \frac{H_i(p)H_j(r)}{b_{pr}^2 - m_{ij}^2} \frac{\mathcal{Y}_{sm}^*(\mathbf{p}_r^*)}{(q_r^*)^s} \frac{1}{2\omega_r^{(j)}L^3}, \quad (3.11)$$

and,

$$[P^{(s)}]_{ps'm';rsm} = \delta_{\mathbf{pr}} \delta_{s's} \delta_{m'm} (-1)^s. \quad (3.12)$$

We note that eq. (3.11) is closely related to eq. (2.27), with two main differences: an overall $2\omega_p L^3$ factor, and the fact that the spherical harmonics in eq. (2.26) are defined with respect to the azimuthal component, and not in the spin-helicity basis.

The final component of \hat{F}_3 is $\hat{\mathcal{K}}_{2,L}$, given by

$$\hat{\mathcal{K}}_{2,L} = \text{diag} \left(\mathcal{K}_{2,L}^{D\pi, I=1/2}, \frac{1}{2} \mathcal{K}_{2,L}^{DD, I=1} \right), \quad (3.13)$$

where each entry corresponds to a modified K matrix for the $\{jk\}$ system with isospin I ,

$$[\mathcal{K}_{2,L}^{jk, I}]_{ps'm';rsm} = \delta_{\mathbf{pr}} 2\omega_p^{(i)} L^3 \delta_{s's} \delta_{m'm} \mathcal{K}_{2,s}^{jk, I}(\mathbf{p}), \quad (3.14)$$

$$[\mathcal{K}_{2,s}^{jk, I}(\mathbf{p})]^{-1} = \frac{\eta_i}{8\pi\sqrt{\sigma_p^{(i)}}} \left\{ q_p^* \cot[\delta_s^{(jk), I}(q_p^*)] + |q_p^*| [1 - H^{(i)}(p)] - H^{(i)}(p) \frac{c_{\text{PV}, s}^{(i)}}{(q_p^*)^{2s}} \right\}, \quad (3.15)$$

where $\delta_s^{(jk), I}$ is the corresponding phase shift for angular momentum s . The constants $c_{\text{PV}, s}^{(i)}$ are to be determined so that $\mathcal{K}_{2,s}^{jk, I}$ does not have a pole in the kinematically allowed range \mathbf{p} [75].

Finally, we describe how the three-particle K matrix, \mathcal{K}_3 , is converted to the matrix form that enters the QC3. One begins with the chosen model form in terms of the momenta, e.g., the threshold expansion given in eq. (2.49). Here, we label the final momenta $\{\mathbf{p}\} \equiv \{\mathbf{p}_1, \mathbf{p}_2, \mathbf{p}_3\}$, where the flavors are $1 = 2 = D$ and $3 = \pi$, and similarly for the initial momenta. One then applies operators that project onto the pairs' angular momenta s', s . The flavor structure of the result takes the form of an outer product [22],

$$\hat{\mathcal{K}}_3 = \mathcal{Y}^{[I=0]} \circ \mathcal{K}_3(\{\mathbf{p}\}; \{\mathbf{k}\}) \circ \mathcal{Y}^{[I=0]\dagger}, \quad (3.16)$$

$$\mathbf{y}^{[I=0]} = \begin{pmatrix} -\mathbf{y}_{(123)}^{[kab]} \\ \sqrt{\frac{1}{2}}\mathbf{y}_{(312)}^{[kab]} \end{pmatrix}, \quad \mathbf{y}^{[I=0]\dagger} = \begin{pmatrix} -\mathbf{y}_{(123)}^{[kab]\dagger}, \sqrt{\frac{1}{2}}\mathbf{y}_{(312)}^{[kab]\dagger} \end{pmatrix}, \quad (3.17)$$

where the operator $\mathbf{y}_{\sigma}^{[kab]}$ is defined through its action on functions $g(\{p\})$ of three on-shell momenta,

$$\left[\mathbf{y}_{\sigma}^{[kab]} \circ g\right]_{ksm} = \frac{1}{4\pi} \int d\Omega_{a^*} Y_{sm}(\hat{a}^*) g(\{p_i\}) \Big|_{p_{\sigma(1)} \rightarrow k, p_{\sigma(2)} \rightarrow a, p_{\sigma(3)} \rightarrow b}, \quad (3.18)$$

where σ is a permutation of $\{123\}$. The explicit decomposition into the ksm basis for the quantities entering the threshold expansion, i.e. those in eq. (2.50), has been presented in ref. [42] for the $\pi^+\pi^+K^+$ and $K^+K^+\pi^+$ systems and implemented numerically in ref. [87]. This work carries over to the $I = 0$ $DD\pi$ system, aside from trivial changes due to differences in meson masses and the nontrivial appearance of negative signs in eq. (3.17) (which are absent in the $\pi^+\pi^+K^+$ and $K^+K^+\pi^+$ systems).

4 Numerical results

In practice, one wishes to apply the framework presented above to the QCD finite-volume $DD\pi$ energies to first constrain parametrizations of \mathcal{K}_2 and \mathcal{K}_3 , then solve the integral equations, and finally determine the pole position of T_{cc}^+ . Given that no $DD\pi$ lattice data exists yet, we illustrate the application of the three-body formalism by making reasonable assumptions about the interactions of the $DD\pi$, DD , and $D\pi$ systems. We study their behavior for different fixed choices of the two- and three-particle parameters and estimate a value for the three-body K matrix.

Numerical solutions of the partial-wave projected three-body integral equations, described in eqs. (2.13) and (2.35), are obtained by fixing the two-body $D\pi$ and DD interactions from the available lattice results and adjusting the unknown three-body K matrix to match our LSZ-reduced amplitude to the result of ref. [9]. We then use our determination of \mathcal{K}_3 in the three-body finite-volume quantization condition to derive corresponding $DD\pi$ and DD^* energy levels and compare them to the analogous two-body results. Finally, we discuss the significance of the left-hand cuts in both the infinite- and finite-volume numerical solutions.

We start with section 4.1, where we provide the values of particle masses, thresholds, and the ERE parameters used to describe interactions in the two-body subchannels. We use a combination of lattice results and a comparison with the heavy-light meson ChPT to interpolate scattering lengths and effective ranges to the pion mass used in ref. [9]. Next, in section 4.2, we focus on the solution to the ladder equation, where the states interact only in pairs and by one-particle exchanges. We first discuss an approximate solution, where the partial-wave mixing is ignored by artificially truncating the DD^* angular momentum space. Then, we present the partial-wave mixing result. In both cases, we find that the ladder amplitude alone cannot describe the lattice data. Thus, in section 4.3, we include a non-zero \mathcal{K}_3 , trying to tune the partial-wave projected integral equations to describe the DD^* scattering. We find that by adjusting a single parameter, \mathcal{K}_3^E , we can match the

DD^* phase shift to the lattice results reasonably well. Again, two models are considered: one neglecting and one including the partial-wave mixing. In both cases, we observe the T_{cc}^+ as a pair of complex poles and study their trajectory as a function of the three-body coupling. The analytic properties of the amplitude obtained in our approach are similar to and confirm those reported in Refs. [13, 20, 21, 24]. In section 4.4, we produce the DD^* amplitude in the $J^P = 0^-$ wave, employing the set of parameters fixed in the $J^P = 1^+$ case. We find no additional bound or virtual states with this quantum number and observe a qualitative agreement between our result and the infinite-volume parametrization extracted from the lattice calculation. Finally, in section 4.5, we determine the form of the three-particle spectrum using the determined scattering parameters as input in QC2 and QC3. We observe a breakdown of the QC2 in the vicinity of the left-hand cut in agreement with the numerical results of ref. [51].

4.1 Physical setup and two-body interactions

We compute the DD^* amplitude for one of the two sets of masses reported in ref. [9],

$$m_\pi \approx 280 \text{ MeV}, \quad m_D \approx 1927 \text{ MeV}, \quad m_{D^*} \approx 2049 \text{ MeV}. \quad (4.1)$$

Throughout this section, we use m_D as a unit of energy. Above values correspond to the ratios $\kappa = m_\pi/m_D = 0.1453$, and $m_{D^*}/m_D = 1.0663$. The three-body threshold is placed at $E_{DD\pi}/m_D = 2.1453$, the DD^* threshold at $E_{DD^*}/m_D = 2.0663$ and the nearest OPE branch point in the DD^* amplitude at $E_2^{\text{lh}}/m_D = 2.0592$. The authors of ref. [9] determined the S -wave DD^* phase shift from the Lüscher method and implemented the ERE parametrization to identify the T_{cc}^+ as a virtual state around the energy $E_{T_{cc}}/m_D = 2.0582$, slightly below the left-hand cut branch point. Subsequent studies reanalyzed the same data set using chiral-EFT-based dynamical equations and incorporating the presence of the OPE in the amplitude [13, 20, 21, 24]. Instead of a single T_{cc}^+ state, they found two complex poles on the second Riemann sheet of the DD^* amplitude, at energies around $E_{T_{cc}}/m_D = 2.0597 \pm 0.0043i$.

To apply the three-body integral equations to the $DD\pi$ scattering, one must specify interactions in the $D\pi$ and DD subchannels. For consistency, the two-body amplitudes should be given for the particle masses of eq. (4.1). While existing lattice studies do not match these values, the available data is sufficient to place nontrivial constraints on the required two-body amplitudes, as we now explain.

Following the description of section 2.2.1, we assume that the $I = 1$ DD channel is weakly repulsive and well-approximated by neglecting all but the lowest partial wave, $s = 0$. To our knowledge, no lattice computations have been performed for this channel, but, like the $I = 1$ KK system, it is not expected to exhibit bound states or resonances. Our model of the reaction depends on a single parameter, the two-body scattering length $a_0^{(2)}$, and our solutions show a negligible dependence on its value. This is due in part to the assumed weakness of the interactions in this channel. More important, however, is that, for our choice of cutoff function, the DD subsystem decouples when its invariant mass falls below the two-pion exchange branch cut. It happens when,

$$E/m_D < 2\sqrt{1 - \kappa^2} + \kappa = 2.1241, \quad (4.2)$$

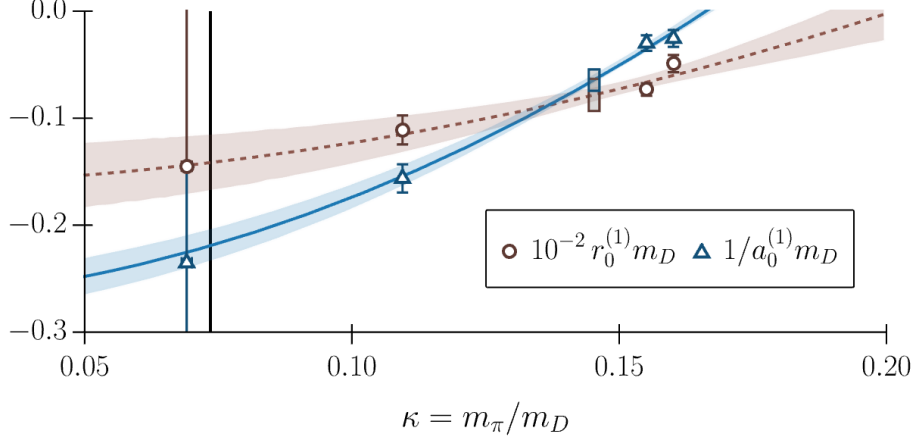


Figure 2: Determination of the $D\pi$ s -wave scattering parameters. Triangles and circles represent entries of Table II in ref. [60], while solid curves represent chiral extrapolation of the form $x = c_0 + c_1\kappa^2$, where the dimensionless parameter $x = 1/a_0^{(1)}m_D$ (solid, blue) or $r_0^{(1)}m_D$ (dashed, brown). Dark blue and brown boxes at $\kappa = 0.1453$ depict the intervals of parameters considered in this work. The black vertical line at $\kappa = 0.0735$ corresponds to the physical ratio, $m_\pi^{\text{phys}}/m_D^{\text{phys}}$.

which lies significantly above the DD^* threshold and slightly below the D^*D^* and $DD\pi$ thresholds. Therefore, from the perspective of DD^* scattering and T_{cc}^+ physics, the DD interactions contribute only at energies near the inelastic thresholds. In practice, we set $m_D a_0^{(2)} = -10^{-2}$.

The $I = 1/2$ $D\pi$ channel is described with four parameters: the s -wave scattering length $a_0^{(1)}$ and effective range $r_0^{(1)}$, together with the p -wave scattering length $a_1^{(1)}$ and effective range $r_1^{(1)}$. Several finite-volume studies of the $D\pi$ reaction are available [56–60] with the most recent work, ref. [60], exploring the s - and p -wave scattering in ensembles corresponding to four different pion masses. In principle, no precise connection can be assumed between the DD^* system considered in ref. [9] and the $D\pi$ lattice studies mentioned above due to different physical parameters, finite-volume and discretization contributions, and other systematic effects, associated, e.g., with the set of the employed interpolation operators or the approximations made in applying the Lüscher method. For this reason, we use the above studies to determine a plausible interval of the two-body parameters rather than trying to fix them exactly. We then study the dependence of our solutions on these values within the constrained ranges.

As in the DD case, we assume weak interactions in the $D\pi$ s -wave scattering and consider two models for the amplitude. In the “spartan” approach, we set $r_0^{(1)} = 0$ and constrain $|a_0^{(1)}| < 1/m_\pi$ such that no bound or virtual states appear in the vicinity of the $D\pi$ threshold. For these values, the physical and spurious pole of the LO ERE move to the complex plane on the first (for positive $a_0^{(1)}$) or the second Riemann sheet (for negative $a_0^{(1)}$), away from the threshold, and do not introduce any important physical effects. The $D\pi$ interactions are expected to be attractive, so we explore only positive values of $a_0^{(1)}$.

In the second approach, we consider an amplitude including a state analogous to the physical $D_0^*(2300)$ meson. This system has been studied extensively on the lattice in refs. [58–60]. To specify this model of the amplitude, we use physical parameters from Tables II and VIII of ref. [60]. Note that we follow the opposite sign convention for the LO term of the ERE than this work. We use the provided values to interpolate to our mass of choice, $\kappa = 0.1453$, by applying the chiral formula $x = c_0 + c_1 \kappa^2$, where the dimensionless quantity x is either $1/a_0^{(1)} m_D$ or $r_0^{(1)} m_D$. The results are shown in figure 2. The estimated scattering length and effective range are,

$$a_0^{(1)} m_D = -15.5 \pm 2.5, \quad r_0^{(1)} m_D = -7.84 \pm 1.50, \quad (4.3)$$

where the chosen ranges are conservative. Assuming the above values of the parameters, the D_0^* appears as a virtual state below the $D\pi$ threshold, in agreement with Fig. 3 of ref. [60].

Regardless of the choice of model, we find that the $J^P = 1^+$ three-body amplitude is largely insensitive to the assumptions about the s -wave interactions. In the subsequent sections, we use the central values from eq. (4.3). The situation changes for the $J^P = 0^-$ DD^* scattering, for which we find a noticeable dependence on the s -wave parameters. We discuss this further in section 4.4.

We now turn to the p -wave $D\pi$ interactions. As discussed above, we use a two-term ERE expansion, eq. (2.22). Under the assumption that the D^* pole position of $\mathcal{M}_{2,1}^{(1)}$ is fixed at a mass given in eq. (4.1), the parameters $a_1^{(1)}$ and $r_1^{(1)}$ are related to each other by eq. (2.23), which depends on the (purely imaginary) binding momentum q_0 , eq. (2.24). For our chosen masses, this momentum is $q_0 = i 0.87 m_\pi$. We choose $r_1^{(1)}$ to be the free parameter and fix it by equating the value of the residue of $\mathcal{M}_{2,1}^{(1)}$ at the pole to the residue computed in terms of the $D^* D\pi$ coupling, $g_{D^* D\pi}$, defined in the continuum literature [88]. As explained in appendix D, we find,

$$r_1^{(1)} = -3|q_0| - \frac{128\pi}{g_{DD^*\pi}^2} \frac{m_{D^*}^5}{m_{D^*}^4 - (m_\pi^2 - m_D^2)^2}. \quad (4.4)$$

In the lattice QCD literature, it is more common to use the coupling g appearing in heavy-quark effective theory. The relation between couplings is $g_{DD^*\pi}^2 = 4g^2 m_D m_{D^*} / f_\pi^2$, where the pion decay constant is taken to be $f_\pi = \sqrt{2} F_\pi = 130$ MeV. Using experimental decay widths, one finds $g_{\text{exp}} \approx 0.57$ [89], while lattice simulations find the range $g_{\text{lat}} \in [0.50, 0.61]$, depending on the pion mass and lattice spacing [57].

We consider values of g in this range, which translates to $r_1^{(1)}/m_D \in [-7.7, -5.3]$ and $a_1^{(1)} M_D^3 \in [24.7, 16.8]$ with the central values $r_1^{(1)}/m_D = -6.5$, $a_1^{(1)} m_D^3 = 19.98296$. The solutions to the integral equations depend noticeably on the assumed values of the p -wave parameters. Therefore, in the following, to provide an idea of the parameter dependence of our DD^* amplitude, we show our main results for three choices of the coupling, $g = 0.4996 \approx 0.50$, $g = 0.5464 \approx 0.55$, and $g = 0.6094 \approx 0.61$. We note that for this set of parameters, the p -wave amplitude has additional poles; a virtual state with $q_0/m_D \approx -0.12i$, as well as a distant physical-sheet pole with $q_0/m_D \approx 3i$. These singularities do

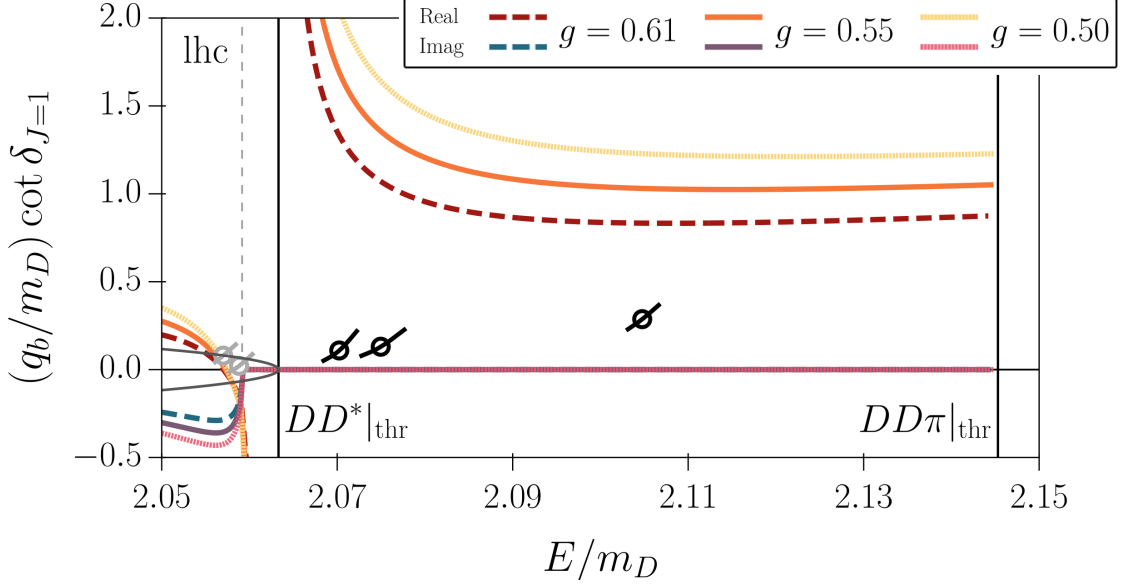


Figure 3: The $J^P = 1^+$ DD^* scattering phase shift, as defined in eq. (2.55), obtained by s -wave truncation of the ladder amplitude. We plot $q_b \cot \delta$ as a function of energy in the vicinity of DD^* and $DD\pi$ thresholds (black, vertical lines). The solution is given for three different values of the $D^* \rightarrow D\pi$ coupling g , as shown in the legend. The phase shift acquires a non-zero imaginary part below the left-hand cut branch point (dashed vertical line). Black and gray points are from the s -wave phase shift extracted using the QC2 in ref. [9]. Points below E_2^{lhc} are highlighted by a lighter, gray color, as they are not expected to be reliable. Gray, solid lines below the DD^* threshold are $\pm|q_b/m_D|$. The absence of a crossing of these lines above the left-hand cut shows the absence of bound or virtual states in this channel.

not affect the amplitude significantly in the integration region (e.g., above the threshold) due to the dominance of the D^* pole.

Finally as explained in ref. [75], to compute the finite-volume spectrum, we need to fix constants introduced in eq. (2.34). We set $c_{\text{PV},1}^{(1)}/m_D^3 = -0.25$ in the p -wave $D\pi$ channel to account for the real-axis D^* pole and $c_{\text{PV},0}^{(1)}/m_D = -0.2$ in the s -wave $D\pi$ channel due to the lattice equivalent of the D_0^* pole.

4.2 The $J^P = 1^+$ ladder amplitude

In the first step, we solve the ladder equation, eq. (2.13), using methods of section 2.2.3 and assuming two-body parameters from the previous subsection. The short-range interactions are ignored by setting $\mathcal{K}_3 = 0$ to investigate the amplitude driven purely by the pair-wise interactions and one-particle exchanges.¹¹ We perform the LSZ reduction of the $DD\pi$ amplitude and extract the DD^* K matrix.

¹¹We remind the reader that this is a scheme-dependent statement that changes its meaning whenever a different choice of the cutoff function is made.

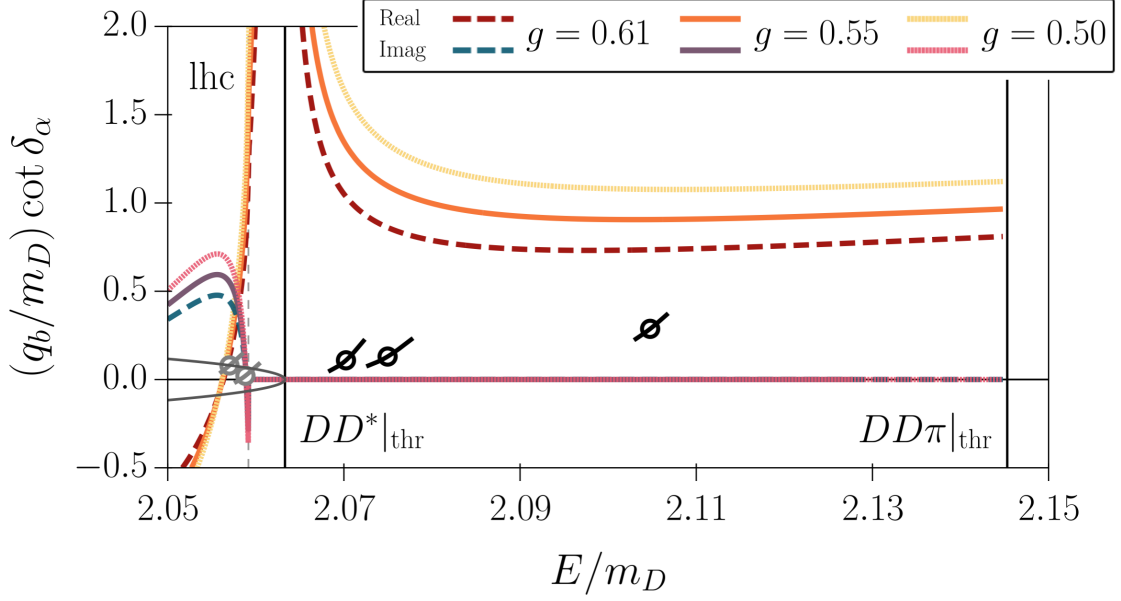


Figure 4: Results for $q_b \cot \delta_\alpha$, as defined in the Blatt-Biedenharn parametrization of eq. (2.57). It is obtained from the LSZ-reduced ladder amplitude including the s - and d -wave mixing. Notation and conventions are as in figure 3. Note that the enhancement in the real parts below the threshold is not a pole, instead peaking at a finite value. The imaginary parts display a sharp dip just below the left-hand cut. Gray, solid lines are $\pm|q_b/m_D|$. The absence of a crossing of these lines above the left-hand cut shows the absence of bound or virtual states in this channel.

We first present the approximate solution obtained by restricting the angular momentum space to the ${}^3S_1 \rightarrow {}^3S_1$ transitions. This is obtained by artificially removing (setting to zero) entries of the integral equation corresponding to $(\ell, s) = (2, 1)$ or $(\ell', s') = (2, 1)$. Although this approximation explicitly violates the unitarity of the amplitude, it is justified, provided this system exhibits small partial-wave mixing. It has been assumed in many preceding studies [9–11, 13] and was additionally investigated in ref. [14] where the authors discussed in detail the effect of the higher partial waves. Our results are shown in figure 3, displayed as $q_b \cot \delta_{J=1}(E)$, as defined in eq. (2.55). They are compared to the lattice data points of ref. [9]. The visible disagreement indicates that a non-zero \mathcal{K}_3 must be included to describe the data. We note that the amplitude exhibits a zero below the threshold, which leads to a pole in the inverse of the DD^* K matrix. This agrees with the studies of this setting based on non-relativistic chiral EFT [90]. The appearance of this zero has also been argued on the grounds of general N/D parametrization of amplitudes constructed from the one-particle exchange interactions [25], independently of the value of the short-range couplings. Moreover, the amplitude has no virtual or bound state pole near the threshold that could be identified with T_{cc}^+ . This can be inferred from the figure, since the real part of $q_b \cot \delta_{J=1}$ does not cross the parabola $\pm|q_b/m_D|$ (gray, solid line) above the E_2^{lhc} .

We display in figure 3 and subsequent figures both the DD^* and $DD\pi$ thresholds, shown as black vertical lines, as well as the left-hand cut (dashed vertical line). In principle, our formalism is valid above the $DD\pi$ threshold, as well as below the left-hand cut. However, for the D^* mass considered here, another threshold, namely that of the D^*D^* , is placed below $E_{DD\pi}$, at $E_{D^*D^*}/m_D = 2.1266$. We cannot investigate the effect of the opening of this new channel, as this would require a four-particle formalism in our approach. Our results effectively assume that it is closed, and are insensitive to its presence. Thus, to avoid clutter, we do not show this threshold on the figures. We do note, however, that it has been recently studied (at a heavier pion mass) in ref. [14] using a multichannel QC2 approach.

The solution of the full ladder equation, including 3S_1 – 3D_1 mixing, is shown in figure 4 in the form of the DD^* K matrix α eigenvalue, as defined in the Blatt-Biedenharn parametrization, eq. (2.57). It is similar to the truncated ladder solution above the DD^* threshold, which hints at the insignificance of the partial-wave mixing in this system. We include the lattice $\cot \delta_{J=1}$ points in the figure for reference, even though they are not, strictly speaking, comparable with the outcome of the partial-wave mixing calculation. Nevertheless, since $\cot \delta_\alpha = \cot \delta_{J=1} + \mathcal{O}(\epsilon^2)$ [91], and we find small values for the mixing angle ϵ (not shown), a qualitative comparison can be made, and we see again that our results do not lie close to the lattice points.

The amplitude exhibits a zero below the threshold in the $(\ell, s) = (0, 1)$ partial wave, which leads to a peak (but no pole) in $\cot \delta_\alpha$ around the same energy. Other matrix elements of the amplitude vanish at the threshold in agreement with the expected $\propto q_b^{2(\ell'+\ell)}$ behavior. Generally speaking, the behavior of the alpha eigenvalue significantly differs from the $\cot \delta_{J=0}$ of the truncated solution below the elastic threshold. Not only has the pole disappeared, but the imaginary part below the lhc changed its sign from negative to positive. This can be explained by the rapid increase of the mixing angle below the threshold, which does not contradict the naïve expectation that $\cot \delta_\alpha \approx \cot \delta_{J=1}$ for energies above E_{DD^*} . We postpone showing results for the mixing angle and $\cot \delta_\beta$ until we consider the full solution with nonzero \mathcal{K}_3 .

4.3 The $J^P = 1^+$ amplitude with non-zero \mathcal{K}_3

After this preliminary discussion, we turn to the complete solution of the combined three-body eqs. (2.13) and (2.35), obtained for non-zero \mathcal{K}_3 . We emphasize again that, although the threshold expansion of \mathcal{K}_3 contains several terms (see eq. (2.49)), at the order we work only the \mathcal{K}_3^E term contributes to the $J^P = 1^+$ channel. As for the ladder amplitude discussed previously, we study the result both in the s -wave truncated and the partial-wave mixing cases.

The results for $\cot \delta_{J=1}$ from the truncated solution are shown in figure 5, at a fixed strength of the three-body parameter, $m_D^2 \mathcal{K}_3^E = 1.9 \cdot 10^5$, and for our standard three values of g . This is the value of the three-body K matrix for which the $g = 0.55$ curve matches reasonably well to the lattice data of ref. [9].¹² It is possible to match the $g = 0.50$ result

¹²We stress again that we do not perform a fit to the available points, but choose to match our solution

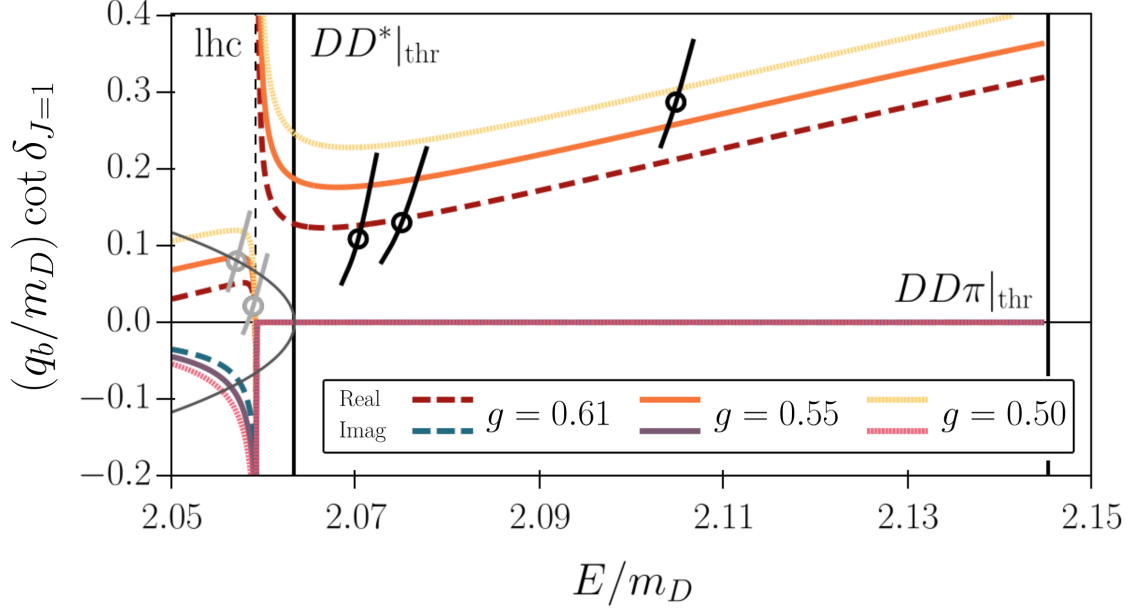


Figure 5: Results for $q_b \cot \delta_{J=1}$ for the s -wave truncated solution with a nonzero value for the three-particle K matrix, $m_D^2 \mathcal{K}_3^E = 1.9 \cdot 10^5$. This value is chosen so that the $g = 0.55$ curve passes through the lattice data points lying above the left-hand cut. Gray, solid lines are $\pm |q_b/m_D|$. Notation as in figure 3.

more closely to the data by decreasing its value to $m_D^2 \mathcal{K}_3^E \approx 1.4 \cdot 10^5$ and to match the $g = 0.61$ result by increasing it to $m_D^2 \mathcal{K}_3^E \approx 2.4 \cdot 10^5$.

A characteristic feature of the $q_b \cot \delta$ curves for s -wave truncated solutions is the presence of a pole between the left-hand cut and the DD^* threshold, corresponding to a zero of the amplitude. This agrees qualitatively with the results obtained using s -wave truncated Lippmann-Schwinger equations in refs. [13, 20, 21, 24]. We find that this zero moves to lower energies as \mathcal{K}_3^E increases, approaching, but not crossing, the left-hand cut. Clearly, this pole invalidates the use of the ERE to describe the amplitude near the left-hand cut, as emphasized in [24]. The half-parabola $|q_b/m_D|$ is not crossed by our solutions, so we find no virtual bound states, in agreement with most examples in the literature [13, 20, 21, 24]. By continuing the amplitude to the unphysical Riemann sheet, using eq. (2.59), we find two subthreshold conjugate complex poles. These have been identified in the above-mentioned studies as corresponding to the T_{cc}^+ . The positions of these poles are given in Table 1 in the first row.

Our result for the full, partial-wave mixing amplitude, obtained for the same non-zero value of the three-body K matrix, $m_D^2 \mathcal{K}_3^E = 1.9 \cdot 10^5$, is presented in three plots, figures 6 to 8. They show the alpha and beta eigenvalues of the Blatt-Biedenharn \mathcal{K}_{DD^*} matrix, and the mixing angle, respectively—see eq. (2.57).

We first note that, above the DD^* threshold, $\cot \delta_\alpha$ (figure 6) is almost identical to

by eye. As mentioned at the beginning of section 2.2.3, our goal is not to perform a rigorous analysis of the lattice data but rather to benchmark the RFT formalism and estimate reasonable values for \mathcal{K}_3^E .

Model	$g = 0.50$	$g = 0.55$	$g = 0.61$
truncated	$2.05755 \pm 0.00457 i$	$2.05396 \pm 0.00589 i$	$2.04941 \pm 0.00662 i$
p.w. mixing	$2.05797 \pm 0.00463 i$	$2.05469 \pm 0.00578 i$	$2.05035 \pm 0.00626 i$

Table 1: Positions of putative T_{cc}^+ poles on the second sheet for the three-body coupling $m_D^2 \mathcal{K}_3^E = 1.9 \cdot 10^5$ and our standard choices of g . The “truncated” model includes only s waves in the DD^* system, while the “p.w. mixing” model includes both s and d waves.

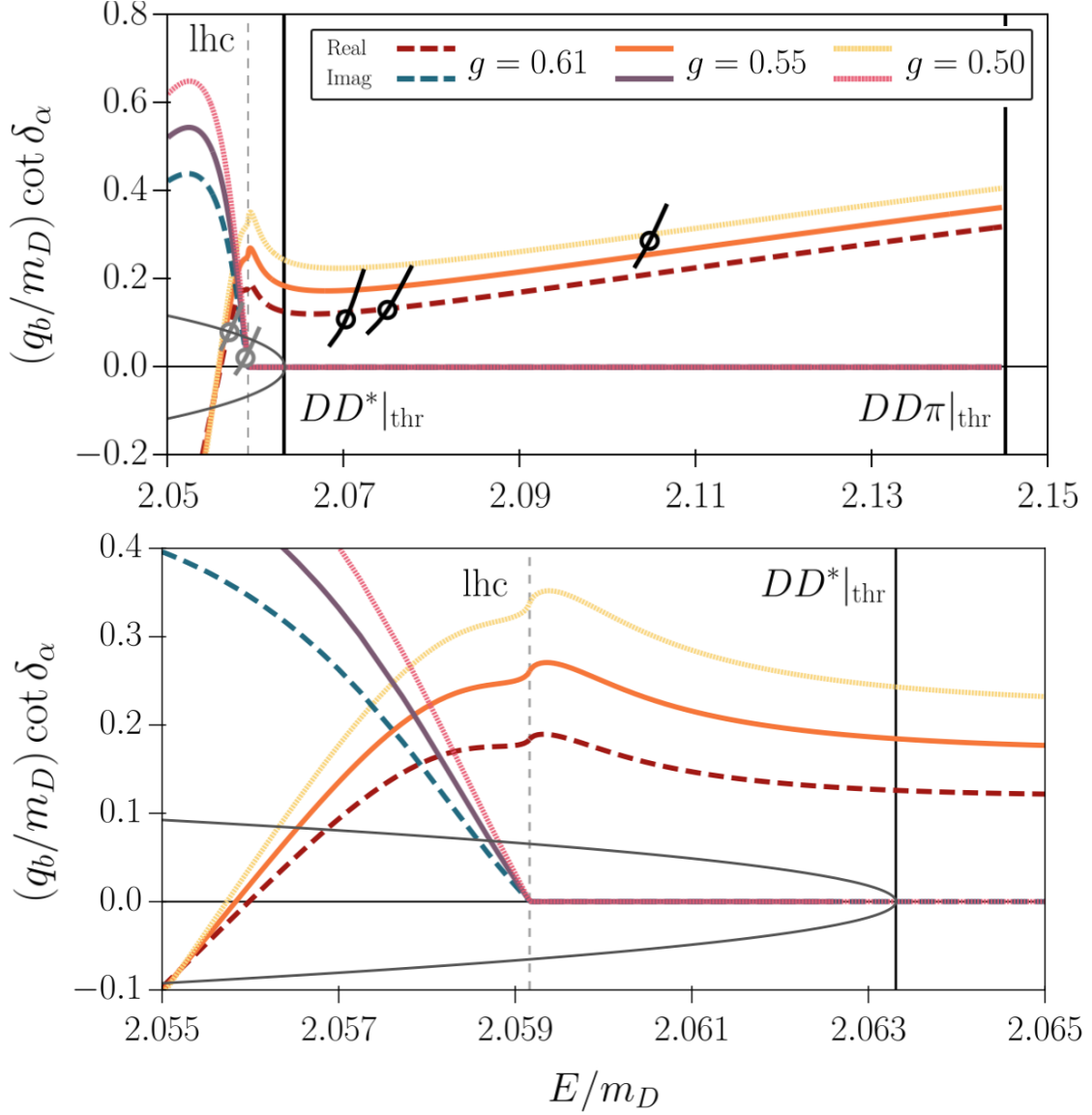


Figure 6: Results for $q_b \cot \delta_\alpha$, obtained from the solution with a nonzero three-body K matrix, $m_D^2 \mathcal{K}_3^E = 1.9 \cdot 10^5$, the same value as used in figure 5. Notation as in figure 4. The lower panel zooms in near the left-hand cut. Gray, solid lines are $\pm |q_b/m_D|$.

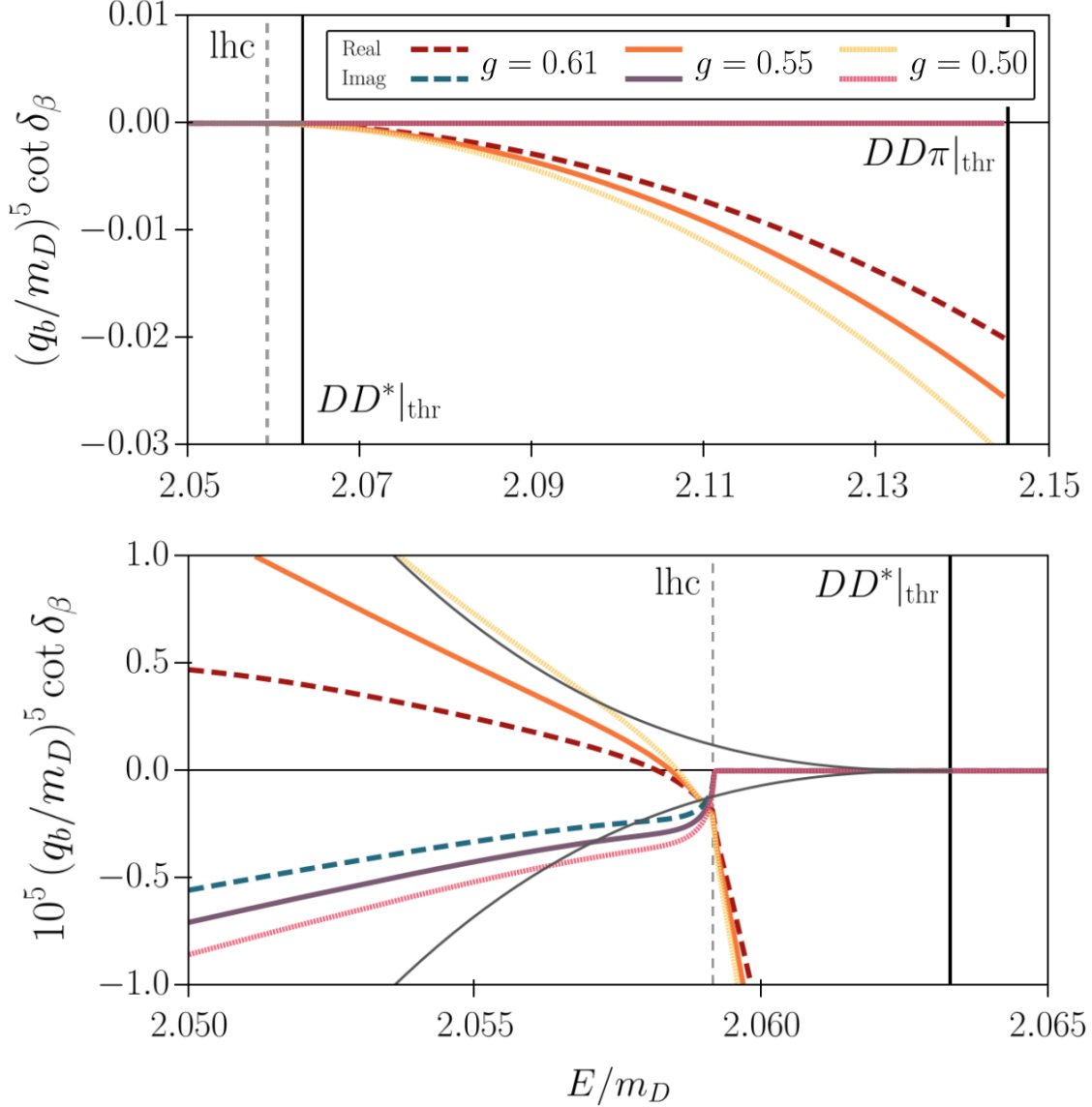


Figure 7: Results for $q_b^5 \cot \delta_\beta$ from the same solution used to display $q_b \cot \delta_\alpha$ in figure 6, using the same format. The lower panel zooms in near the left-hand cut. Gray, solid lines are $\pm |q_b/m_D|^5$.

the truncated model's $\cot \delta_{J=1}$ (figure 5). This can be understood by the fact that the mixing angle $\epsilon \approx -\pi/64$ for $E > E_{DD^*}$, nearly decoupling the 3S_1 and 3D_1 sectors of the K matrix. Furthermore, we find that the β eigenvalue, shown in figure 7, is an order of magnitude smaller than the α eigenvalue.

Below the DD^* threshold, however, the situation is quite different. The mixing angle rises rapidly and the behavior of $\cot \delta_\alpha$ differs markedly from that of $\cot \delta_{J=1}$ in the truncated model. In particular, $\cot \delta_\alpha$ has no pole, behaving fairly smoothly, and its imaginary part below the left-hand cut has the opposite sign to that in the truncated model. These results show the importance of including the d -wave channel in this energy regime.

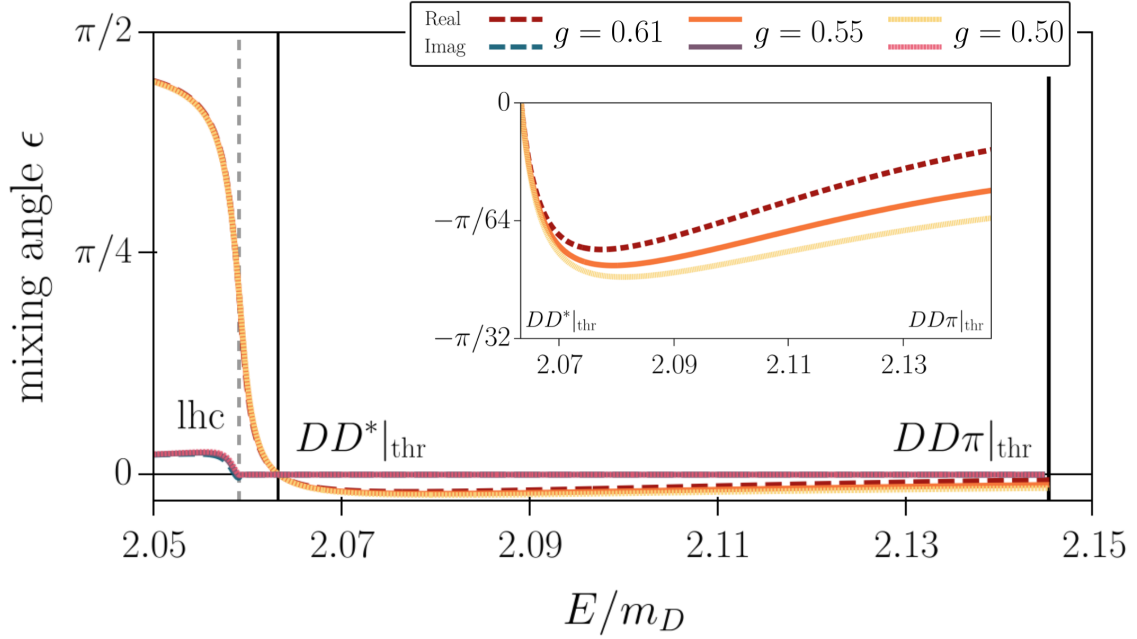


Figure 8: Results for the mixing angle ϵ from the same solution as that used for figures 6 and 7, and using the same format. The inset shows the result for ϵ in the physical region, where it is purely real.

Neither $\cot \delta_\alpha$ nor $\cot \delta_\beta$ satisfies the corresponding bound or virtual state conditions, as can be seen from the lower panels of figures 6 and 7. Instead, as in the truncated model, we find two subthreshold complex poles. Their positions are listed in Table 1 in the bottom row. We observe relatively small shifts between the truncated and partial-wave mixing cases. We also note that these values are of the same order as those presented in Fig. 7 of ref. [20].

We have extended the above investigations to a large range of values of \mathcal{K}_3^E , to explore the possible manifestations of the T_{cc}^+ pole. Our results are summarized in figure 9, where we show the pole trajectories for $g = 0.55$. Starting from negative \mathcal{K}_3^E , increasing its value leads to an evolution of the model's spectrum from two subthreshold complex poles to a pair of virtual states. These separate on the real axis, with one moving to the DD^* threshold, and subsequently moving onto the first sheet and becoming, for large enough \mathcal{K}_3^E , a bound state. As \mathcal{K}_3^E increases further, its binding energy increases, and the pole eventually moves below the left-hand cut, where we no longer trace its evolution. The companion pole remains a virtual state. In the s -wave truncated model, its position asymptotes with increasing \mathcal{K}_3^E to the left-hand branch point and the pole does not cross this singularity. By contrast, in the partial-wave mixing case, we find that this pole keeps moving to the left and crosses E_2^{lhc} at $m_D^2 \mathcal{K}_3^E \approx 4 \cdot 10^5$. This is another example of an important difference between the two models below the DD^* threshold.

Overall, the determined trajectory resembles the results reported in the literature (see figures 11 and 12 in ref. [13] and figure 3 in ref. [20]) although there different model

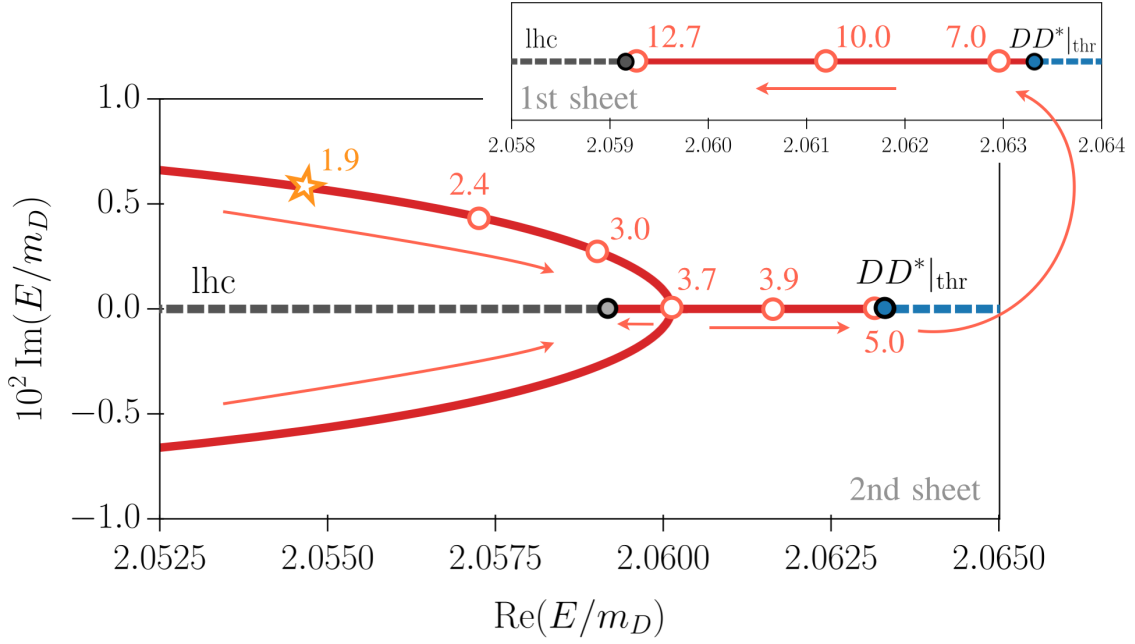


Figure 9: Trajectories of the putative T_{cc}^+ poles (red, solid lines) in the partial-wave mixing model, as a function of \mathcal{K}_3^E , for the central value of the $D\pi$ p -wave coupling, $g = 0.55$. Pink dots represent the position of the poles at the given values of $m_D^2 \mathcal{K}_3^E / 10^5$. The orange star indicates the position of the pole for $m_D^2 \mathcal{K}_3^E = 1.9 \cdot 10^5$, the value chosen so that our DD^* amplitude matches the data of ref. [9]. The arrows indicate the motion of the poles as \mathcal{K}_3^E is increased. Dashed lines indicate the placement of the right- and left-hand cuts, which emerge respectively from the DD^* threshold (blue dot) and left-hand branch point (grey dot). For further discussion, see the text.

parameters (charm quark and pion mass) were varied.

4.4 The $J^P = 0^-$ amplitude

The lattice calculations of ref. [9] also report results for the phase shift in the $\ell = 1$, $J^P = 0^-$ DD^* channel. Indeed, in the finite-volume analysis, in moving frames, the energies of states in certain irreducible representations (irreps) depend on the interactions in both the $J^P = 1^+$ and 0^- channels. Thus, at some level of precision, one must include the 0^- channel in the calculation.

Thus motivated, we have solved the integral equations also for this channel. This requires performing the LSZ reduction on the ${}^3P_0 \rightarrow {}^3P_0$ element of the $DD\pi$ amplitude, $\mathcal{M}_{3;11;11}^{(11)0}$. We employ the parametrization of eq. (2.55) to present our result in the form of $q_b^3 \cot \delta_{J=0}$ in figure 10, providing also a comparison with the result from ref. [9]. A new feature of this channel is that the $\mathcal{K}_3^{\text{iso},0}$, $\mathcal{K}_3^{\text{iso},1}$, and \mathcal{K}_3^B terms in the threshold expansion of the three-particle K matrix, eq. (2.49), contribute in addition to \mathcal{K}_3^E . However, we find that the resulting $J^P = 0^-$ phase shift is largely unaffected by any of the three-particle couplings at the order in the threshold expansion we consider—the dominant contribution is from

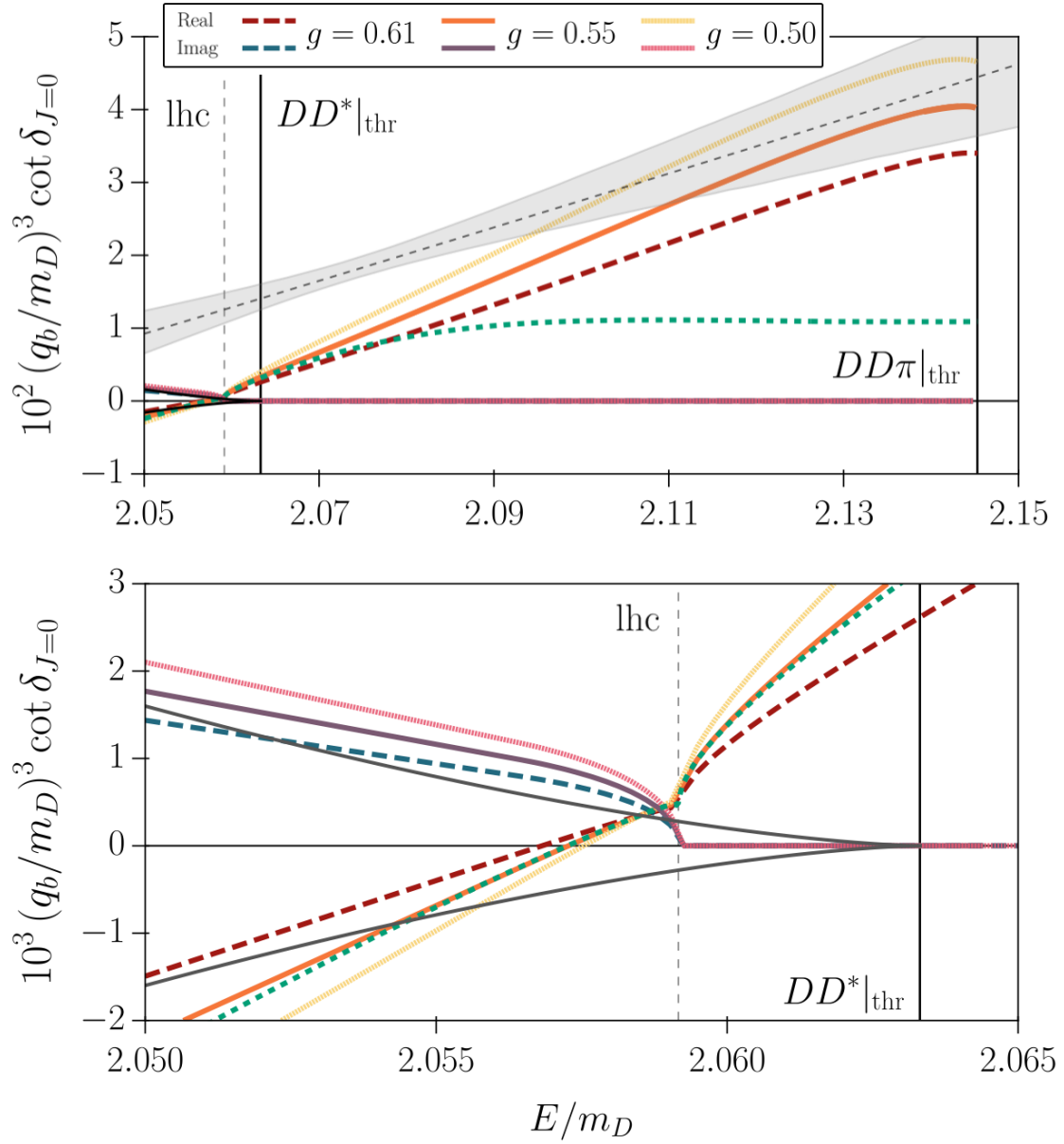


Figure 10: Results for $q_b^3 \cot \delta_{J=0}$, i.e. the DD^* interaction in the $\ell = 1$, $J^P = 0^-$ channel. As denoted in the legend, these are obtained for our standard values of the coupling g , with $m_D^2 \mathcal{K}_3^E = 1.9 \cdot 10^5$, $\mathcal{K}_3^{\text{iso},0} = \mathcal{K}_3^{\text{iso},1} = \mathcal{K}_3^B = 0$, and with our standard choice of the $D\pi$ s -wave scattering parameters (eq. (4.3)). In addition, we present as a green dashed line, the result obtained using the spartan model for the $D\pi$ s -wave interaction, as described in the text. The gray band centered around the dashed gray line is the result of a two-parameter ERE fit to the lattice spectrum using the QC2, as reported in ref. [9]. Dark gray lines correspond to $\pm |q_b/m_D|^3$, crossings of which above the left-hand cut correspond to bound or virtual states. The lower plot zooms in on the subthreshold region, showing the absence of any such crossings.

the ladder amplitude. In particular, the clear disagreement in slope with the result from ref. [9] is not resolved by adding the $\mathcal{K}_3^{\text{iso},0}$, $\mathcal{K}_3^{\text{iso},1}$, or \mathcal{K}_3^B contributions. We note, however, that our result is consistent with that reported in ref. [21]—in both approaches $q_b^3 \cot \delta_{J=0}$ has a considerably larger slope than that from ref. [9]. We speculate that this difference may be due to the fact that the lattice data are fit using an ERE parametrization that does not include the effects of the one-pion exchange. We do find agreement with ref. [9] on the absence of virtual or bound states in this channel.

Finally, we note that the $J^P = 0^-$ solution, unlike that for $J^P = 1^+$, displays considerable dependence on the s -wave $D\pi$ scattering parameters, particularly at higher energies. This is true even given our assumption, discussed in section 4.1, of weak, attractive interactions in this subchannel. We recall that our main solutions are based on the ERE parameters in eq. (4.3), which lead to a D_0^* resonance. To illustrate the dependence on the choice of interaction, we have repeated the calculation (for $g = 0.55$) using the spartan $D\pi$ s -wave model, with $m_D a_0^{(1)} = 3.0$, and $r_0^{(1)} = 0$. The result is shown in figure 10 by the green, dashed curve. Although for this case the $J^P = 1^+$ phase shifts do not deviate visibly from the results presented above, the slope of $q_b^3 \cot \delta_{J=0}$ significantly decreases at higher energies. We stress, however, that the behavior near the DD^* threshold and the left-hand cut remains largely unchanged.

4.5 Comparison with the finite-volume energies

In the previous sections, we presented numerical results obtained by solving infinite-volume integral equations at a pion mass $m_\pi = 280$ MeV corresponding to the lattice ensemble of ref. [9]. We used values for the two-body scattering parameters that included the D^* and D_0^* in the $D\pi$ subchannel and were motivated by existing lattice results. We then tuned the three-body K matrix to match the DD^* s -wave phase shift results from ref. [9].

In this section, we present the numerical results obtained from the finite-volume formalism described in section 3, in particular the three-particle $DD\pi$ quantization condition QC3 and the two-particle DD^* QC2. The motivations for these two calculations are somewhat different. The aims in applying the QC3 are several. First, we wish to demonstrate that the formalism developed in ref. [22], in which the D^* is not treated as a separate external field, but rather appears as a bound state in the p -wave $D\pi$ system, works as expected. This approach avoids the need to use a $2 \leftrightarrow 3$ formalism along the lines of ref. [92]. The approach followed here has been previously used successfully in model systems of scalar particles with a shallow bound state [49, 51, 75], but here the new features are a binding momentum that is comparable to m_π and a bound state having spin.

Second, we wish to show that the QC3 successfully predicts the energy levels that lie at or below the left-hand cut due to single-pion exchange (those that are greyed out in the figures above). This is the major reason for using the three-particle formalism to describe the DD^* system [22].

Third, we want to see how well the levels predicted by the QC3 match those obtained in ref. [9]. We stress that we are not attempting a fit of this data using the QC3, but aiming for an “eyeball” comparison. This does, however, provide a consistency check of the entire QC3 formalism. And, finally, we wish to investigate which energy levels are

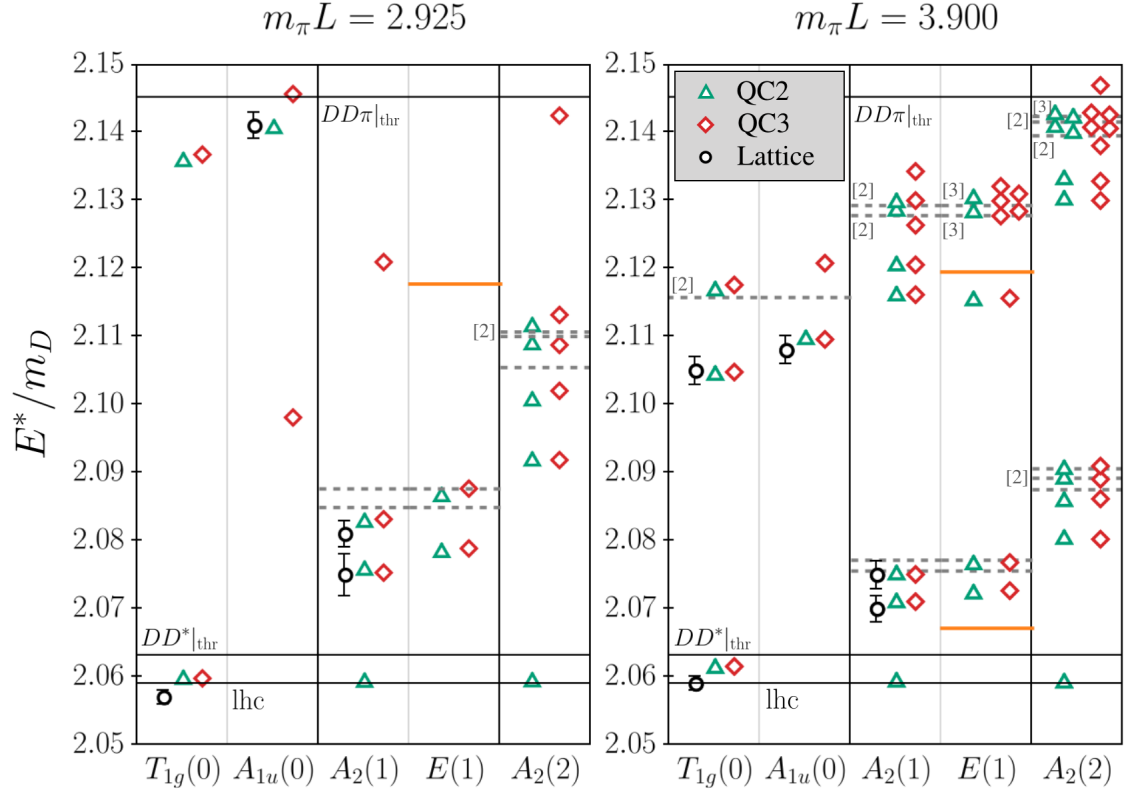


Figure 11: Finite-volume energy levels predicted by the QC3 (red diamonds) and QC2 (green triangles), compared to the levels found in a lattice computation [9] (black circles, with error bars.) Results are given for the c.m. frame energies. Levels are sorted horizontally according to their finite-volume irreps, using a notation described in the text. Details of the QC3 and QC2 methodology are described in the text. For the QC3 and QC2, only levels lying at or below the $DD\pi$ threshold are shown. Solid lines correspond to the positions of thresholds and the left-hand cut. Dashed lines correspond to the noninteracting DD^* energy levels. For the $T_{1g}(0)$ irrep, there is a non-interacting level lying underneath the DD^* threshold line for both values of L . The degeneracy of the noninteracting levels is denoted by a number next to the line, except if the level is nondegenerate. DD levels appear in the $E(1)$ irrep, and their noninteracting energies are shown as orange lines. Note the extra energy levels produced by the QC2 near the left-hand cut.

the most important for future lattice studies to focus on, in order to best constrain the underlying K matrix parameters.

As concerns the DD^* QC2, our main aim here is to investigate the manner in which it breaks down as one approaches the left-hand cut. A subsidiary aim is to see how well it matches the predictions of the QC3 in regions (i.e. above the DD^* threshold) where both QC2 and QC3 are valid. Differences between the results can arise from the dropped exponentially suppressed terms. For the quark masses we consider, the exponentially suppressed effects in the QC2 are dominated by the binding momentum of the D^* , $|q_0| \approx 0.87m_\pi$.

These effects, due to $D\pi$ loops, are automatically included in the QC3. However, the dropped finite-volume effects appear to be numerically small for the parameters used in the lattice simulations of ref. [9, 13]. The measured D^* masses on the two lattices used in these works are consistent within part per mille errors [93]. Furthermore, applying the QC2 to the $D\pi$ system with the p -wave ERE interaction used below, we find that the D^* on the smaller lattice is heavier, but only by about a part per mille. Angular-momentum truncation in the two-body quantization condition can also lead to differences between QC2 and QC3, but these are small in practice due to threshold suppression.

We now turn to the results, shown in figure 11. We determine the finite-volume spectrum for two values of the box size, $m_\pi L = 2.925$ and $m_\pi L = 3.9$, equal to those used in ref. [9].¹³ For the QC3 results, we set the K matrices to the central values used in the final results from the integral equations, i.e. those displayed in figures 5 to 8 and 10. Specifically, we set $g = 0.55$, $m_D^2 \mathcal{K}_3^E = 1.9 \cdot 10^5$, $\mathcal{K}_3^{\text{iso},0} = \mathcal{K}_3^{\text{iso},1} = \mathcal{K}_3^B = 0$, and $m_D a_0^{(2)} = -10^{-2}$, and use the s -wave $D\pi$ parameters of eq. (4.3). For the QC2, we use as input the phase shifts for the $J^P = 0^-, 1^+$ DD^* channels obtained from the solution to the integral equations using the same central values for the underlying parameters.

The results displayed in figure 11 are for the three irreps for which results are provided by ref. [9], together with two additional irreps, $E(1)$ and $A_2(2)$, to which the T_{cc}^+ channel contributes. The notation for irreps is standard in the lattice literature; see, e.g., ref. [94]. For example, $T_{1g}(0)$ indicates the T_{1g} irrep of the little group associated with a dimensionless total squared momentum $d^2 = 0$, where $\mathbf{d} = L/(2\pi) \mathbf{P}$. Of the quantum numbers studied above in infinite volume, the $J^P = 1^+$ irrep subduces into $T_{1g}(0)$, $A_2(1)$, $E(1)$, and $A_2(2)$, while $J^P = 0^-$ subduces into $A_{1u}(0)$, $A_2(1)$, and $A_2(2)$. Higher partial waves contribute to all irreps, but we do not consider such waves in this work.

The QC3 predictions in the figure are shown as red diamonds and can be compared to the results of ref. [9], shown as black circles with error bars. We note that, while with the QC3 we show levels up to the $DD\pi$ threshold, lattice levels are available in general only up to a lower energy. Thus the absence of a lattice level corresponding to one predicted by the QC3 does not necessarily indicate a disagreement. As discussed in section 3.2, the QC3 is strictly valid only up to the D^*D^* threshold, which lies at $E^*/m_D = 2.127$, slightly below the $DD\pi$ threshold. We expect the impact on the higher levels shown in the figure to be small since they lie close to the threshold.

Consider first the $T_{1g}(0)$ irrep on the two lattices. To good approximation, this channel picks out the tetraquark quantum numbers. The lowest level corresponds, in the noninteracting limit, to a DD^* pair with both at rest, whose energy is that of the DD^* threshold (which is noted in the figure). The lattice and QC3 levels lie below this, as expected for an attractive interaction, with the former lying at (for the larger volume) or below (the smaller volume) the left-hand cut. For our chosen parameters, the QC3 levels do not reach

¹³The exponentially-suppressed terms that are not included in the QC3 are generically of size $\exp(-m_\pi L)$. The rule of thumb used in lattice simulations is that one should take $m_\pi L \gtrsim 4$ to minimize these effects. The smaller volume used in ref. [9] clearly violates this inequality. However, as noted in section 3.1, there is numerical and theoretical evidence that these dropped effects have an additional suppression in systems including D mesons.

this low. However, were we to use the parameters corresponding to $g = 0.61$, the QC3 level on the smaller lattice would lie below the left-hand cut. This illustrates that the QC3 can predict levels at or below this cut.

The excited $T_{1g}(0)$ levels correspond in the noninteracting limit to a D and D^* with opposite momenta of unit dimensionless length. This “free” level is doubly degenerate, and the QC3 predicts that one of these levels is lowered by interactions, while the other is slightly pushed up. This can be seen on the larger volume, by comparing to the horizontal dashed line.¹⁴ Only the lower of the two levels is available from the lattice, and the agreement is good. On the smaller volume, only the lower level falls below the $DD\pi$ threshold (with the free energy lying above this threshold) and the corresponding lattice level is not available.

We next consider the $A_{1u}(0)$ irrep, which is sensitive primarily to the $J^P = 0^-$ channel, with no contributions from the tetraquark channel. On the larger volume, the QC3 finds two levels, the lower of which corresponds to the same free DD^* level with moving D and D^* as appears in the $T_{1g}(0)$ irrep, although this level has degeneracy 1 in the $A_{1u}(0)$ case. The upper level corresponds to the free $DD\pi$ state with all particles at rest, lowered substantially from the noninteracting energy by the subchannel interactions. We make this identification by gradually turning on the interactions and tracking the levels. On the smaller volume, the order of the two levels is inverted, with the lower level (around $E^*/m_D = 2.1$) being the (much lowered) $DD\pi$ state. The absence of lattice states corresponding to these “ $DD\pi$ ” levels on the two volumes is likely due to ref. [9] not including $DD\pi$ operators.

Next, we consider the irreps in moving frames. Lattice levels are available only for the $A_2(1)$ case, which we discuss first. The lower pair of nearly degenerate free levels correspond to a moving D with a D^* at rest, or vice versa. Both levels are lowered by interactions, and the matching of QC3 results to those from the lattice is good on both volumes. On the larger volume, the first excited $A_2(1)$ levels fall within our energy range, with each free level being doubly degenerate. The QC3 finds these four levels, and also a fifth level that corresponds to a $DD\pi$ level with one of the D s moving, the free energy of which lies just above the displayed energy range at $E^*/m_D \approx 2.16$. On the smaller volume, the single level at $E^*/m_D \approx 2.12$ is also a lowered $DD\pi$ level (whose free energy is $E^*/M_D \approx 2.171$).

The next irrep is the $E(1)$, which we include as the tetraquark contributes to this channel, but $J^P = 0^-$ does not. Thus it is more sensitive to tetraquark properties than the $A_2(1)$, which has contributions from both channels. The pattern of predicted levels is similar to that for the $A_2(1)$, with two main differences. First, we find that the lower pair of levels lie above the corresponding levels in the $A_2(1)$ irrep. Second, the first excited pair of levels, whose free energies match those in the $A_2(1)$ irrep, have a degeneracy of 3 rather than 2. The QC3 finds all these levels, some shifted down and others up relative to the free energies.

¹⁴The free energies are given by $E^*(\mathbf{p}, \mathbf{k}) = \sqrt{E(\mathbf{p}, \mathbf{k})^2 - (\mathbf{p} + \mathbf{k})^2}$ where $E(\mathbf{p}, \mathbf{k}) = \omega_p^D + \omega_k^{D^*}$, and \mathbf{p} and \mathbf{k} are the finite-volume momenta of the D and D^* , respectively.

Parity is not conserved in moving frames, and this leads to mixing between $J^P = 1^+$ and $J^P = 1^-$ states in some irreps, such as the $E(1)$ irrep. This is an issue in the three-body formalism, since DD and $DD\pi$ states with $J^P = 1^-$ can mix, and two-to-three transitions are not included in the QC3 [22] (although doing so would be possible with an extended formalism). However, this mixing is likely to be small, and we only expect it to induce important finite-volume effects if the DD and $DD\pi$ levels lie close to each other. For this reason, we show in the figure the position of the noninteracting DD levels in the $E(1)$ irrep. On the smaller volume, the DD level is well separated from the QC3 levels, while on the larger volume, mixing may be more of an issue.

The final irrep we consider is the $A_2(2)$, which we include to show how moving frames with larger momenta can provide additional constraints. The tetraquark contributes to this channel, as does $J^P = 0^-$, but there is no mixing with DD states. This irrep offers more states (four) in the lower band than $A_2(1)$. In the upper band (only present on the larger volume) the topmost level is likely a lowered $DD\pi$ state.

We have investigated the sensitivity of these results to the parameters in \mathcal{K}_3 . By far the greatest sensitivity is to \mathcal{K}_3^E , which impacts all levels. If we set $\mathcal{K}_3^E = 0$ (rather than the standard value of $1.9 \cdot 10^5$) then the QC3 prediction for the lightest $T_{1g}(0)$ state for the smaller volume moves above the DD^* threshold, and the splitting between the two lowest $A_2(1)$ states is more than halved on both volumes. This demonstrates that a nonzero \mathcal{K}_3 is needed to have a reasonable description of the lattice data, just as was the case when solving the integral equations.

The other parameters in \mathcal{K}_3 , namely $\mathcal{K}_3^{\text{iso},0}$, $\mathcal{K}_3^{\text{iso},1}$, and \mathcal{K}_3^B , do not contribute to the $T_{1g}(0)$ and $E(1)$ levels. For the other irreps, their contributions to the energies of the levels shown are an order of magnitude smaller than those of \mathcal{K}_3^E , if we choose these parameters to have the same size as \mathcal{K}_3^E .

Finally, we turn to the results from the QC2, which are shown as green triangles in figure 11. Again we have displayed all levels up to the $DD\pi$ threshold, ignoring the coupling to the D^*D^* channel. We observe that there is a good matching with the QC3 (and lattice) levels in the expected region, i.e., away from the left-hand cut, with the exception that the QC2 is missing states in the $A_{1u}(0)$ and $A_2(1)$ irreps that are predicted by the QC3. These missing states are, however, those that, as discussed above, correspond to $DD\pi$ states shifted down by interactions. Thus it is not surprising that they are missed by the QC2, which does not have a $DD\pi$ component. Additionally, the QC2 misses some excited $E(1)$ and $A_2(2)$ states, which is likely due to our truncation of the QC2 to $J < 2$. Overall, however, the use of the QC2 in refs. [9, 13] for the levels above the DD^* threshold appears justified.

The situation is different close to the left-hand cut. We know that the QC2 breaks down at, and likely slightly above, this cut. We find evidence of this in the appearance of solutions in the $A_2(1)$ and $A_2(2)$ irreps slightly above this cut, that are not present in the QC3 and thus clearly spurious. On the other hand, we note that the levels slightly above the cut that are predicted in the $T_{1g}(0)$ irrep do match well with those from the QC2.

5 Summary and outlook

In this work, we have described and implemented numerically the infinite-volume integral equations and the three-body finite-volume quantization condition for the $I = 0$ $DD\pi$ system. These steps complete the formalism proposed in ref. [22] and provide a ready-to-use methodology for the rigorous lattice determination of the properties of the T_{cc}^+ . The approach applies to computations at both physical and heavier quark masses. In particular, unlike the traditional two-body formalism, it remains valid for energies near or on the left-hand cut associated with one-pion exchange in the DD^* system.

The first part of our analysis involves solving the RFT partial-wave projected three-body integral equations, extending previous studies. Specifically, this is the first application of these equations to hadrons with unequal masses, which requires the consideration of two distinct pair-spectator channels. In addition, we include multiple two-body and three-body partial waves, using the results of ref. [67] and appendix A. We also consider for the first time terms beyond the isotropic approximation in the threshold expansion of the three-body K matrix. This requires an extension of previous implementations of the integral equations. These methods are easily generalizable to other three-body systems of interest.

In the integral equations, we use a model of $D\pi$ and DD interactions based on existing lattice data and effective theories, and estimate values for the unknown three-body parameter \mathcal{K}_3^E by matching the amplitude to existing DD^* results [9]. By implementing LSZ reduction, we obtain the DD^* elastic amplitude and find that the T_{cc}^+ manifests as a pair of subthreshold complex poles on the unphysical Riemann sheet, in agreement with the literature. We investigate the DD^* phase shifts and the T_{cc}^+ pole position for different interaction models, including and excluding partial-wave mixing. We find that partial-wave mixing between s and d waves in the DD^* system is unimportant for physical kinematics, but its inclusion has a significant impact on the phase shifts below the DD^* threshold.

In the second part, we implement the three-particle quantization condition (QC3) for the $DD\pi$ system, using it to describe the DD^* energy levels down to and below the onset of the left-hand cut. This tests the strategy proposed in ref. [22], in which the D^* is introduced in the QC3 as a pole in the $D\pi$ p -wave amplitude. Our predicted energies match those obtained from lattice QCD. We also explore the limitations of the two-particle DD^* quantization condition. While it produces energy levels consistent with those from the QC3 above the elastic threshold, it breaks down near the left-hand cut, as expected. This confirms the advantage of using the three-particle approach in this system.

Looking forward, we suggest several extensions of the lattice calculations that would allow for a more robust study of the T_{cc}^+ . First, our results show that $DD\pi$ -like states are intermingled with those that are qualitatively DD^* -like. Since in finite volume these states mix, it is important to include $DD\pi$ interpolating operators in the lattice calculations. Second, extending the spectrum up to the D^*D^* or $DD\pi$ thresholds would lead to additional constraints on the K matrices. Similarly, additional finite-volume irreps could be studied, which may be good windows into the properties of T_{cc}^+ . Examples are the $E(1)$ and $A_2(2)$ irreps in figure 11. Finally, results for the $I = 1$ DD and $I = 1/2$ $D\pi$ channels (the latter for both s and p waves) are needed in the three-body description of the T_{cc}^+ .

Other infinite-volume approaches [16, 19, 95, 96] have been developed for the analysis of the T_{cc}^+ and related systems. While these methods differ from ours in their technical implementation, preliminary investigations indicate that the nonrelativistic limit of our equations leads to a formalism that is essentially equivalent to that of these approaches. A careful comparison is left for future work. Moreover, we note that the integral equations described here provide a general parametrization for the three-meson amplitudes and may be also used in the phenomenological description of experimental data for the $T_{cc}^+ \rightarrow DD\pi$ decay, similar to refs. [16, 19]. We also leave this for future work.

In summary, this proof-of-concept study presents key ideas in the three-body treatment of T_{cc}^+ and opens the door for further studies in Lattice QCD. Although the parametrizations of the K matrices can be refined as more lattice QCD data becomes available, the overall workflow established in this work will remain unchanged. Given the recent advances in lattice QCD results for three-hadron scattering [52, 54, 65, 97–111], we expect substantial progress for the $DD\pi$ system in the near term, and anticipate that the strategy outlined here will play a central role.

Acknowledgments

We wish to thank Saša Prelovšek for pointing us a discrepancy between our preliminary results and the literature, which helped to resolve a critical issue in our study. We also thank Raúl Briceño and Andrew Jackura for insightful conversations about the partial-wave projection of the OPE amplitude. We thank Jeremy Green for discussions related to finite-volume irreps. Furthermore, we are grateful to Vadim Baru, Raúl Briceño, Meng Lin Du, Max Hansen, Andrew Jackura, Saša Prelovšek, and Haobo Yan for many other valuable discussions regarding this work. We also thank Saša Prelovšek and Madanagopalan Padmanath for sharing with us data from ref. [9]. SMD and SRS acknowledge the financial support through the U.S. Department of Energy Contract No. DE-SC0011637. FRL acknowledges partial support by the USDOE Contract No. DE-SC0011090 and DE-SC0021006, and the Mauricio and Carlota Botton Fellowship. This work contributes to the goals of the USDOE ExoHad Topical Collaboration, contract DE-SC0023598.

A Partial-wave projection of OPE and \mathcal{K}_3

As described in the main text, we project the integral equations onto definite total angular momentum in the three-body c.m. frame prior to solving them. The rotation invariance of each quantity in the integral equations then propagates this projection separately onto each term. Thus we need to determine the projection of the OPE kernel G , the two-particle amplitude \mathcal{M}_2 , and the three-particle K matrix. We discuss details of this projection in this appendix. We note that a very general formula for the projection of G has been derived in ref. [67], including results that we need. Our discussion here offers an alternative presentation, which we hope will be useful to the readers. Our explicit results agree with those of ref. [67]. We make extensive use of the discussion of angular momentum projections given in ref. [69].

A.1 Basic results

Following the discussion in the main text, on-shell states of three spinless particles of given E , and having $\mathbf{P} = 0$, can be described by the momentum of the spectator, \mathbf{k} , the pair's spin s , and the helicity λ of the pair relative to its momentum, $-\mathbf{k}$. Here we consider the kinematic variables used in the main text for the initial state, although the following considerations apply equally well to the final state. The following discussion is independent of the flavor of the spectator, which enters only into the kinematics, so we keep the flavor index implicit. Since the three-particle state is analogous to a solid body, we can obtain a general state from that in which \mathbf{k} is aligned along the z axis by applying a rotation specified in the standard manner by three Euler angles. To be completely explicit, this state is given by

$$|\alpha, \beta, \gamma; -\lambda\rangle \equiv \mathcal{U}[R(\alpha, \beta, \gamma)]\{\mathcal{U}[L_z(k)]|0, 0\rangle \otimes \mathcal{U}[L_z(-k)]|s, -\lambda\rangle\}, \quad (\text{A.1})$$

where $|0, 0\rangle$ and $|s, -\lambda\rangle$ are, respectively, the states in which the spectator and the pair are at rest. We use the standard notation for angular momentum eigenstates, $|s, m\rangle$, with m

the azimuthal component of the spin along the z axis. For the pair, we have $m = -\lambda$, since the helicity is determined relative to $-\mathbf{k} = k(-\hat{z})$. The unitary operators in eq. (A.1) implement the boosts and rotations (defined in an active sense), with, for example, $L_z(k)$ indicating the boost that brings the spectator from rest to the momentum $k\hat{z}$.

Following ref. [69], the projection onto a state of definite total angular momentum J and azimuthal component M is achieved by integrating with an appropriate Wigner D function,¹⁵

$$|JM, -\lambda\rangle = \frac{\sqrt{2J+1}}{8\pi^2} \int d\alpha dc_\beta d\gamma D_{M\mu}^{J*}(\alpha, \beta, \gamma) |\alpha, \beta, \gamma; -\lambda\rangle, \quad (\text{A.2})$$

where $c_\beta \equiv \cos \beta$, and μ can, at this state, take any value satisfying $|\mu| \leq J$. Using the result

$$D_{M\mu}^{J*}(\alpha, \beta, \gamma) = D_{M\mu}^{J*}(\alpha, \beta, 0) e^{i\gamma\mu}, \quad (\text{A.3})$$

together with,

$$|\alpha, \beta, \gamma; -\lambda\rangle = |\alpha, \beta, 0; -\lambda\rangle e^{i\gamma\lambda}, \quad (\text{A.4})$$

one can do the integral over γ ; this sets $\mu = -\lambda$ and yields,

$$|JM, -\lambda\rangle = \frac{\sqrt{2J+1}}{4\pi} \int d\alpha dc_\beta D_{M-\lambda}^{J*}(\alpha, \beta, 0) |\alpha, \beta, 0; -\lambda\rangle. \quad (\text{A.5})$$

We stress that these states transform correctly under rotations for any allowed choice of λ . Conversion to the LS basis is then achieved by the following unitary transformation [69],

$$|JM; \ell s\rangle = \sqrt{\frac{2\ell+1}{2J+1}} \sum_\lambda |JM; -\lambda\rangle \langle J, -\lambda | \ell, m_\ell = 0; s, -\lambda\rangle. \quad (\text{A.6})$$

To implement the above-described projection, and in particular the integral over the Euler angles α and β for both initial and final states, we will need to determine the dependence of the quantities to be projected (G , \mathcal{M}_2 , and $\mathcal{K}_{\text{df},3}$) on the angles denoted $\Omega_k^* = (\vartheta_k^*, \varphi_k^*)$ and $\Omega_p^* = (\vartheta_p^*, \varphi_p^*)$ in the main text (see section 2.1). Focusing on the initial spectator, we recall that the angles Ω_k^* are determined relative to a coordinate system in which the z axis is aligned with the direction of the pair's momentum in the c.m. frame. Thus we need to define this system. To do so, we start with an arbitrarily chosen right-handed triplet of axes (i.e. a space-fixed coordinate system). We then apply the Euler rotation $R(\phi, \theta, 0)$ that brings \hat{z} to the direction of the pair, $\hat{q} \equiv -\hat{k}$. (We use \hat{q} for brevity and generality.) This implies that the resulting y axis (whose direction is denoted \hat{y}_q) lies in the original xy plane. The explicit forms are given by¹⁶

$$\hat{z}_q = \hat{q}, \quad \hat{y}_q = \frac{\hat{z} \times \hat{q}}{\sqrt{1 - (\hat{q} \cdot \hat{z})^2}}, \quad \text{and} \quad \hat{x}_q = \hat{y}_q \times \hat{z}_q = \frac{\hat{q}(\hat{q} \cdot \hat{z}) - \hat{z}}{\sqrt{1 - (\hat{q} \cdot \hat{z})^2}}. \quad (\text{A.7})$$

We note that the “ q basis” triplet $\{\hat{x}_q, \hat{y}_q, \hat{z}_q\}$ is invariant under the boost along \hat{q} that connects the pair's rest frame to the three-body c.m. frame.

¹⁵We use a different normalization from ref. [69], chosen so that a state that is independent of the angles projects with unchanged normalization onto $J = 0$.

¹⁶These expressions are ambiguous as $\hat{q} \rightarrow \pm\hat{z}$, but this ambiguity cancels in the final results.

Further kinematic results that we will need are the components of the quantities \mathbf{k}_p^* (\mathbf{p}_k^*) relative to the above-described coordinate systems for the final (initial) pair. These quantities, defined in the main text below eq. (2.27), are, respectively, the initial (final) spectator momentum boosted to the final (initial) pair's c.m. frame. Focusing on the initial spectator, and keeping in mind that the final pair momentum is $\hat{q} = -\hat{p}$, we find,

$$\begin{aligned} (\mathbf{k}_p^*)_{z_{-p}} &= -\gamma_p(\beta_p \omega_k + k c_\Theta), \\ \frac{(\mathbf{k}_p^*)_{x_{-p}}}{k} &= \frac{(\hat{p} c_\Theta - \hat{k}) \cdot \hat{z}}{\sqrt{1 - (\hat{p} \cdot \hat{z})^2}}, \\ \frac{(\mathbf{k}_p^*)_{y_{-p}}}{k} &= -\frac{\hat{z} \cdot \hat{p} \times \hat{k}}{\sqrt{1 - (\hat{p} \cdot \hat{z})^2}}. \end{aligned} \quad (\text{A.8})$$

Here $c_\Theta = \cos \Theta$, with Θ the angle between \mathbf{p} and \mathbf{k} . Analogous equations hold for the components of \mathbf{p}_k^* relative to coordinate system with $\hat{q} = -\hat{k}$, and are obtained by $p \leftrightarrow k$ interchange.

A.2 Projection formula for OPE kernel G

We first project onto JM states with given pair helicities, and later convert to the LS basis. Using the results above, the first step yields,

$$G_{s'\lambda';s\lambda}^{(ij)JM}(p, k) = \frac{2J+1}{(4\pi)^2} \int_{\Omega_p} \int_{\Omega_k} D_{M,-\lambda'}^J(\Omega_p) D_{M,-\lambda}^{J*}(\Omega_k) G_{s'\lambda';s\lambda}^{(ij)}(\mathbf{p}, \mathbf{k}), \quad (\text{A.9})$$

where we are using the shorthand $\int_{\Omega_p} \equiv \int d\alpha_p d\cos\beta_p$, while Ω_p stands for the rotation $R(\alpha_p, \beta_p, 0)$ that brings \hat{z} into the direction \hat{p} , and similarly with $p \rightarrow k$. The equality of the initial and final values of J and M , which is built into this expression, is due to the overall rotation invariance of $G^{(ij)}$.

Pulling out factors that are independent of the orientations of \mathbf{p} and \mathbf{k} , we can rewrite eq. (A.9) as,

$$G_{s'\lambda';s\lambda}^{(ij)JM}(p, k) = \frac{H_{ij}(p, k)}{(q_p^*)^{s'}(q_k^*)^s} \mathcal{G}_{s'\lambda';s\lambda}^{(ij)JM}(p, k), \quad (\text{A.10})$$

where,

$$\mathcal{G}_{s'\lambda';s\lambda}^{(ij)JM}(p, k) = \frac{2J+1}{(4\pi)^2} \int_{\Omega_p} \int_{\Omega_k} D_{M,-\lambda'}^J(\Omega_p) D_{M,-\lambda}^{J*}(\Omega_k) \frac{\mathcal{Y}_{s'\lambda'}^*(\mathbf{k}_p^*) \mathcal{Y}_{s\lambda}(\mathbf{p}_k^*)}{b_{\mathbf{p}\mathbf{k}}^2 - m_{ij}^2 + i\epsilon}. \quad (\text{A.11})$$

Here $\mathcal{Y}_{\ell m}(\mathbf{p}) = \sqrt{4\pi} p Y_{\ell m}(\hat{p})$ are harmonic polynomials normalized following the RFT conventions [22]. It follows from rotation invariance that this expression is independent of M , as can be checked explicitly. Thus, we can replace the factor of $2J+1$ with a sum over M , which allows the two Wigner D matrices to be combined, using their unitarity. The result (with superscript M now dropped) is,

$$\mathcal{G}_{s'\lambda';s\lambda}^{(ij)J}(p, k) = \frac{1}{(4\pi)^2} \int_{\Omega_p} \int_{\Omega_k} D_{-\lambda', -\lambda}^{J*}(\Omega_p^{-1} \Omega_k) \frac{\mathcal{Y}_{s'\lambda'}^*(\mathbf{k}_p^*) \mathcal{Y}_{s\lambda}(\mathbf{p}_k^*)}{b_{\mathbf{p}\mathbf{k}}^2 - m_{ij}^2 + i\epsilon}. \quad (\text{A.12})$$

To perform the integrals over the orientations of \hat{p} and \hat{k} we proceed as follows. First, we treat the reaction plane as a solid body defined by the ordered vectors \mathbf{p} and \mathbf{k} , and integrate over its orientation with the standard Euler angles.¹⁷ In order to make it easier to use in the results given above for the orientation of the helicity axes, the $\alpha = \beta = \gamma = 0$ configuration is chosen to be that in which \hat{p} is aligned along the z axis, while \hat{k} lies in the xz plane with positive x component. Second, we integrate the angle Θ between \mathbf{p} and \mathbf{k} . These steps correspond to the variable transformation,

$$\int_{\Omega_p} \int_{\Omega_k} = \int d\alpha d\beta d\gamma d\Theta. \quad (\text{A.13})$$

We thus need to express the rotations characterized by Ω_p and Ω_k in terms of the new angles. For Ω_p this is straightforward,

$$R(\Omega_p) = R(\alpha, \beta, 0). \quad (\text{A.14})$$

To obtain Ω_k , we can first rotate from \hat{p} to \hat{k} while they are in the xz plane and then do the full solid-body rotation. This does not, however, lead to an orientation, i.e. a rotation described by two Euler angles; to obtain this, we must add an initial rotation about the lab z axis,

$$R(\Omega_k) = R(\alpha', \beta', 0) = R(\alpha, \beta, \gamma) R(0, \Theta, 0) R(0, 0, -\delta). \quad (\text{A.15})$$

Explicit expressions for α' , β' and δ in terms of α , β , γ , and Θ can be obtained, but will not be needed in the following. What we do require is the result,

$$R(\Omega_p^{-1} \Omega_k) = R(\gamma, \Theta, -\delta). \quad (\text{A.16})$$

which follows from eqs. (A.14) and (A.15). Thus the Wigner D matrix needed in eq. (A.12) is given by,

$$D_{-\lambda', -\lambda}^{J*}(\Omega_p^{-1} \Omega_k) = e^{-i\gamma\lambda'} d_{-\lambda', -\lambda}^J(\Theta) e^{i\delta\lambda}, \quad (\text{A.17})$$

where we have used the reality of the d^J matrices.

We also need to express the x and y components of \mathbf{k}_p^* in its helicity basis, given by eq. (A.8), in terms of the new angles, and similarly for \mathbf{p}_k^* . After some effort, we find,

$$(\mathbf{k}_p^*)_{x-p} = k s_\Theta c_\gamma, \quad (\mathbf{k}_p^*)_{y-p} = -k s_\Theta s_\gamma, \quad (\text{A.18})$$

where $s_\Theta = \sin \Theta$, etc., and,

$$(\mathbf{p}_k^*)_{x-k} = -p s_\Theta c_\delta, \quad (\mathbf{p}_k^*)_{y-k} = p s_\Theta s_\delta. \quad (\text{A.19})$$

It follows that the phases of the harmonic polynomials entering $\mathcal{G}^{(ij)}$, eq. (A.12), are

$$\mathcal{Y}_{s'\lambda'}^*(\mathbf{k}_p^*) \propto e^{i\gamma\lambda'}, \quad \mathcal{Y}_{s\lambda}(\mathbf{p}_k^*) \propto e^{-i\delta\lambda}, \quad (\text{A.20})$$

with the proportionality constants being functions only of Θ . This shows that the unprojected $G^{(ij)}$ depends on angles other than Θ , although not on α . However, in the projected

¹⁷Denoted α , β , and γ , which should not be confused with the earlier use of the same symbols for different angles in eq. (A.2).

version eq. (A.12) the dependence on γ and δ cancels between the phases in the harmonic polynomials and those in the Wigner D functions, as can be seen by comparing eqs. (A.17) and (A.20).

The conclusion is that the integrand in eq. (A.12) depends only on Θ , allowing the integral over the other three angles to be done trivially. Using the result,

$$d_{-\lambda', -\lambda}^J(\Theta) = d_{\lambda, \lambda'}^J(\Theta), \quad (\text{A.21})$$

we obtain the final equation,

$$\mathcal{G}_{s'\lambda'; s\lambda}^{(ij)J}(p, k) = \frac{1}{2} \int dc_{\Theta} d_{\lambda, \lambda'}^J(\Theta) \frac{\mathcal{Y}_{s'\lambda'}^*(\mathbf{k}_p^*) \mathcal{Y}_{s\lambda}(\mathbf{p}_k^*)}{b_{ij}^2 - m_k^2 + i\epsilon} \Big|_{\alpha=\beta=\gamma=0}. \quad (\text{A.22})$$

Since the full integrand of eq. (A.12) is independent of α , β , and γ , we can set these angles to any value. The choice $\alpha = \beta = \gamma = 0$ is the simplest, since it sets $\delta = 0$ and thus removes the phase dependence from the Wigner D matrix in eq. (A.17).

Finally, converting to the LS basis using eq. (A.6), we obtain,

$$\begin{aligned} \mathcal{G}_{\ell' s'; \ell s}^{(ij)J}(p, k) &= \frac{\sqrt{(2\ell' + 1)(2\ell + 1)}}{2J + 1} \sum_{\lambda' \lambda} \langle J, -\lambda' | \ell', 0; s', -\lambda' \rangle \langle J, -\lambda | \ell, 0; s, -\lambda \rangle \\ &\times \frac{1}{2} \int dc_{\Theta} d_{\lambda, \lambda'}^J(\Theta) \frac{\mathcal{Y}_{s'\lambda'}^*(\mathbf{k}_p^*) \mathcal{Y}_{s\lambda}(\mathbf{p}_k^*)}{b_{\mathbf{p}\mathbf{k}}^2 - m_{ij}^2 + i\epsilon} \Big|_{\alpha=\beta=\gamma=0}, \end{aligned} \quad (\text{A.23})$$

leading to the final form for the projection of G in the LS basis,

$$G_{\ell' s'; \ell s}^{(ij)J}(p, k) = \frac{H_{ij}(p, k)}{(q_p^*)^{s'} (q_k^*)^s} \mathcal{G}_{\ell' s'; \ell s}^{(ij)J}(p, k). \quad (\text{A.24})$$

The integrals that we require in eq. (A.23) can be brought to the form,

$$I^{(n)}(z_{ij}) = \int \frac{dc_{\Theta}}{2} \frac{c_{\Theta}^n}{(z_{ij}(p, k) - c_{\Theta} + i\epsilon)}, \quad (\text{A.25})$$

where

$$z_{ij}(p, k) = \frac{(E - \omega_p - \omega_k)^2 - p^2 - k^2 - m_{ij}^2}{2pk}. \quad (\text{A.26})$$

The cases that we need are,

$$I^{(0)}(z) = \frac{1}{2} \log \left(\frac{z + 1 + i\epsilon}{z - 1 + i\epsilon} \right), \quad (\text{A.27})$$

$$I^{(1)}(z) = z I^{(0)}(z) - 1, \quad (\text{A.28})$$

$$I^{(2)}(z) = z^2 I^{(0)}(z) - z, \quad (\text{A.29})$$

$$I^{(3)}(z) = z^3 I^{(0)}(z) - z^2 - \frac{1}{3}. \quad (\text{A.30})$$

These integrals can be expressed in terms of Legendre polynomials of the second kind as,

$$\begin{aligned} I^{(0)}(z) &= Q_0(z), \\ I^{(1)}(z) &= Q_1(z), \\ I^{(2)}(z) &= \frac{2}{3} Q_2(z) + \frac{1}{3} Q_0(z), \\ I^{(3)}(z) &= \frac{2}{5} Q_3(z) + \frac{3}{5} Q_1(z), \end{aligned} \quad (\text{A.31})$$

with the proviso that the logarithmic cut runs between the singular points at $z = -1$ and $z = 1$. This ensures that the OPE singularity leads to an imaginary part in the kinematic regime where the exchanged particle can go on shell. We note that all Legendre polynomials have their logarithmic cut at the same position in the z variable, implying that inclusion of higher partial waves in the integral equations does not introduce additional singularities compared to the purely s -wave scenario (defined as $J = 0$, $(\ell' s'; \ell s) = (00; 00)$.)

In appendix B we give the explicit forms for the projected G in terms of the $Q_i(z)$.

A.3 Projection of \mathcal{K}_3

We consider the threshold expansion for \mathcal{K}_3 given in eq. (2.49). The first step is to express \mathcal{K}_3 in the $\{ks\lambda\}$ basis. This has been carried out in ref. [42], and we can carry over the results with only two adjustments. The first is that here we use the helicity basis, as discussed for G above. The second adjustment arises from our use of standard complex spherical harmonics (as opposed to the real versions used in ref. [42]). Thus we must specify which harmonics are complex conjugated. With our choice, the final state spherical harmonic that is pulled out of \mathcal{K}_3 (which depends on the direction of the primary member of the final state pair in the pair c.m. frame) is not conjugated, while the corresponding initial-state harmonic is conjugated. This implies that the harmonic functions that appear in the resulting helicity-basis form of \mathcal{K}_3 have the same conjugation structure as for G , namely the final-state harmonic is conjugated while the initial-state one is not. One result of this structure is that the phase cancellation described above for G between eqs. (A.17) and (A.20) applies to \mathcal{K}_3 as well. This can be shown by an extension of the methods used above.

Thus, again, all angles except Θ can be trivially integrated, leading to the master formula

$$\begin{aligned} \mathcal{K}_{3;\ell' s'; \ell s}^{(ij)J} = & \frac{\sqrt{(2\ell' + 1)(2\ell + 1)}}{2J + 1} \sum_{\lambda' \lambda} \langle J, -\lambda' | \ell', 0; s', -\lambda' \rangle \langle J, -\lambda | \ell, 0; s, -\lambda \rangle \\ & \times \int \frac{dc_\Theta}{2} d_{\lambda, \lambda'}^J(\Theta) \mathcal{K}_{3; s' \lambda'; s \lambda}^{(ij)}(\mathbf{p}, \mathbf{k}) \Big|_{\alpha=\beta=\gamma=0}. \end{aligned} \quad (\text{A.32})$$

We recall that the superscript (ij) refers to the flavors of the final- and initial-state spectators, respectively.

In appendix C we give the explicit forms for the projections of \mathcal{K}_3 onto the channels of interest. To our knowledge, these results have not been presented previously. The integrals involved are all elementary. The only subtlety in the computation is the need to write the Cartesian Kronecker delta in the helicity basis. We do so using

$$\delta_{ij} = (\hat{x}_{-p})_i (\hat{x}_{-p})_j + (\hat{y}_{-p})_i (\hat{y}_{-p})_j + (\hat{z}_{-p})_i (\hat{z}_{-p})_j, \quad (\text{A.33})$$

where, in the final-state pair basis, and for $\alpha = \beta = \gamma = 0$,

$$\hat{x}_{-p} = (1, 0, 0), \quad \hat{y}_{-p} = (0, 1, 0), \quad \hat{z}_{-p} = (0, 0, 1), \quad (\text{A.34})$$

while in the initial-state pair basis

$$\hat{x}_{-p} = (c_\Theta, 0, -s_\Theta), \quad \hat{y}_{-p} = (0, 1, 0), \quad \hat{z}_{-p} = (s_\Theta, 0, c_\Theta). \quad (\text{A.35})$$

A.4 Projection of \mathcal{M}_2

We close this appendix with a derivation of the result eq. (2.15) for the projected form of \mathcal{M}_2 . The starting point is the form for this quantity prior to projection, given in the description of integral equations in sec. VII of ref. [38],

$$\mathcal{M}_{2;s'\lambda';s\lambda}^{(ij)}(\mathbf{p}, \mathbf{k}) = \delta_{ij}\eta_i 2\omega_k (2\pi)^3 \delta^3(\mathbf{p} - \mathbf{k}) \delta_{s's} \delta_{\lambda'\lambda} \mathcal{M}_{2,s}^{(i)}(p). \quad (\text{A.36})$$

Notation is explained in the main text.

The projection onto definite J, M is given, as in eq. (A.9), by

$$\mathcal{M}_{2;s'\lambda';s\lambda}^{(ij)JM}(p, k) = \frac{2J+1}{(4\pi)^2} \int_{\Omega_p} \int_{\Omega_k} D_{M,-\lambda'}^J(\Omega_p) D_{M,-\lambda}^{J*}(\Omega_k) \mathcal{M}_{2;s'\lambda';s\lambda}^{(ij)}(\mathbf{p}, \mathbf{k}). \quad (\text{A.37})$$

Writing the delta function as

$$\delta^{(3)}(\mathbf{p} - \mathbf{k}) = \frac{1}{p^2} \delta(p - k) \delta^{(2)}(\Omega_p - \Omega_k), \quad (\text{A.38})$$

performing the Ω_k integral to set $\Omega_k = \Omega_p$, and using,

$$\int_{\Omega} D_{\mu_1 m_1}^{j_1*}(\Omega) D_{\mu_2 m_2}^{j_2}(\Omega) = \frac{4\pi}{2j_1+1} \delta_{j_1 j_2} \delta_{\mu_1 \mu_2} \delta_{m_1 m_2}, \quad (\text{A.39})$$

we find,

$$\mathcal{M}_{2;s'\lambda';s\lambda}^{(ij)JM}(p, k) = \delta_{ij}\eta_i \tilde{\delta}(p - k) \delta_{s's} \delta_{\lambda'\lambda} \mathcal{M}_{2,s}^{(i)}(p), \quad (\text{A.40})$$

where $\tilde{\delta}(p - k)$ is defined in eq. (2.17). The lack of dependence on M is manifest.

Next we convert to the LS basis using eq. (A.6), which yields

$$\begin{aligned} \mathcal{M}_{2;\ell's';\ell s}^{(ij)J}(p, k) &= \frac{2\ell+1}{2J+1} \sum_{\lambda} \langle J, -\lambda | \ell', 0; s', -\lambda' \rangle \langle J, -\lambda | \ell, 0; s, -\lambda \rangle \\ &\quad \times \eta_i \delta_{ij} \delta_{s's} \delta_{\lambda'\lambda} \tilde{\delta}(p - k) \mathcal{M}_{2,s}^{(i)}(p). \end{aligned} \quad (\text{A.41})$$

Using the unitarity of the transformation in eq. (A.6), one immediately finds the result given in eq. (2.15) of the main text.

A similar derivation holds for the phase-space matrix $\tilde{\rho}$ that appears in the integral equations.

B Expressions for the partial-wave projection of OPE

To keep the formulas compact, we define relativistic factors as

$$\beta_p = \frac{p}{E - \omega_p}, \quad \gamma_p = \frac{1}{\sqrt{1 - \beta_p^2}}, \quad g_{pk} = \frac{\beta_p \gamma_p \omega_k}{k}, \quad (\text{B.1})$$

and analogous formulas with $k \leftrightarrow p$. We also abbreviate z_{ij} as simply z . Following ref. [67], we use the spectroscopic notation $(J, \ell, s) \equiv {}^{2s+1}\ell_J$ to denote transitioning pair-spectator states.

In the following, results in which $\{\ell', s'\}$ and $\{\ell, s\}$ are interchanged are not given in off-diagonal cases. The missing results are simply obtained by switching momenta, $p \leftrightarrow k$, and switching the corresponding spectator masses.

We also stress that the following results only hold for allowed choices of i and j . In particular, if $i = 2$, so that the final-state pair consists of two D mesons in a symmetric ($I = 1$) state, then the pair spin s' must be even. There is no such constraint for $i = 1$. Similar comments apply to the initial state and the corresponding index j .

Finally, in ref. [67] it is noted that a check on the results is obtained by expanding the expressions for $G^{(ij)}$ about $p = 0$ and $k = 0$ for fixed σ_p and σ_k . One expects that the projected G will have a leading dependence

$$G_{\ell' s'; \ell s}^{(ij)J}(p, k) \propto p^{\ell'} k^{\ell}, \quad (\text{B.2})$$

due to angular-momentum barrier factors. This expectation holds for all the following results.

B.1 $J^P = 1^+$

The $^1P_1 \rightarrow ^1P_1$ amplitude

$$G_{10;10}^{(ij)1}(p, k) = \frac{H_{ij}(p, k)}{2pk} Q_1(z). \quad (\text{B.3})$$

The $^1P_1 \rightarrow ^3S_1$ amplitude

$$G_{01;10}^{(ij)1}(p, k) = -\frac{H_{ij}(p, k)}{2pq_p^*} \left[\frac{1}{3}(\gamma_p + 2) Q_0(z) + g_{pk} Q_1(z) + \frac{2}{3}(\gamma_p - 1) Q_2(z) \right]. \quad (\text{B.4})$$

The $^1P_1 \rightarrow ^3D_1$ amplitude

$$G_{21;10}^{(ij)1}(p, k) = \frac{H_{ij}(p, k)}{\sqrt{2}pq_p^*} \left[\frac{1}{3}(\gamma_p - 1) Q_0(z) + g_{pk} Q_1(z) + \frac{1}{3}(2\gamma_p + 1) Q_2(z) \right]. \quad (\text{B.5})$$

The $^3S_1 \rightarrow ^3S_1$ amplitude

$$\begin{aligned} G_{01;01}^{(ij)1}(p, k) = & \frac{H_{ij}(p, k)}{2q_p^* q_k^*} \left[\frac{1}{3} \{g_{kp}(\gamma_p + 2) + g_{pk}(\gamma_k + 2)\} Q_0(z) \right. \\ & + \left\{ g_{pk} g_{kp} + \frac{1}{5}(-2 + 2\gamma_p + 2\gamma_k + 3\gamma_p \gamma_k) \right\} Q_1(z) \\ & \left. + \frac{2}{3} \{g_{kp}(\gamma_p - 1) + g_{pk}(\gamma_k - 1)\} Q_2(z) + \frac{2}{5}(\gamma_k - 1)(\gamma_p - 1) Q_3(z) \right]. \end{aligned} \quad (\text{B.6})$$

The $^3D_1 \rightarrow ^3S_1$ amplitude

$$\begin{aligned} G_{01;21}^{(ij)1}(p, k) = & -\frac{H_{ij}(p, k)}{\sqrt{2}q_p^* q_k^*} \left[\frac{1}{3} \{g_{kp}(\gamma_p + 2) + g_{pk}(\gamma_k - 1)\} Q_0(z) \right. \\ & + \left\{ g_{pk} g_{kp} + \frac{1}{5}(1 - \gamma_p + 2\gamma_k + 3\gamma_p \gamma_k) \right\} Q_1(z) \\ & \left. + \frac{1}{3} \{g_{kp}(2\gamma_p - 2) + g_{pk}(2\gamma_k + 1)\} Q_2(z) + \frac{1}{5}(\gamma_p - 1)(2\gamma_k + 1) Q_3(z) \right]. \end{aligned} \quad (\text{B.7})$$

The ${}^3D_1 \rightarrow {}^3D_1$ amplitude

$$G_{21;21}^{(ij)1}(p, k) = \frac{H_{ij}(p, k)}{2q_p^* q_k^*} \left[\frac{2}{3} \{g_{kp}(\gamma_p - 1) + g_{pk}(\gamma_k - 1)\} Q_0(z) \right. \\ \left. + \left\{ 2g_{kp}g_{pk} + \frac{1}{5}(-1 - 2\gamma_p - 2\gamma_k + 6\gamma_p\gamma_k) \right\} Q_1(z) \right. \\ \left. + \frac{2}{3} \{g_{kp}(2\gamma_p + 1) + g_{pk}(2\gamma_k + 1)\} Q_2(z) + \frac{1}{5}(1 + 2\gamma_k)(1 + 2\gamma_p) Q_3(z) \right]. \quad (\text{B.8})$$

B.2 $J^P = 0^-$

The ${}^1S_0 \rightarrow {}^1S_0$ amplitude

$$G_{00;00}^{(ij)0}(p, k) = \frac{H_{ij}(p, k)}{2pk} Q_0(z). \quad (\text{B.9})$$

The ${}^1S_0 \rightarrow {}^3P_0$ amplitude

$$G_{11;00}^{(ij)0}(p, k) = \frac{\sqrt{3}H_{ij}(p, k)}{2pq_p^*} [g_{pk} Q_0(z) + \gamma_p Q_1(z)]. \quad (\text{B.10})$$

The ${}^3P_0 \rightarrow {}^3P_0$ amplitude

$$G_{11;11}^{(ij)0} = \frac{H_{ij}(p, k)}{2q_k^* q_p^*} \left[(3g_{pk}g_{kp} + \gamma_k\gamma_p) Q_0(z) + 3(g_{pk}\gamma_k + g_{kp}\gamma_p) Q_1(z) + 2\gamma_k\gamma_p Q_2(z) \right]. \quad (\text{B.11})$$

C Expressions for the partial-wave projection of \mathcal{K}_3

This appendix provides explicit expressions for the partial wave projection of \mathcal{K}_3 , based on the master formula given in eq. (A.32). To write the results compactly, we introduce some notation in addition to that used in the previous appendix,

$$\omega_{q_p^*}^- = \sqrt{(q_p^*)^2 + m_D^2} - \sqrt{(q_p^*)^2 + m_\pi^2}, \quad (\text{C.1})$$

$$p_p^* = \gamma_p(p + \omega_p\beta_p), \quad (\text{C.2})$$

$$\omega_{p_p^*} = \gamma_p(\omega_p + \beta_p p), \quad (\text{C.3})$$

as well as the analogous expressions with $p \rightarrow k$. Since the \mathcal{K}_3 matrix is symmetric under interchanges of final and initial states, we provide only the minimal number of non-zero elements necessary to reproduce all partial-wave and flavor compositions.

The expected threshold behavior is the same as for G , eq. (B.2), and this expectation holds for all the following results.

We stress that the results in this appendix do not include the symmetry factors discussed at the end of section 2.2.2 in the main text.

C.1 $J^P = 1^+$

The isotropic and \mathcal{K}_3^B terms do not contribute. For the former this result is trivial since an internal p -wave is required to create $J = 1$; for the latter this is a nontrivial result.

The $^1P_1 \rightarrow ^1P_1$ amplitude

$$\mathcal{K}_{3;10;10}^{(11)1}(p, k) = \frac{1}{6} \mathcal{K}_3^E \frac{1}{M^2} (p - \gamma_p \beta_p \omega_{q_p^*}^-) (k - \gamma_k \beta_k \omega_{q_k^*}^-), \quad (\text{C.4})$$

$$\mathcal{K}_{3;10;10}^{(12)1}(p, k) = -\frac{1}{3} \mathcal{K}_3^E \frac{1}{M^2} (p - \gamma_p \beta_p \omega_{q_p^*}^-) k, \quad (\text{C.5})$$

$$\mathcal{K}_{3;10;10}^{(22)1}(p, k) = \frac{2}{3} \mathcal{K}_3^E \frac{pk}{M^2}. \quad (\text{C.6})$$

The $^1P_1 \rightarrow ^3S_1$ amplitude

$$\mathcal{K}_{3;01;10}^{(11)1}(p, k) = -\frac{1}{9} \mathcal{K}_3^E \frac{1}{M^2} q_p^* (\gamma_p + 2) (k - \gamma_k \beta_k \omega_{q_k^*}^-), \quad (\text{C.7})$$

$$\mathcal{K}_{3;01;10}^{(12)1}(p, k) = \frac{2}{9} \mathcal{K}_3^E \frac{1}{M^2} q_p^* (\gamma_p + 2) k, \quad (\text{C.8})$$

$$\mathcal{K}_{3;01;10}^{(22)1}(p, k) = 0. \quad (\text{C.9})$$

The $^1P_1 \rightarrow ^3D_1$ amplitude

$$\mathcal{K}_{3;21;10}^{(11)1}(p, k) = \frac{\sqrt{2}}{9} \mathcal{K}_3^E \frac{1}{M^2} q_p^* (\gamma_p - 1) (k - \gamma_k \beta_k \omega_{q_k^*}^-), \quad (\text{C.10})$$

$$\mathcal{K}_{3;21;10}^{(12)1}(p, k) = -\frac{2\sqrt{2}}{9} \mathcal{K}_3^E \frac{1}{M^2} q_p^* (\gamma_p - 1) k, \quad (\text{C.11})$$

$$\mathcal{K}_{3;21;10}^{(22)1}(p, k) = 0. \quad (\text{C.12})$$

The $^3S_1 \rightarrow ^3S_1$ amplitude

$$\mathcal{K}_{3;01;01}^{(11)1}(p, k) = \frac{2}{27} \mathcal{K}_3^E \frac{1}{M^2} q_p^* (\gamma_p + 2) q_k^* (\gamma_k + 2), \quad (\text{C.13})$$

$$\mathcal{K}_{3;1;01;01}^{(12)}(p, k) = 0, \quad (\text{C.14})$$

$$\mathcal{K}_{3;1;01;01}^{(22)}(p, k) = 0. \quad (\text{C.15})$$

The $^3S_1 \rightarrow ^3D_1$ amplitude

$$\mathcal{K}_{3;21;01}^{(11)1}(p, k) = -\frac{2\sqrt{2}}{27} \mathcal{K}_3^E \frac{1}{M^2} q_p^* q_k^* (\gamma_p - 1) (\gamma_k + 2), \quad (\text{C.16})$$

$$\mathcal{K}_{3;1;21;01}^{(12)}(p, k) = 0, \quad (\text{C.17})$$

$$\mathcal{K}_{3;1;21;01}^{(22)}(p, k) = 0. \quad (\text{C.18})$$

$$(\text{C.19})$$

The $^3D_1 \rightarrow ^3D_1$ amplitude

$$\mathcal{K}_{3;21;21}^{(11)1}(p, k) = \frac{4}{27} \mathcal{K}_3^E \frac{1}{M^2} q_p^* (\gamma_p - 1) q_k^* (\gamma_k - 1), \quad (\text{C.20})$$

$$\mathcal{K}_{3;1;21;21}^{(12)}(p, k) = 0, \quad (\text{C.21})$$

$$\mathcal{K}_{3;1;21;21}^{(22)}(p, k) = 0. \quad (\text{C.22})$$

Separated momentum dependence Given the elements above, it is possible to cast the $J^P = 1^+$ three-body K matrix into the form of eq. (2.38) with $a_{\max} = 1$. The corresponding non-zero “left” functions are,

$$\mathcal{K}_{L,10}^{(1)}(p) = \sqrt{\frac{\mathcal{K}_3^E}{6}} \frac{p - \gamma_p \beta_p \omega_{q_p^*}^-}{M}, \quad (\text{C.23})$$

$$\mathcal{K}_{L,01}^{(1)}(p) = -\sqrt{\frac{2\mathcal{K}_3^E}{27}} \frac{q_p^*(\gamma_p + 2)}{M}, \quad (\text{C.24})$$

$$\mathcal{K}_{L,21}^{(1)}(p) = \sqrt{\frac{4\mathcal{K}_3^E}{27}} \frac{q_p^*(\gamma_p - 1)}{M}, \quad (\text{C.25})$$

$$\mathcal{K}_{L,10}^{(2)}(p) = -\sqrt{\frac{2\mathcal{K}_3^E}{3}} \frac{p}{M}, \quad (\text{C.26})$$

where we have now dropped the trivial index a . The “right” functions are obtained from the above expressions by replacing labels $L \leftrightarrow R$, momenta $p \leftrightarrow k$, and the corresponding spectator’s masses when appropriate. In this case, matrix \mathcal{I} of eq. (2.43) becomes a number.

C.2 $J^P = 0^-$

In the following, we use the abbreviation $\mathcal{K}_3^{\text{iso}} = \mathcal{K}_3^{\text{iso},0} + \mathcal{K}_3^{\text{iso},1} \Delta$.

$^1S_0 \rightarrow ^1S_0$ elements

$$\begin{aligned} \mathcal{K}_{3;00;00}^{(11)0}(p, k) &= \mathcal{K}_3^{\text{iso}} + \mathcal{K}_3^B \frac{1}{M^2} \left[E(\omega_p + \omega_k) - 6m_D^2 + \omega_{k^*} \omega_{q_k^*}^- + \omega_{p^*} \omega_{q_p^*}^- \right] \\ &\quad + \mathcal{K}_3^E \frac{1}{M^2} \left[2m_\pi^2 - \frac{1}{2}(E - \omega_{q_p^*}^- \gamma_p - \omega_p)(E - \omega_{q_k^*}^- \gamma_k - \omega_k) \right], \end{aligned} \quad (\text{C.27})$$

$$\begin{aligned} \mathcal{K}_{3;00;00}^{(12)0}(p, k) &= \mathcal{K}_3^{\text{iso}} + \mathcal{K}_3^B \frac{1}{M^2} \left[E\omega_p - 3m_D^2 + \omega_{p^*} \omega_{q_p^*}^- + (\sigma_k - 4m_D^2) \right] \\ &\quad + \mathcal{K}_3^E \frac{1}{M^2} \left[2m_\pi^2 - (E - \omega_{q_p^*}^- \gamma_p - \omega_p)\omega_k \right], \end{aligned} \quad (\text{C.28})$$

$$\begin{aligned} \mathcal{K}_{3;00;00}^{(22)0}(p, k) &= \mathcal{K}_3^{\text{iso}} + \mathcal{K}_3^B \frac{1}{M^2} \left[(\sigma_k - 4m_D^2) + (\sigma_p - 4m_D^2) \right] \\ &\quad + \mathcal{K}_3^E \frac{2}{M^2} (m_\pi^2 - \omega_p \omega_k). \end{aligned} \quad (\text{C.29})$$

$^1S_0 \rightarrow ^3P_0$ elements

$$\mathcal{K}_{3;11;00}^{(11)0}(p, k) = -\mathcal{K}_3^B \frac{2}{\sqrt{3}} \frac{1}{M^2} p_p^* q_p^* - \mathcal{K}_3^E \frac{1}{\sqrt{3}} \frac{1}{M^2} q_p^* \beta_p \gamma_p (E - \omega_{q_k^*}^- \gamma_k - \omega_k), \quad (\text{C.30})$$

$$\mathcal{K}_{3;11;00}^{(12)0}(p, k) = -\frac{2}{\sqrt{3}} \mathcal{K}_3^B \frac{1}{M^2} p_p^* q_p^* - \frac{2}{\sqrt{3}} \mathcal{K}_3^E \frac{1}{M^2} q_p^* \beta_p \gamma_p \omega_k, \quad (\text{C.31})$$

$$\mathcal{K}_{3;11;00}^{(12)0}(p, k) = 0. \quad (\text{C.32})$$

The $^3P_0 \rightarrow ^3P_0$ elements

$$\mathcal{K}_{3;11;11}^{(11)0}(p, k) = -\frac{2}{3} \mathcal{K}_3^E \frac{1}{M^2} q_p^* \beta_p \gamma_p q_k^* \beta_k \gamma_k, \quad (\text{C.33})$$

$$\mathcal{K}_{3;11;11}^{(12)0}(p, k) = 0 \quad (\text{C.34})$$

$$\mathcal{K}_{3;11;11}^{(22)0}(p, k) = 0. \quad (\text{C.35})$$

Separated momentum dependence Below we provide the “left” and “right” functions reproducing the above partial-wave projected $J^P = 0^-$ \mathcal{K}_3 matrix. In the most general case, when all coefficients are non-zero, it requires $a_{\max} = 4$. The $a \leq 2$ “left” functions involve only \mathcal{K}^{iso} and \mathcal{K}^E terms,

$$\mathcal{K}_{L,00}^{1,(1)}(p) = i\sqrt{\frac{\mathcal{K}_3^E}{2}} \frac{E - \omega_{q_p^*}^- \gamma_p - \omega_p}{M}, \quad \mathcal{K}_{L,00}^{2,(1)}(p) = \sqrt{\mathcal{K}_3^{\text{iso}} + 2\mathcal{K}_3^E} \frac{m_\pi^2}{M^2}, \quad (\text{C.36})$$

$$\mathcal{K}_{L,11}^{1,(1)}(p) = i\sqrt{\frac{2\mathcal{K}_3^E}{3}} \frac{q_p^* \beta_p \gamma_p}{M}, \quad \mathcal{K}_{L,11}^{2,(1)}(p) = 0, \quad (\text{C.37})$$

$$\mathcal{K}_{L,00}^{1,(2)}(p) = i\sqrt{2\mathcal{K}_3^E} \frac{\omega_p}{M}, \quad \mathcal{K}_{L,00}^{2,(2)}(p) = \sqrt{\mathcal{K}_3^{\text{iso}} + 2\mathcal{K}_3^E} \frac{m_\pi^2}{M^2}. \quad (\text{C.38})$$

The corresponding “right” functions are obtained by replacing momenta $p \leftrightarrow k$ and the corresponding masses. To include \mathcal{K}_3^B terms we need to add new non-symmetric terms,

$$\mathcal{K}_{L,00}^{3,(1)}(p) = \mathcal{K}_3^B \frac{E\omega_p - 3m_D^2 + \omega_{p_p^*} \omega_{q_p^*}^-}{M^2}, \quad \mathcal{K}_{R,00}^{3,(1)}(k) = 1, \quad (\text{C.39})$$

$$\mathcal{K}_{L,00}^{4,(1)}(p) = 1, \quad \mathcal{K}_{R,00}^{4,(1)}(k) = \mathcal{K}_3^B \frac{E\omega_k - 3m_D^2 + \omega_{k_k^*} \omega_{q_k^*}^-}{M^2}, \quad (\text{C.40})$$

$$\mathcal{K}_{L,11}^{3,(1)}(p) = -\mathcal{K}_3^B \frac{2}{\sqrt{3}} \frac{q_p^* p_p^*}{M^2}, \quad \mathcal{K}_{R,11}^{3,(1)}(k) = 0, \quad (\text{C.41})$$

$$\mathcal{K}_{L,11}^{4,(1)}(p) = 0, \quad \mathcal{K}_{R,11}^{4,(1)}(k) = -\mathcal{K}_3^B \frac{2}{\sqrt{3}} \frac{q_k^* k_k^*}{M^2}, \quad (\text{C.42})$$

$$\mathcal{K}_{L,00}^{3,(2)}(p) = \mathcal{K}_3^B \frac{\sigma_p - 4m_D^2}{M^2}, \quad \mathcal{K}_{R,00}^{3,(2)}(k) = 1, \quad (\text{C.43})$$

$$\mathcal{K}_{L,00}^{4,(2)}(p) = 1, \quad \mathcal{K}_{R,00}^{4,(2)}(k) = \mathcal{K}_3^B \frac{\sigma_k - 4m_D^2}{M^2}. \quad (\text{C.44})$$

D Residue of D^* pole

In this appendix we derive the result eq. (4.4) used in the main text, which provides the relation between the effective range in p -wave $D\pi$ scattering amplitude to the $DD^*\pi$ coupling. We simplify the notation by writing this amplitude as $\mathcal{M}_{2,1}$, using s for the square of the two-particle c.m. frame energy, and denoting the magnitude of the momentum of each particle in this frame as q and the phase shift simply as $\delta(q)$.

We first observe that it follows from the physical crossing condition described after eq. (2.23) that the p -wave amplitude,

$$\mathcal{M}_{2,1}^{-1} = \frac{1}{8\pi\sqrt{s}} \frac{1}{q^2} \left(q^3 \cot \delta(q) - iq^3 \right), \quad (\text{D.1})$$

must have a positive residue at a physical bound-state pole (as already incorporated into the form eq. (2.52) used in the LSZ reduction of \mathcal{M}_3). We thus introduce a (real, positive) $D^*D\pi$ coupling constant, $g_{D^*D\pi}$, by taking the following form for the inverse amplitude close to the pole,

$$\mathcal{M}_{2,1}^{-1} = -\frac{2}{q_0^2} \frac{s - m_{D^*}^2}{g_{D^*D\pi}^2} \left[1 + \mathcal{O}(s - m_{D^*}^2) \right], \quad (\text{D.2})$$

The overall factors are chosen so that the coupling constant agrees with that used in the chiral perturbation theory (ChPT) literature [88], as discussed further below. Note that the residue is positive because the momentum at the bound state, q_0 is imaginary. We will use the two-term ERE expansion, $q^3 \cot \delta = -1/a_0 + rq^2/2$ (again with a simplified notation), in which case q_0 is given by eq. (2.24). Matching the derivatives of eqs. (D.1) and (D.2) at the pole position yields

$$g_{D^*D\pi}^2 = -\frac{128\pi m_{D^*}}{1 - (m_D^2 - m_\pi^2)^2/m_{D^*}^4} \frac{1}{r + 3|q_0|}. \quad (\text{D.3})$$

In order for the right-hand side to be positive, we must have $r < -3|q_0|$. The result eq. (D.3) leads immediately to eq. (4.4).

We now explain why the form eq. (D.2) agrees with conventions used in ChPT. The coupling constant is defined by [88],

$$\langle D^0(p_1)\pi^+(p_2)|D^{*+}(p_1+p_2)\rangle = -(\epsilon \cdot p_2)g_{D^*D\pi} = -\sqrt{2}\langle D^+(p_1)\pi^0(p_2)|D^{*+}(p_1+p_2)\rangle, \quad (\text{D.4})$$

where ϵ is the D^* polarization vector, and the second equality follows from isospin symmetry. The decay widths are then,

$$\Gamma(D^{*+} \rightarrow D^0\pi^+) = \frac{g_{D^*D\pi}^2 q^3}{24\pi m_{D^*}^2} = 2\Gamma(D^{*+} \rightarrow D^+\pi^0). \quad (\text{D.5})$$

To match the normalization of $\mathcal{M}_{2,1}$ we need to project onto $I = 1/2$ and $\ell = 1$. For the former, we use,

$$\langle D\pi, I = 1/2, m_I = 1/2 | = \sqrt{\frac{2}{3}}\langle D^0\pi^+ | - \sqrt{\frac{1}{3}}\langle D^+\pi^0 | \quad (\text{D.6})$$

to obtain,

$$\langle D(p_1)\pi(p_2), I = 1/2 | D^{*+}(p_1+p_2)\rangle = -\sqrt{\frac{3}{2}}(\epsilon \cdot p_2)g_{D^*D\pi}. \quad (\text{D.7})$$

Using this, and summing over polarizations, the pole contribution to \mathcal{M}_2 is,

$$\mathcal{M}_2(I = 1/2) = -\frac{3}{2}g_{D^*D\pi}^2 \frac{\mathbf{q}'_\pi \cdot \mathbf{q}_\pi}{s - m_{D^*}^2}, \quad (\text{D.8})$$

with \mathbf{q}'_π and \mathbf{q}_π being the final and initial pion momenta in the c.m. frame. An equivalent result can be obtained by using the effective Lagrangian and Feynman rules in ref. [63]. The projection onto $\ell = 1$ can be done using

$$\mathbf{a} \cdot \mathbf{b} = \frac{4\pi}{3}ab \sum_m Y_{1m}(\hat{a})Y_{1m}^*(\hat{b}), \quad (\text{D.9})$$

and leads to

$$\mathcal{M}_{2,1}(I = 1/2) = -\frac{1}{2}g_{D^*D\pi}^2 \frac{q^2}{s - m_{D^*}^2}, \quad (\text{D.10})$$

which agrees with eq. (D.2).

References

- [1] **LHCb** Collaboration, R. Aaij et al., *Observation of an exotic narrow doubly charmed tetraquark*, *Nature Phys.* **18** (2022), no. 7 751–754, [[arXiv:2109.01038](#)].
- [2] **LHCb** Collaboration, R. Aaij et al., *Study of the doubly charmed tetraquark T_{cc}^+* , *Nature Commun.* **13** (2022), no. 1 3351, [[arXiv:2109.01056](#)].
- [3] L. Heller and J. A. Tjon, *On the Existence of Stable Dimesons*, *Phys. Rev. D* **35** (1987) 969.
- [4] S. Zouzou, B. Silvestre-Brac, C. Gignoux, and J. M. Richard, *FOUR QUARK BOUND STATES*, *Z. Phys. C* **30** (1986) 457.
- [5] H. J. Lipkin, *A MODEL INDEPENDENT APPROACH TO MULTI - QUARK BOUND STATES*, *Phys. Lett. B* **172** (1986) 242–247.
- [6] J. Carlson, L. Heller, and J. A. Tjon, *Stability of Dimesons*, *Phys. Rev. D* **37** (1988) 744.
- [7] D. Janc and M. Rosina, *The $T_{cc} = DD^*$ molecular state*, *Few Body Syst.* **35** (2004) 175–196, [[hep-ph/0405208](#)].
- [8] H.-X. Chen, W. Chen, X. Liu, Y.-R. Liu, and S.-L. Zhu, *An updated review of the new hadron states*, *Rept. Prog. Phys.* **86** (2023), no. 2 026201, [[arXiv:2204.02649](#)].
- [9] M. Padmanath and S. Prelovsek, *Signature of a Doubly Charm Tetraquark Pole in DD^* Scattering on the Lattice*, *Phys. Rev. Lett.* **129** (2022), no. 3 032002, [[arXiv:2202.10110](#)].
- [10] Y. Lyu, S. Aoki, T. Doi, T. Hatsuda, Y. Ikeda, and J. Meng, *Doubly Charmed Tetraquark T_{cc}^+ from Lattice QCD near Physical Point*, *Phys. Rev. Lett.* **131** (2023), no. 16 161901, [[arXiv:2302.04505](#)].
- [11] S. Chen, C. Shi, Y. Chen, M. Gong, Z. Liu, W. Sun, and R. Zhang, *$T_{cc}^+(3875)$ relevant DD^* scattering from $N_f = 2$ lattice QCD*, *Phys. Lett. B* **833** (2022) 137391, [[arXiv:2206.06185](#)].
- [12] E. Ortiz-Pacheco, S. Collins, L. Leskovec, M. Padmanath, and S. Prelovsek, *Doubly charmed tetraquark: isospin channels and diquark-antidiquark interpolators*, [[arXiv:2312.13441](#)].
- [13] S. Collins, A. Nefediev, M. Padmanath, and S. Prelovsek, *Towards the quark mass dependence of T_{cc}^+ from lattice QCD*, [[arXiv:2402.14715](#)].
- [14] T. Whyte, D. J. Wilson, and C. E. Thomas, *Near-threshold states in coupled $DD^* - D^*D^*$ scattering from lattice QCD*, [[arXiv:2405.15741](#)].
- [15] M. Albaladejo, *$T_{cc}+$ coupled channel analysis and predictions*, *Phys. Lett. B* **829** (2022) 137052, [[arXiv:2110.02944](#)].
- [16] M.-L. Du, V. Baru, X.-K. Dong, A. Filin, F.-K. Guo, C. Hanhart, A. Nefediev, J. Nieves, and Q. Wang, *Coupled-channel approach to $T_{cc}+$ including three-body effects*, *Phys. Rev. D* **105** (2022), no. 1 014024, [[arXiv:2110.13765](#)].
- [17] N. N. Achasov and G. N. Shestakov, *Triangle singularities in the $T_{cc}+\rightarrow D^*+D0\rightarrow\pi+D0D0$ decay width*, *Phys. Rev. D* **105** (2022), no. 9 096038, [[arXiv:2203.17100](#)].
- [18] J.-Z. Wang, Z.-Y. Lin, and S.-L. Zhu, *Cut structures and an observable singularity in the three-body threshold dynamics: The $T_{cc}+$ case*, *Phys. Rev. D* **109** (2024), no. 7 L071505, [[arXiv:2309.09861](#)].
- [19] X. Zhang, *Relativistic three-body scattering and the $D^0D^{*+} - D^+D^{*0}$ system*, *Phys. Rev. D* **109** (2024), no. 9 094010, [[arXiv:2402.02151](#)].

- [20] M. Abolnikov, V. Baru, E. Epelbaum, A. A. Filin, C. Hanhart, and L. Meng, *Internal structure of the $T_{cc}(3875)^+$ from its light-quark mass dependence*, [arXiv:2407.04649](#).
- [21] L. Meng, V. Baru, E. Epelbaum, A. A. Filin, and A. M. Gasparian, *Solving the left-hand cut problem in lattice QCD: $T_{cc}(3875)^+$ from finite volume energy levels*, *Phys. Rev. D* **109** (2024), no. 7 L071506, [[arXiv:2312.01930](#)].
- [22] M. T. Hansen, F. Romero-López, and S. R. Sharpe, *Incorporating $DD\pi$ effects and left-hand cuts in lattice QCD studies of the $T_{cc}(3875)^+$* , *JHEP* **06** (2024) 051, [[arXiv:2401.06609](#)].
- [23] M. Lüscher, *Volume Dependence of the Energy Spectrum in Massive Quantum Field Theories. 2. Scattering States*, *Commun.Math.Phys.* **105** (1986) 153–188.
- [24] M.-L. Du, A. Filin, V. Baru, X.-K. Dong, E. Epelbaum, F.-K. Guo, C. Hanhart, A. Nefediev, J. Nieves, and Q. Wang, *Role of Left-Hand Cut Contributions on Pole Extractions from Lattice Data: Case Study for $T_{cc}(3875)^+$* , *Phys. Rev. Lett.* **131** (2023), no. 13 131903, [[arXiv:2303.09441](#)].
- [25] M.-L. Du, F.-K. Guo, and B. Wu, *Effective range expansion with the left-hand cut*, [arXiv:2408.09375](#).
- [26] A. B. a. Raposo and M. T. Hansen, *Finite-volume scattering on the left-hand cut*, *JHEP* **08** (2024) 075, [[arXiv:2311.18793](#)].
- [27] R. Bubna, H.-W. Hammer, F. Müller, J.-Y. Pang, A. Rusetsky, and J.-J. Wu, *Lüscher equation with long-range forces*, *JHEP* **05** (2024) 168, [[arXiv:2402.12985](#)].
- [28] R. A. Briceño and Z. Davoudi, *Three-particle scattering amplitudes from a finite volume formalism*, *Phys. Rev.* **D87** (2013), no. 9 094507, [[arXiv:1212.3398](#)].
- [29] K. Polejaeva and A. Rusetsky, *Three particles in a finite volume*, *Eur. Phys. J. A* **48** (2012) 67, [[arXiv:1203.1241](#)].
- [30] M. T. Hansen and S. R. Sharpe, *Relativistic, model-independent, three-particle quantization condition*, *Phys. Rev.* **D90** (2014), no. 11 116003, [[arXiv:1408.5933](#)].
- [31] M. T. Hansen and S. R. Sharpe, *Expressing the three-particle finite-volume spectrum in terms of the three-to-three scattering amplitude*, *Phys. Rev.* **D92** (2015), no. 11 114509, [[arXiv:1504.04248](#)].
- [32] H.-W. Hammer, J.-Y. Pang, and A. Rusetsky, *Three-particle quantization condition in a finite volume: 1. The role of the three-particle force*, *JHEP* **09** (2017) 109, [[arXiv:1706.07700](#)].
- [33] H. W. Hammer, J. Y. Pang, and A. Rusetsky, *Three particle quantization condition in a finite volume: 2. General formalism and the analysis of data*, *JHEP* **10** (2017) 115, [[arXiv:1707.02176](#)].
- [34] M. Mai and M. Döring, *Three-body Unitarity in the Finite Volume*, *Eur. Phys. J.* **A53** (2017), no. 12 240, [[arXiv:1709.08222](#)].
- [35] A. W. Jackura, S. M. Dawid, C. Fernández-Ramírez, V. Mathieu, M. Mikhasenko, A. Pilloni, S. R. Sharpe, and A. P. Szczepaniak, *Equivalence of three-particle scattering formalisms*, *Phys. Rev. D* **100** (2019), no. 3 034508, [[arXiv:1905.12007](#)].
- [36] M. T. Hansen, F. Romero-López, and S. R. Sharpe, *Generalizing the relativistic quantization condition to include all three-pion isospin channels*, *JHEP* **07** (2020) 047, [[arXiv:2003.10974](#)].

- [37] J.-Y. Pang, J.-J. Wu, and L.-S. Geng, *DDK system in finite volume*, *Phys. Rev. D* **102** (2020), no. 11 114515, [[arXiv:2008.13014](#)].
- [38] T. D. Blanton and S. R. Sharpe, *Relativistic three-particle quantization condition for nondegenerate scalars*, *Phys. Rev. D* **103** (2021), no. 5 054503, [[arXiv:2011.05520](#)].
- [39] T. D. Blanton and S. R. Sharpe, *Equivalence of relativistic three-particle quantization conditions*, *Phys. Rev. D* **102** (2020), no. 5 054515, [[arXiv:2007.16190](#)].
- [40] T. D. Blanton and S. R. Sharpe, *Three-particle finite-volume formalism for $\pi^+\pi^+K^+$ and related systems*, *Phys. Rev. D* **104** (2021), no. 3 034509, [[arXiv:2105.12094](#)].
- [41] F. Müller, J.-Y. Pang, A. Rusetsky, and J.-J. Wu, *Relativistic-invariant formulation of the NREFT three-particle quantization condition*, *JHEP* **02** (2022) 158, [[arXiv:2110.09351](#)].
- [42] T. D. Blanton, F. Romero-López, and S. R. Sharpe, *Implementing the three-particle quantization condition for $\pi^+\pi^+K^+$ and related systems*, *JHEP* **02** (2022) 098, [[arXiv:2111.12734](#)].
- [43] Z. T. Draper, M. T. Hansen, F. Romero-López, and S. R. Sharpe, *Three relativistic neutrons in a finite volume*, *JHEP* **07** (2023) 226, [[arXiv:2303.10219](#)].
- [44] R. A. Briceño, A. W. Jackura, D. A. Pefkou, and F. Romero-López, *Electroweak three-body decays in the presence of two- and three-body bound states*, *JHEP* **05** (2024) 279, [[arXiv:2402.12167](#)].
- [45] Q.-C. Xiao, J.-Y. Pang, and J.-J. Wu, *Lattice spectra of DDK three-body system with Lorentz covariant kinematic*, [arXiv:2408.16590](#).
- [46] Y. Feng, F. Gil, M. Döring, R. Molina, M. Mai, V. Shashtry, and A. Szczepaniak, *A unitary coupled-channel three-body amplitude with pions and kaons*, [arXiv:2407.08721](#).
- [47] R. A. Briceño, M. T. Hansen, and S. R. Sharpe, *Three-particle systems with resonant subprocesses in a finite volume*, *Phys. Rev. D* **99** (2019), no. 1 014516, [[arXiv:1810.01429](#)].
- [48] R. A. Briceño, M. T. Hansen, and S. R. Sharpe, *Numerical study of the relativistic three-body quantization condition in the isotropic approximation*, *Phys. Rev. D* **98** (2018), no. 1 014506, [[arXiv:1803.04169](#)].
- [49] A. W. Jackura, R. A. Briceño, S. M. Dawid, M. H. E. Islam, and C. McCarty, *Solving relativistic three-body integral equations in the presence of bound states*, *Phys. Rev. D* **104** (2021), no. 1 014507, [[arXiv:2010.09820](#)].
- [50] A. W. Jackura, *Three-body scattering and quantization conditions from S -matrix unitarity*, *Phys. Rev. D* **108** (2023), no. 3 034505, [[arXiv:2208.10587](#)].
- [51] S. M. Dawid, M. H. E. Islam, and R. A. Briceño, *Analytic continuation of the relativistic three-particle scattering amplitudes*, *Phys. Rev. D* **108** (2023), no. 3 034016, [[arXiv:2303.04394](#)].
- [52] **Hadron Spectrum** Collaboration, M. T. Hansen, R. A. Briceño, R. G. Edwards, C. E. Thomas, and D. J. Wilson, *Energy-Dependent $\pi^+\pi^+\pi^+$ Scattering Amplitude from QCD*, *Phys. Rev. Lett.* **126** (2021) 012001, [[arXiv:2009.04931](#)].
- [53] S. M. Dawid, M. H. E. Islam, R. A. Briceño, and A. W. Jackura, *Evolution of Efimov states*, *Phys. Rev. A* **109** (2024), no. 4 043325, [[arXiv:2309.01732](#)].
- [54] M. Garofalo, M. Mai, F. Romero-López, A. Rusetsky, and C. Urbach, *Three-body resonances in the φ^4 theory*, *JHEP* **02** (2023) 252, [[arXiv:2211.05605](#)].

- [55] R. A. Briceño, C. S. R. Costa, and A. W. Jackura, *Partial-wave projection of relativistic three-body amplitudes*, [arXiv:2409.15577](#).
- [56] D. Mohler, S. Prelovsek, and R. M. Woloshyn, *$D\pi$ scattering and D meson resonances from lattice QCD*, *Phys. Rev. D* **87** (2013), no. 3 034501, [[arXiv:1208.4059](#)].
- [57] D. Becirevic and F. Sanfilippo, *Theoretical estimate of the $D^* \rightarrow D\pi$ decay rate*, *Phys. Lett. B* **721** (2013) 94–100, [[arXiv:1210.5410](#)].
- [58] G. Moir, M. Peardon, S. M. Ryan, C. E. Thomas, and D. J. Wilson, *Coupled-Channel $D\pi$, $D\eta$ and $D_s\bar{K}$ Scattering from Lattice QCD*, *JHEP* **10** (2016) 011, [[arXiv:1607.07093](#)].
- [59] **Hadron Spectrum** Collaboration, L. Gayer, N. Lang, S. M. Ryan, D. Tims, C. E. Thomas, and D. J. Wilson, *Isospin-1/2 $D\pi$ scattering and the lightest D_0^* resonance from lattice QCD*, *JHEP* **07** (2021) 123, [[arXiv:2102.04973](#)].
- [60] H. Yan, C. Liu, L. Liu, Y. Meng, and H. Xing, *Pion mass dependence in $D\pi$ scattering and the $D_0^*(2300)$ resonance from lattice QCD*, [arXiv:2404.13479](#).
- [61] H. Georgi, *An Effective Field Theory for Heavy Quarks at Low-energies*, *Phys. Lett. B* **240** (1990) 447–450.
- [62] M. B. Wise, *Chiral perturbation theory for hadrons containing a heavy quark*, *Phys. Rev. D* **45** (1992), no. 7 R2188.
- [63] M. B. Wise, *Combining chiral and heavy quark symmetry*, in *CCAST Symposium on Particle Physics at the Fermi Scale*, pp. 71–114, 5, 1993. [hep-ph/9306277](#).
- [64] F. Gil-Domínguez, A. Giachino, and R. Molina, *Quark mass dependence of the $T_{cc}(3875)^+$ pole*, [arXiv:2409.15141](#).
- [65] **GWQCD** Collaboration, M. Mai, A. Alexandru, R. Brett, C. Culver, M. Döring, F. X. Lee, and D. Sadasivan, *Three-Body Dynamics of the $a_1(1260)$ Resonance from Lattice QCD*, *Phys. Rev. Lett.* **127** (2021), no. 22 222001, [[arXiv:2107.03973](#)].
- [66] S. M. Dawid, *Infinite volume, three-body scattering formalisms in the presence of bound states*, *PoS LATTICE2021* (2022) 520, [[arXiv:2111.05418](#)].
- [67] A. W. Jackura and R. A. Briceño, *Partial-wave projection of the one-particle exchange in three-body scattering amplitudes*, *Phys. Rev. D* **109** (2024), no. 9 096030, [[arXiv:2312.00625](#)].
- [68] **JPAC** Collaboration, A. Jackura, C. Fernandez-Ramirez, V. Mathieu, M. Mikhasenko, J. Nys, A. Pilloni, K. Saldaña, N. Sherrill, and A. P. Szczepaniak, *Phenomenology of Relativistic $3 \rightarrow 3$ Reaction Amplitudes within the Isobar Approximation*, *Eur. Phys. J. C* **79** (2019), no. 1 56, [[arXiv:1809.10523](#)].
- [69] S. U. Chung, *Spin Formalisms*, <https://suchung.web.cern.ch/spinfm1.pdf>.
- [70] J. M. Blatt and J. D. Jackson, *On the Interpretation of Neutron-Proton Scattering Data by the Schwinger Variational Method*, *Phys. Rev.* **76** (1949) 18–37.
- [71] H. A. Bethe, *Theory of the Effective Range in Nuclear Scattering*, *Phys. Rev.* **76** (1949) 38–50.
- [72] J. R. Taylor, *Scattering Theory: The Quantum Theory of Nonrelativistic Collisions*. John Wiley & Sons, Inc., New York, 1972.
- [73] S. K. Adhikari and J. A. Torreão, *Effective range expansion revisited*, *Phys. Lett. B* **119** (1982) 245–248.

- [74] M. Ebert, H. W. Hammer, and A. Rusetsky, *An alternative scheme for effective range corrections in pionless EFT*, *Eur. Phys. J. A* **57** (2021), no. 12 332, [[arXiv:2109.11982](#)].
- [75] F. Romero-López, S. R. Sharpe, T. D. Blanton, R. A. Briceño, and M. T. Hansen, *Numerical exploration of three relativistic particles in a finite volume including two-particle resonances and bound states*, *JHEP* **10** (2019) 007, [[arXiv:1908.02411](#)].
- [76] M. Mikhasenko, Y. Wunderlich, A. Jackura, V. Mathieu, A. Pilloni, B. Ketzer, and A. P. Szczepaniak, *Three-body scattering: Ladders and Resonances*, [arXiv:1904.11894](#).
- [77] D. Sadasivan, M. Mai, H. Akdag, and M. Döring, *Dalitz plots and lineshape of $a_1(1260)$ from a relativistic three-body unitary approach*, *Phys. Rev. D* **101** (2020), no. 9 094018, [[arXiv:2002.12431](#)]. [Erratum: *Phys.Rev.D* 103, 019901 (2021)].
- [78] D. Sadasivan, A. Alexandru, H. Akdag, F. Amorim, R. Brett, C. Culver, M. Döring, F. X. Lee, and M. Mai, *Pole position of the $a_1(1260)$ resonance in a three-body unitary framework*, *Phys. Rev. D* **105** (2022), no. 5 054020, [[arXiv:2112.03355](#)].
- [79] H. Lehmann, K. Symanzik, and W. Zimmermann, *On the formulation of quantized field theories*, *Nuovo Cim.* **1** (1955) 205–225.
- [80] W. Zimmermann, *On the bound state problem in quantum field theory*, *Nuovo Cim.* **10** (1958) 597–614.
- [81] Z. Fried, *Bound states in the Lehmann, Symanzik and Zimmermann formulation of field theory*. PhD thesis, 1960.
- [82] J. M. Blatt and L. C. Biedenharn, *The Angular Distribution of Scattering and Reaction Cross Sections*, *Rev. Mod. Phys.* **24** (1952) 258–272.
- [83] M. Luscher, *Volume Dependence of the Energy Spectrum in Massive Quantum Field Theories. 1. Stable Particle States*, *Commun. Math. Phys.* **104** (1986) 177.
- [84] M. Luscher, *Volume Dependence of the Energy Spectrum in Massive Quantum Field Theories. 2. Scattering States*, *Commun. Math. Phys.* **105** (1986) 153–188.
- [85] R. A. Briceño, *Two-particle multichannel systems in a finite volume with arbitrary spin*, *Phys. Rev. D* **89** (2014), no. 7 074507, [[arXiv:1401.3312](#)].
- [86] T. D. Blanton, F. Romero-López, and S. R. Sharpe, *Implementing the three-particle quantization condition including higher partial waves*, *JHEP* **03** (2019) 106, [[arXiv:1901.07095](#)].
- [87] Z. T. Draper, A. D. Hanlon, B. Hörz, C. Morningstar, F. Romero-López, and S. R. Sharpe, *Interactions of πK , $\pi\pi K$ and $KK\pi$ systems at maximal isospin from lattice QCD*, *JHEP* **05** (2023) 137, [[arXiv:2302.13587](#)].
- [88] V. M. Belyaev, V. M. Braun, A. Khodjamirian, and R. Ruckl, *$D^* D \pi$ and $B^* B \pi$ couplings in QCD*, *Phys. Rev. D* **51** (1995) 6177–6195, [[hep-ph/9410280](#)].
- [89] **BaBar** Collaboration, J. P. Lees et al., *Measurement of the $D^*(2010)^+$ natural line width and the $D^*(2010)^+ - D^0$ mass difference*, *Phys. Rev. D* **88** (2013), no. 5 052003, [[arXiv:1304.5009](#)]. [Erratum: *Phys.Rev.D* 88, 079902 (2013)].
- [90] S. Prelovšek and A. Nefediev. Private communication.
- [91] R. A. Briceño, Z. Davoudi, T. Luu, and M. J. Savage, *Two-nucleon systems in a finite volume. II. $^3S_1 - ^3D_1$ coupled channels and the deuteron*, *Phys. Rev. D* **88** (2013), no. 11 114507, [[arXiv:1309.3556](#)].

- [92] R. A. Briceño, M. T. Hansen, and S. R. Sharpe, *Relating the finite-volume spectrum and the two-and-three-particle S matrix for relativistic systems of identical scalar particles*, *Phys. Rev. D* **95** (2017), no. 7 074510, [[arXiv:1701.07465](#)].
- [93] M. Padmanath and S. Prelovšek. Private communication.
- [94] C. Morningstar, J. Bulava, B. Fahy, J. Foley, Y. Jhang, K. Juge, D. Lenkner, and C. Wong, *Extended hadron and two-hadron operators of definite momentum for spectrum calculations in lattice QCD*, *Phys. Rev. D* **88** (2013), no. 1 014511, [[arXiv:1303.6816](#)].
- [95] L. Meng and E. Epelbaum, *Two-particle scattering from finite-volume quantization conditions using the plane wave basis*, *JHEP* **10** (2021) 051, [[arXiv:2108.02709](#)].
- [96] V. Baru, A. A. Filin, C. Hanhart, Y. S. Kalashnikova, A. E. Kudryavtsev, and A. V. Nefediev, *Three-body $D\bar{D}\pi$ dynamics for the $X(3872)$* , *Phys. Rev. D* **84** (2011) 074029, [[arXiv:1108.5644](#)].
- [97] S. R. Beane, W. Detmold, T. C. Luu, K. Orginos, M. J. Savage, and A. Torok, *Multi-Pion Systems in Lattice QCD and the Three-Pion Interaction*, *Phys. Rev. Lett.* **100** (2008) 082004, [[arXiv:0710.1827](#)].
- [98] W. Detmold, M. J. Savage, A. Torok, S. R. Beane, T. C. Luu, K. Orginos, and A. Parreno, *Multi-Pion States in Lattice QCD and the Charged-Pion Condensate*, *Phys. Rev. D* **78** (2008) 014507, [[arXiv:0803.2728](#)].
- [99] W. Detmold, K. Orginos, M. J. Savage, and A. Walker-Loud, *Kaon Condensation with Lattice QCD*, *Phys. Rev. D* **78** (2008) 054514, [[arXiv:0807.1856](#)].
- [100] W. Detmold and B. Smigielski, *Lattice QCD study of mixed systems of pions and kaons*, *Phys. Rev. D* **84** (2011) 014508, [[arXiv:1103.4362](#)].
- [101] M. Mai and M. Döring, *Finite-Volume Spectrum of $\pi^+\pi^+$ and $\pi^+\pi^+\pi^+$ Systems*, *Phys. Rev. Lett.* **122** (2019), no. 6 062503, [[arXiv:1807.04746](#)].
- [102] B. Hörz and A. Hanlon, *Two- and three-pion finite-volume spectra at maximal isospin from lattice QCD*, *Phys. Rev. Lett.* **123** (2019), no. 14 142002, [[arXiv:1905.04277](#)].
- [103] T. D. Blanton, F. Romero-López, and S. R. Sharpe, *$I = 3$ three-pion scattering amplitude from lattice QCD*, *Phys. Rev. Lett.* **124** (2020), no. 3 032001, [[arXiv:1909.02973](#)].
- [104] C. Culver, M. Mai, R. Brett, A. Alexandru, and M. Döring, *Three pion spectrum in the $I = 3$ channel from lattice QCD*, *Phys. Rev. D* **101** (2020), no. 11 114507, [[arXiv:1911.09047](#)].
- [105] M. Mai, M. Döring, C. Culver, and A. Alexandru, *Three-body unitarity versus finite-volume $\pi^+\pi^+\pi^+$ spectrum from lattice QCD*, *Phys. Rev. D* **101** (2020) 054510, [[arXiv:1909.05749](#)].
- [106] M. Fischer, B. Kostrzewa, L. Liu, F. Romero-López, M. Ueding, and C. Urbach, *Scattering of two and three physical pions at maximal isospin from lattice QCD*, *Eur. Phys. J. C* **81** (2021), no. 5 436, [[arXiv:2008.03035](#)].
- [107] A. Alexandru, R. Brett, C. Culver, M. Döring, D. Guo, F. X. Lee, and M. Mai, *Finite-volume energy spectrum of the $K^-K^-K^-$ system*, *Phys. Rev. D* **102** (2020), no. 11 114523, [[arXiv:2009.12358](#)].
- [108] R. Brett, C. Culver, M. Mai, A. Alexandru, M. Döring, and F. X. Lee, *Three-body*

- interactions from the finite-volume QCD spectrum*, *Phys. Rev. D* **104** (2021), no. 1 014501, [[arXiv:2101.06144](#)].
- [109] T. D. Blanton, A. D. Hanlon, B. Hörz, C. Morningstar, F. Romero-López, and S. R. Sharpe, *Interactions of two and three mesons including higher partial waves from lattice QCD*, *JHEP* **10** (2021) 023, [[arXiv:2106.05590](#)].
- [110] **NPLQCD, QCDSF** Collaboration, S. R. Beane et al., *Charged multihadron systems in lattice QCD+QED*, *Phys. Rev. D* **103** (2021), no. 5 054504, [[arXiv:2003.12130](#)].
- [111] H. Yan, M. Garofalo, M. Mai, U.-G. Meißner, and C. Urbach, *The ω -meson from lattice QCD*, [arXiv:2407.16659](#).